

STUDIES ON INTERACTION OF A ROTATING RELATIVISTIC
ELECTRON BEAM WITH PLASMA

BY
KAMLESH KUMAR JAIN

A THESIS
SUBMITTED FOR THE DEGREE OF
DOCTOR OF PHILOSOPHY
OF THE

GUJARAT UNIVERSITY

MAY 1982

043



B11673

PHYSICAL RESEARCH LABORATORY
AHMEDABAD
INDIA

THE LIBRARY
PHYSICAL RESEARCH LABORATORY
NAVRANGPURA
AHMEDABAD-380 009

TO MY PARENTS

C O N T E N T S

CERTIFICATE

ACKNOWLEDGEMENTS

ABSTRACT OF THE THESIS

Chapter I	<u>INTRODUCTION</u>	1 - 24
1.1	Intense electron beam	3
1.2	Beam propagation characteristics	6
1.3	Rotating relativistic electron beam	8
1.4	Theoretical studies on rotating REB-plasma interaction	12
1.4.1	Return current process	13
1.4.2	Magnetosonic wave	19
1.5	Experiments on beam-plasma interaction	21
1.6	Scope of the thesis	23
Chapter II	<u>EXPERIMENTAL DEVICE AND DIAGNOSTICS</u>	25 - 68
2.1	Vacuum chamber	27
2.2	Magnetic field configuration	27
2.3	Gas injected washer plasma gun	31
2.4	Relativistic electron beam generator	38
2.4.1	Marx generator	42
2.4.2	Co-axial water line	45
2.4.3	High voltage holding switch	48

2.4.4	Field emission diode	48
2.4.5	Beam characteristics	50
2.5	Automatic control unit	50
2.6	Diagnostics	53
2.6.1	Time of flight mass spectrometer	53
2.6.2	Voltage divider	55
2.6.3	Rogowskii coil	58
2.6.4	Faraday cup	58
2.6.5	Electron beam probe	60
2.6.6	Magnetic probe	62
2.6.7	Diamagnetic loop	64
2.6.8.	Fast particle detector	67
2.7	Grounding and shielding	68

Chapter III GENERATION AND PROPAGATION OF

	<u>ROTATING REB</u>	69 - 98
3.1	Introduction	69
3.2	Experimental set-up	73
3.3	Experimental results	76
3.3.1	Passage of REB through cusp magnetic field	76
3.3.2	Enhancement of cusp transmission in vacuum	81
3.3.3	Rotating electron beam propagation	83

3.4	Discussion	91
3.4.1	REB rotation	91
3.4.2	Cusp transmission enhancement	94
3.4.3	Propagation characteristics	97

Chapter IV	<u>MAGNETIC RESPONSE OF THE PLASMA</u>	99 - 147
------------	--	----------

4.1	Experimental set-up	100
4.2	Experimental results	103
4.2.1	Net axial currents	103
4.2.2	Net azimuthal currents	105
4.2.3	Induced axial magnetic field	113
4.2.4	Trapped return current layer	113
4.2.5	Scaling laws for azimuthal return current decay	122
4.3	Numerical studies on the magnetic response of the plasma	128
4.3.1	Numerical results	130
4.3.2	Comparison with experi- mental results	137
4.4	Discussions	140
4.4.1	Return currents	140
4.4.2	Absence of gross plasma Oscillation	143

4.4.3 Decoupling and shrinking
of return current layer 144

4.4.4 Decay characteristics 145

Chapter V CONCLUSION 148 - 154

5.1 Scope for future research 151

REFERENCES 155 - 160

C E R T I F I C A T E

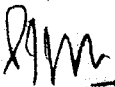
I hereby declare that the work presented in this thesis is original and has not formed the basis for the award of any degree or diploma by any University or Institution.

Kamlesh Kumar Jain

KAMLESH KUMAR JAIN

(AUTHOR)

Certified by:



P. I. JOHN

Professor-in-charge

A C K N O W L E D G E M E N T S

I wish to express my deep sense of gratitude and appreciation for the expert guidance, constant encouragement and keen interest shown by my thesis adviser, Professor P.I. John throughout this investigation. I consider it a privilege to have been associated with him in carrying out the thesis work. I am grateful to him.

It is a pleasure to acknowledge the advice and helpful discussions with Professor Y.C. Saxena and Dr. S.K. Mattoo. My sincere thanks **are** due to Dr. A.M. Punithavelu for his help, especially during the initial stages of the experiment and for his frank comments and suggestions. I wish to thank Professors P.K. Kaw, A. Sen and A.K. Sundaram for the discussions that proved to be very valuable in this work.

I owe immensely to my colleagues Sekar, Venkat and Dhiraj for their co-operation and the lively discussions I had with them. Their friendly help and nice company made my period of the thesis work a pleasant one.

My thanks are due to Mr. Pathak who was always available to render me assistance. I express my sincere thanks to Messrs. Lali, Pujara, Bhatt, Suthar, Shaikh and Vinchi for their technical assistance at various phases of the experiment.

A thank you goes out to Ashok, Ambastha, Avinash, Chitra, Gopa, Goswami, Harish, Hussain, Kar, KK, Manab, Mohan, Nautiyal, Patro, Pawar, Pankaj, Rajesh, Rhama, Rao, Sahu, Syamlal and Neeraj for the friendly atmosphere provided by them. Special thanks are due to Chandra for his great help through reprints and good humour. Thanks are due to Velu for the critical perusal of the manuscript and to Sekar and Anand for their help in proof-reading.

I would like to express my gratefulness to the personnel of the Library, Workshop, Drafting and Photography sections for their co-operation and help during the course of the work. Thanks are extended to Mr. Ravindran Nair for typing this thesis with his fantastic speed and to Mr. Murlidhar for the neat cyclostyling.

Finally, I am indebted to my wife, Hema (who for a while suspected that this work would 'go on forever'), for her patience and understanding.

ABSTRACT OF THE THESIS

The work presented in this thesis is on an experimental study on the interaction of a rotating relativistic electron beam with the plasma. Specifically two aspects, rotating electron beam propagation characteristics and magnetic response of the plasma to the beam are investigated in detail.

Experimental studies on the passage of the electron beam through the nonadiabatic cusp have shown that only 8% of the electron beam particles are able to cross the cusp in vacuum. A technique for improving the transmission of the intense electron beam through a cusp magnetic field in vacuum using dielectric drift tubes has been demonstrated. The plasma produced by the material of the dielectric tube increases the

transmission efficiency by a factor of four over vacuum values. The study of the rotating electron beam propagation shows that in the presence of the plasma density 10^{11} - 10^{13} cm⁻³, the rotating beam propagates to distances more than 150.0 cm. While traversing through the plasma, the rotating beam loses a significant fraction of its axial energy and thereafter piles up at the end of the electrical termination.

The response of the plasma to the rotating electron beam is found to be of magnetic diffusion type over a plasma density range 10^{11} - 10^{13} cm⁻³. Excitation of the axial and azimuthal return currents by the rotating beam are observed. An attempt has been made to identify the physical mechanism responsible for the generation of the azimuthal return current. This azimuthal return current leads to a reduction of the external magnetic field by 45% at the axis. It is found that the main contribution to the diamagnetic loop signal is from the diamagnetic effect of the azimuthal return current and not from plasma heating, as was attributed to, in the earlier experiments. Trapping of the azimuthal return current layer in the magnetic mirror region is observed and it has been shown that the

magnetic mirror field plays an important role in the formation of the trapped return current layer. The observed decay of the azimuthal return current cannot be explained by either classical process or by the expected turbulent processes. Numerical results on the magnetic response of the plasma to the beam are presented to facilitate comparison with the experimental results.

CHAPTER I

INTRODUCTION

In recent years, plasma physics research has been aimed at the ultimate goal of controlled fusion energy release. This requires heating of plasma to high temperature and confinement for periods long enough to satisfy Lawson criteria. Confinement of the plasma is desired to ensure that there are enough collisions for the fusion reaction to proceed efficiently and the heating is essential to accelerate the nuclei to velocities sufficient to overcome their mutual electrical repulsion, when they encounter each other. Presently plasma confinement schemes can be broadly divided into two classes. In the first class, magnetic field confines a plasma by

controlling its individual charged particle. Magnetic mirror and toroidal devices are well known examples of this class. In another approach known as inertial confinement, plasma particles are restrained by their own inertia from flying apart.

As in the case of confinement, different heating methods are also being pursued to raise the plasma temperature. For low density plasmas, one of the earliest methods suggested for achieving the necessary temperature was to pass large electric currents through plasma. This method is inefficient at high temperatures due to the small resistivity of the hot plasma. Neutral beams and RF waves are used for the auxiliary heating of Tokamaks plasma and have shown encouraging results. These techniques are considered for heating of the plasma in some of the major Tokamak devices in future. Lasers, as a possible source of energy for heating the plasma also received some attention. The enthusiasm with laser driven plasma heating has waned recently, primarily because of the nonavailability of lasers with adequate energies. One of the recent attractive candidates for the plasma heating is the relativistic electron beam (REB) which is already available in the megajoule energy range. The intense relativistic electron beams offer great promise as an excellent tool for depositing

large amounts of energy into the plasma.

1.1 INTENSE ELECTRON BEAM

Recent technological advances have placed at our disposal intense relativistic electron beam devices capable of delivering megajoule energy in submicrosecond time scales. At present there are generators capable of producing electron beams of energy up to 5 MeV with currents in mega-Amperes range and pulse duration of the order of 100 nanoseconds (Bernstein and Smith, 1971). In addition to the development of high power beam generators, there have been intensive efforts to exploit the unique attributes of these beams. In early stages, such beams were used for flash X-ray production and material studies (Oswald et al, 1966). More recently, the electron beams are being used to excite high pressure gases (Bagratashoili et al, 1973), for high power microwave generation (Nation, 1970) and collective ion acceleration (Graybill and Uglum, 1970).

The idea of using intense relativistic electron beams for fusion oriented research came in the early 1960's. The REB fusion schemes are divided into two classes. Firstly, these beams can be used for pellet fusion - a submillimeter size solid pellet surrounded by shells of heavy material can be compressed to 10^3 - 10^4 times normal solid state density and at the same time heated to fusion

temperatures by irradiation with powerful electron beams. The beams deposit their energy through classical processes. According to a calculation by Rudakov and Samarsky (1973), focusing a 1.0 Mega Joule beam of 1.0 MeV in 10 nanoseconds on a pellet, few mm in diameter, should produce a significant release of thermonuclear energy. The most essential requirement of the beam-pellet fusion scheme is that, the beam should be focused to the size of the pellet with current density reaching a value of 10^8 - 10^9 Amps/cm². Current densities of over 10^6 A/cm² have already been achieved (Yonas et al, 1974) by focusing the beam within the diode. The compression of the deuterium - tritium pellet has not yet been tested, however, theoretical calculations indicate compressions of a few hundred times the solid state densities.

Another potential approach of REB being applied to fusion is the direct electron beam heating of a high density plasma. To date, a number of experimental (Altyntsev et al, 1971, Kapetanacos and Hammer 1973, Ekdahl et al, 1974 and Wharton 1977) and theoretical (Hammer & Rostoker 1970, Lee and Sudan 1971, Lovelace and Sudan 1971, Chu and Rostoker 1973, Thode and Sudan 1975, Thode 1976) studies have been made in order to study the feasibility of using relativistic electron beams for heating plasma to thermonuclear temperatures.

An understanding of the beam-plasma interaction is also significant in space research. Phenomena are often observed in space where high intensity electron beams play an important role in the presence of a background plasma, resulting in type III and type IV bursts in solar flares (Wild and Swerd, 1972) and VLF emissions in the magnetosphere.

The classical binary collisional interaction of the beam electrons with plasma particles is very weak due to the high energy of the beam and as a result the collisional stopping power of a plasma to an REB is in Kilometers. Therefore, it is only collective interactions which can result in an efficient plasma heating. Theoretically there are two well known collective interaction mechanisms which results in an anomalous plasma heating, namely, two stream instability (Fainberg et al. 1970, Toepfer and Poukey 1973, Ferch and Sudan 1975, Papadopoulos 1975) and return current heating (Cox and Bennet 1970, Hammer and Rostoker 1970, Lee and Sudan 1971). The electron - electron two stream instability is driven by the relative drift between the beam and the plasma electrons. Linear, quasilinear and wave-wave scattering models have been proposed for energy transfer and each of these interactions has its own interaction length. In the return current heating mechanism, drifting plasma electrons

excite the ion acoustic instability, resulting in a large effective collision frequency. On account of this, plasma resistivity is enhanced, so that a large amount of the beam energy is dissipated into the plasma. A complete account of these theoretical studies is available in the review by Breizman and Ryutov (1974). In several beam injection experiments, reported so far, plasma heating amounting to 10-20% transfer of the beam energy has been observed under various conditions. These high rates of energy deposition in the plasma imply that collective mechanisms are responsible for the energy transfer.

1.2 BEAM PROPAGATION CHARACTERISTICS

The propagation of a relativistic electron beam is strongly influenced by the self fields of the beam electrons. An unneutralised 10 Kamps relativistic electron beam with a radius of 2.0 cm generates on its surface, electric fields of over 1 MV/cm. Thus, when an electron beam is injected into a vacuum chamber, the Coulomb repulsion quickly blows it apart in the radial direction. The dispersive force of this radial electric field is reduced by a factor of $1/\gamma^2$ (γ is the relativistic mass factor) due to presence of self magnetic fields. Still, the electrostatic repulsive force due to the space charge effects exceeds the pinching force due to the self magnetic fields and hence such a beam

simply diverges in vacuum. The space charge electrostatic force can be nullified by injecting the beam into a neutralising medium such as a neutral gas or plasma.

Even after an electron beam is space charge neutralised, the current carried by a propagating beam is limited due to the following reasons.

When the beam current is small the particle trajectories under the action of the self magnetic fields remains sinusoidal. As the current increases, the particle gains transverse velocity and when the current is increased above a certain critical value, known as "Alfven critical current" (Alfven, 1939), the self magnetic fields of the beam push the beam particles back to the cathode, where the beam was produced. The value of the Alfven's critical current is obtained by the consideration that a particle's Larmor orbit in the maximum field of the beam should be equal to the beam radius,

$$I_A = 17000 \beta \gamma \quad \text{Amperes} \quad \dots\dots\dots (1.1)$$

Where

$$\beta = v/c$$

$$\gamma = \sqrt{1 - \beta^2}$$

v is the beam velocity

However, there are a number of techniques to overcome the above mentioned limitation on the current.

If the beam is hollowed out, the limitation on the current will arise only when particles can execute a Larmor orbit within the thickness of the hollow beam. Thus, by making the beam hollow we have higher limiting currents. Another way to achieve arbitrarily high currents is by injecting the beam into a plasma medium, the net current density is thus reduced and so also the self field of the beam, facilitating larger beam currents (Lawson 1959, 1977). The beam currents can be increased beyond the critical value if an external magnetic field B_z , much stronger than the self magnetic field B_0 is applied. Under this condition, the electron drifts predominantly in the z direction and so the beam is "forced" to propagate even though the beam current is more than critical value.

1.3 ROTATING RELATIVISTIC ELECTRON BEAM

As mentioned in the earlier section, a laminar relativistic electron beam can deposit a significant part of its energy into plasma as a result of several collective interactions between the beam and plasma particles. The experimental results have shown that optimum energy thus, transferred from the beam to the plasma, takes place at $n_p = n_b$ (where n_p is the plasma density and n_b is the beam density). At a plasma density much higher than the beam density, the energy coupling efficiency falls

drastically. This result indicates that the laminar electron beams are not well suited for heating even a moderate density plasma. Keeping these factors in view, Chu and Rostoker (1974) suggested a new scheme which is characterised by a relatively high coupling efficiency at $n_p \gg n_b$. The method suggested was to use a rotating electron beam in place of the laminar beam. By a rotating beam, it is meant that each beam electron, in addition to its axial velocity, is gyrating about the beam axis under the influence of an externally applied axial magnetic field. The rotating electron beam itself is obtained by either injecting the laminar beam at nearly right angles to the field lines of a uniform magnetic field or by passing a non-rotational hollow beam through an axially symmetric nonadiabatic cusp magnetic field.

The rotating relativistic electron beam has number of other advantages over the laminar beam. A rotating electron beam is capable of creating a reversed magnetic field configuration (figure 1.1) and a plasma confined in such a configuration of fields is stable against one of the most destructive perturbations i.e. MHD instabilities. This field reversal configuration with closed field lines exhibits favourable confinement properties for high β plasmas. As far as plasma heating is concerned, rotating

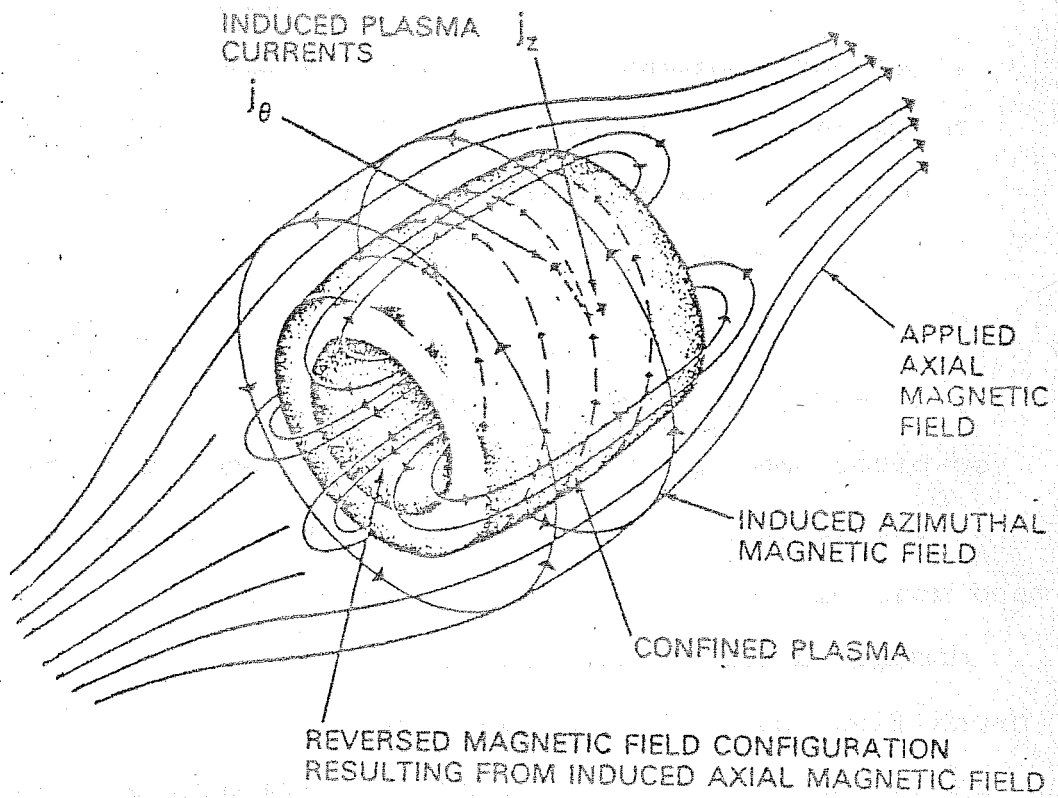


Figure 1.1 Rotating relativistic electron beam produced reversed magnetic field configuration.

beams can transfer their energy to the plasma not only through excitation of microturbulence, but also via other mechanisms such as electrostatic acceleration of ions by the equilibrium electric field, excitation of magnetosonic waves and also joule heating. According to the calculations of Chu and Rostoker, the stopping power of the plasma is enhanced for a rotating beam by a factor $2 (c/v_{||})^3$, where $v_{||}$ is beam's axial velocity.

Historically, in 1958 Christofilos (1958) suggested that stable confinement of a fusion plasma could be achieved by producing field reversal configuration. It was proposed to use a rotating relativistic electron beam trapped in a magnetic mirror thus producing a minimum B configuration. This suggestion lead to the well known "ASTRON" experiments. In these experiments, the primary aim was to trap a rotating beam in the magnetic mirror to form an E layer, which in turn would produce field reversal. A 200 nanosecond long, 600 Amps, 6 MeV beam was injected into a magnetic well. It was found that the electrons do not get trapped as should have been expected from the adiabatic theory. To improve the trapping efficiency, resistive rings were introduced in the drift region so as to dissipate some of the axial energy of the beam and thus, increase the probability of

trapping the beam. Although a trapping efficiency of 60% was achieved, field reversal to the extent of only 40% were obtained. To improve this further, stacking of a series of beam pulses were tried out; but this also did not produce the desired results and the whole Astron programme was terminated in 1973.

The availability of high power electron beam generators has made it possible to produce field reversal in a single pulse (Andrew et al, 1971). The induced plasma currents, that result from the interaction of a rotating electron beam with a plasma, are capable of creating the field reversal configuration. Reverse fields created by the induced plasma currents have been observed when a rotating electron beam is injected into an initially neutral gas (Kapetanakis et al, 1975). Field reversal configuration even in the absence of external magnetic field has been observed recently (Sethian, 1978).

1.4 THEORETICAL STUDIES ON ROTATING REB-PLASMA INTERACTION

Most of the theoretical works on rotating relativistic electron beam-plasma interaction deal with macroscopic collective process. The macroscopic mechanism essentially include effects which are unique to intense rotating electron beam. The rotating beam induced return current processes are studied in detail

to determine beam-plasma coupling efficiency. The electron beam rotating across field lines exerts a large transverse pressure against the confining field, which can result in radial oscillations in the plasma. Theoretical studies related to this oscillatory magnetosonic mode, both in linear and nonlinear regimes have been carried out extensively.

1.4.1 Return Current Process

Recently several papers have been devoted to the study of rotating beam induced counter currents and their effects on the beam itself. The common conclusion arrived at by these authors (Chu and Rostoker 1974, Molvig and Rostoker 1977 a) is that under certain conditions both axial and angular return currents are excited by the rotating beam and they are equal in magnitude to the beam currents. It has been shown that these return currents serve as efficient channels through which the beam can strongly interact with the plasma. The physical mechanism for the return current generation can be understood from the following:

As the rotating electron beam enters the plasma, time varying magnetic fields associated with its front induces an electric field with components $E_z = -\frac{1}{c} \frac{\partial A_z}{\partial t}$ and $E_\theta = -\frac{1}{c} \frac{\partial A_\theta}{\partial t}$. The azimuthal electric field E_θ produces a plasma electron drift $V_r = c E_\theta / B_z$, where

B_z is external magnetic field, which results in a charge separation and hence a radial electric field.

The radial electric field E_r produces a plasma electron drift $V_\theta = c E_r / B_z$ as shown in figure 1.2. The corresponding angular plasma current $j_{\theta p} = -n_p e V_\theta$, thus generated, neutralises the original beam current $j_{\theta b} = n_b e V_\perp$.

But in cases when plasma ions are magnetised, the angular return current is of mainly resistive type and is generated by the electric field E_θ i.e. $j_{\theta p} = \sigma E_\theta$ where σ is plasma conductivity. The conventional axial return current is developed essentially by the axial electric field E_z as $J_z = \sigma E_z$.

The first theoretical model on the return current response of the plasma to the rotating electron beam was given by Chu and Rostoker (1974). Interaction of the hollow rotating relativistic electron beam front with a dense plasma ($n_p \gg n_b$) is studied. The model is based on the assumptions that the plasma electrons are magnetised while ions are not and the annular beam thickness is large compared to the plasma skin depth. It is found that on injection of the rotating beam into the plasma, the system becomes slightly over charge neutralised. The excess positive charge inside the beam thickness produces a radial electric field that drives the azimuthal return current, similar to the axial return

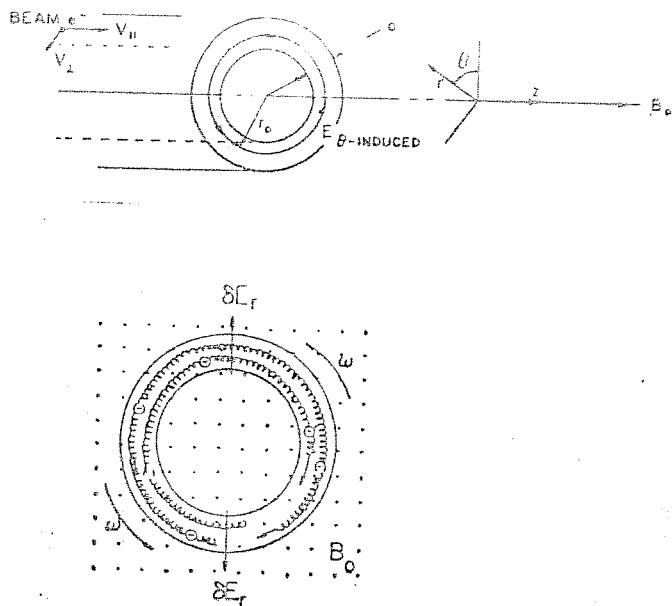


Figure 1.2 Drift motion of plasma electrons due to radial electric field.

current in the straight beam case. The radial electric field sustaining the angular return current also electrostatically accelerates the ions. Thus, arises the major difference, ion heating is due to ion sound turbulence in the case of laminar beam injection while in case of rotating beam, the ions are electrostatically heated.

Chu and Rostoker's magnetic diffusion model has predicted decay lengths for the return currents. The two decay lengths obtained are:

$$l_{||} = \frac{a^2 + \lambda^2}{\lambda^2} \frac{v_o}{v_e} \dots\dots\dots (1.2)$$

for axial return current

and

$$l_{\perp} = \frac{a^2 + \lambda^2}{\lambda^2 \left(1 + \frac{\omega_e \omega_i}{v_e v_i}\right)} \frac{v_o}{v_e} \dots\dots\dots (1.3)$$

for angular return current

Where

a is the beam radius

λ is the plasma skin depth

v_o is the initial beam velocity

v_e is the electron collision frequency

v_i is the ion collision frequency

ω_e is the electron cyclotron frequency

ω_i is the ion cyclotron frequency.

The time decay of axial return current results

from collisional damping of the electron current alone, as does the first term in the expression for the angular return current. The second term in the case of angular return current is due to radial flow of ions under the influence of electric field E_r . The ion flow neutralises the radial electric field, necessary to sustain J_{θ} leading to the decay of the angular return current.

Further work (Molvig and Rostoker, 1977 a) on this subject was more or less an extension of the Chu and Rostoker model. In Molvig's treatment, classical form of friction term is used in the fluid equation for determining the plasma response, in contrast to Langevin form. However, it is found that the response of the plasma to the rotating beam is identical to the one obtained by Chu and Rostoker.

Molvig and Rostoker have also extended the model to include realistic beam profiles, beam risetimes and boundary conditions. Finite beam rise times and presence of conducting boundary affect the amplitude and the decay of the return currents. During the rise time, the initial portion of the angular return current already begins to diffuse before the beam current reaches its peak value. The return current decay competes with the rise of the beam current and limits the maximum

angular return current to less than the full neutralising value. However, there is no such rise time limitations on the axial return current. When the beam-plasma system is enclosed by a conducting wall, the net axial counter current decays. The difference between the beam current and the return current flowing in the plasma is carried by the conducting wall. Similar behaviour also holds good for the angular return current.

The axial force experienced by the rotating beam due to return current decay has been determined from the magnetic diffusion model. The calculated stopping length for the rotating beam is

$$l_s = \frac{1}{2} \frac{n_p}{n_b} \left(\frac{v_{||}}{c} \right)^3 \frac{\gamma c}{\nu_e} \quad \dots (1.4)$$

Where

n_p is the plasma density

n_b is the beam density

$v_{||}$ is the beam axial velocity

γ is the relativistic mass factor

ν_e is the electron collision frequency.

The stopping length is smaller by a factor $2 (c/v_{||})^3$ over that for a non-rotating beam. Hence, even if a plasma is transparent to straight beam, it can stop a rotating beam. According to the model, the beam energy lost is shared among electrons, ions and the magnetic field.

An apparently different return current model was given by Berk and Pearlstein (1976) for long pulse electron beams. The model has predicted that only for beam rise times short compared with the Alfvén time L/V_A (L is radius of conducting boundary and V_A is Alfvén velocity), angular return current will completely cancel the beam current. In case of longer rise times, return current will oscillate with much smaller amplitude. Further, axial return current neutralisation will take place only if the beam pulse is smaller than magnetic diffusion time.

1.4.2 Magnetosonic Wave

The radial gross oscillations of the plasma identified as magnetosonic mode have been observed in the rotating electron beam-plasma interaction. As the angular beam current $j_{b\theta}$ builds up, a radial electric field E_r is established in the beam annular section, which drives a drift plasma angular return current $j_{p\theta}$ and simultaneously excites a magnetosonic wave with wavelength ' $2a$ ' and frequency $\pi V_A/a$ (where ' a ' is the beam radius and V_A is Alfvén speed). During the first half cycle of the mode, the plasma ions and electrons are driven radially outward by E_r and $j_{p\theta} \times B_z$ force respectively. The "Frozen in." field lines also

move radially with the plasma, resulting in a diamagnetic field configuration inside the beam cross-section and paramagnetic outside. Simultaneously, the energy density decreases at a rate $\delta_{b0} E_0$. During the second half cycle, E_0 reverses its sign and so the beam regains part of the energy, lost during the first half cycle.

A nonturbulent model valid in linear regime was given by Chu et al (1975) to explain the experimentally observed magnetosonic oscillations (Kapetanakis et al., 1973). Main features of the proposed model are that it does not resort to collisions or instabilities and operates mainly in dense plasmas. It has been found from the model that the rotating electron beam pulse rapidly transfers energy to the ions of the plasma through excitation of the magnetosonic mode. The beam energy transfer efficiency scales linearly with the beam axial density rather than the beam volume density.

Further studies on the magnetosonic mode which includes nonlinear effects were carried out by Molvig and Rostoker (1977 b). When $\Delta B \ll B_0$ (where ΔB is the wave field and B_0 is the external magnetic field), dissipation balances the nonlinearity to produce a

shock type flow resembling that of the linear theory. The only nonlinear modification is an increase of the magnetosonic wave speed to $V_s \approx V_A M_s$ where $M_s = 1 + \frac{\Delta B}{B_0}$ is the Mach number.

1.5 EXPERIMENTS ON BEAM-PLASMA INTERACTION

The availability of the intense electron beam generator soon resulted in experimental studies related to straight beam - plasma interaction. Several beam injection experiments (Korn et al. 1973, Miller 1975, Goldenbaum et al. 1974) at various laboratories were performed with an aim to determine energy coupling efficiency and identify the interaction mechanism. Plasma heating amounting to 10-20% of the beam energy has been observed under various experimental conditions. The observed energy deposition is greater than as explained by classical process.. The rate of energy deposition in the plasma from the beam agree with the calculations, which take into account collective processes such as two-stream or return current instabilities.

The first experiment on rotating beam-plasma interaction was performed by Kapetanakis et al. (1973) essentially to study the dependence of energy transfer on the plasma density. A 500 KeV, 20-40 KA electron

beam was injected into a preformed plasma confined by a uniform magnetic field. The optimum energy transfer occurred at the plasma density ($\approx 10^{14} \text{ cm}^{-3}$) which was two orders of magnitude greater than the beam density ($5 \times 10^{11} \text{ cm}^{-3}$). A remarkable result obtained was that the plasma undergoes radial oscillations, characterised as magnetosonic modes. Ion heating was indicated although no attempt was made in this experiment to measure the ion temperature.

The rotating relativistic electron beam-plasma interaction through magnetic perturbations and radial oscillations was studied in another experiment (Roberson 1978). The experimental system was similar to the one described above. Field reversal configuration created by the induced plasma currents was also observed at $3 \times 10^{13} \text{ cm}^{-3}$ plasma density. Another significant result of this experiment was that the beam propagation and braking depend upon the background plasma density. An attempt was made to compare the braking of the beam with existing theoretical models and magnetic perturbations with numerical calculations. From these calculations, inferred plasma conductivity ($\sim 5 \times 10^{11} \text{ sec}^{-1}$) was found to be proportional to the density. The origin of this anomalous conductivity has not been determined.

1.6 SCOPE OF THE THESIS

From the experiments, reviewed above, we notice that the experimental studies on interaction of a rotating REB with plasma has received scant attention so far. Although coupling between the rotating electron beam and the plasma through magnetic perturbation has been established, many phenomena related to the interaction mechanism are far from understood.

The diamagnetism registered was attributed only to the plasma heating and the magnetic field due to the angular return current was completely ignored in all the earlier experiments; whereas the present work aims to study the proportion in which the beam energy is shared between the plasma and the induced magnetic field. In the present experiment we also study the spatial and temporal evolution of the angular return current, which is of great importance while determining the resultant magnetic field configuration. The effect of the external mirror magnetic field on the behaviour of the return current is also a subject matter of the present investigation. An important problem in such an interaction, is related to the decay of the return current. This experiment addresses itself to the question of the return current decay under various experimental condit-

ions. The propagation of the REB in vacuum as well as plasma filled non-adiabatic cusp magnetic field has also been studied extensively.

The experimental device, its operating characteristics, automatic control unit and various diagnostics elements used in the course of the investigation are described in chapter II. The performance of a modified version of the washer type plasma gun, in which gas is injected externally is reported.

Results on the study of rotating electron beam propagation in vacuum and plasma and a discussion are presented in Chapter III. A technique for improving the transmission of intense electron beam through a cusp magnetic field in vacuum by using dielectric drift tubes has been demonstrated.

In Chapter IV, the magnetic response of the plasma to the rotating relativistic electron beam is studied and discussed. Observational evidence for the generation and trapping of a return current layer in the magnetic mirror is presented. This chapter also includes the numerical results on the response of the plasma to the rotating electron beam. The main results of the thesis work are briefly summarised in the last chapter.

CHAPTER II

EXPERIMENTAL DEVICE AND DIAGNOSTICS

A schematic of the experimental device, designed and set up to study the interaction of the intense rotating relativistic electron beam with the mirror trapped plasma is shown in figure 2.1. It consists of a vacuum chamber, system of magnetic field coils, plasma gun and a relativistic electron beam generator. A number of diagnostics have been deployed at various places for measuring the desired experimental parameters. For sequential operation of the various events in the experiment, an automatic control unit has been developed. The details of the experimental device and diagnostics are described in the following sections.

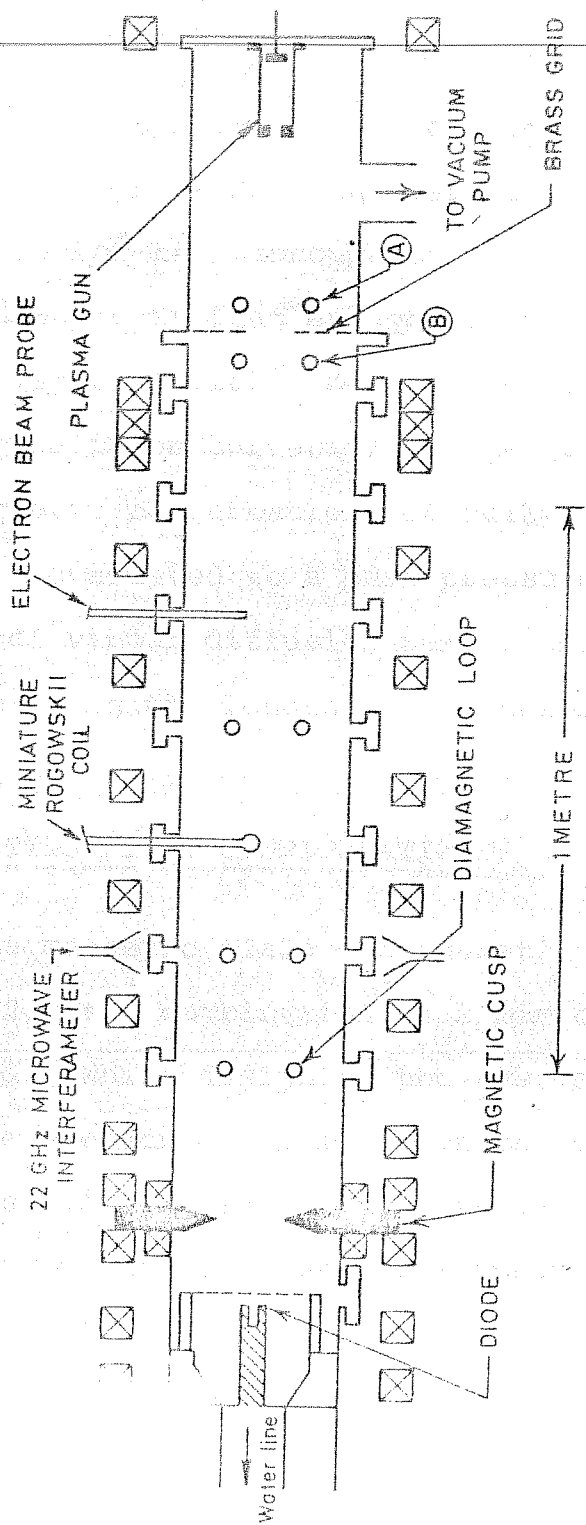


Figure 2.1 A schematic of the experimental set-up.

2.1 VACUUM CHAMBER

The chamber is a 30 cm diameter, 2.3 meter long and 3 mm wall thickness stainless steel tube. The magnetic diffusion time through the walls corresponds to $50 \mu \text{ sec}$ which is fast enough for the penetration of external magnetic field, but long enough for the resistive decay of the image currents, so that the flux displaced by diamagnetic perturbations is fully conserved. The chamber is evacuated to a base pressure of 10^{-5} Torr with the help of vapour diffusion pumps. Nineteen ports are available along the length of the chamber for diagnostics purposes.

2.2 MAGNETIC FIELD CONFIGURATION

The magnetic field configuration, shown in figure 2.2, is a combination of a mirror and a nonadiabatic cusp field. While designing the system of magnetic field coils, the procedure was based on the minimisation of a weighted sum of the squared deviations from the desired field profile and the power dissipated in the coils for a given coil configuration. Details about this procedure is reported in a separate note (Saxena et al, 1979).

MIRROR CUM CUSP MAGNETIC FIELD CONFIGURATION

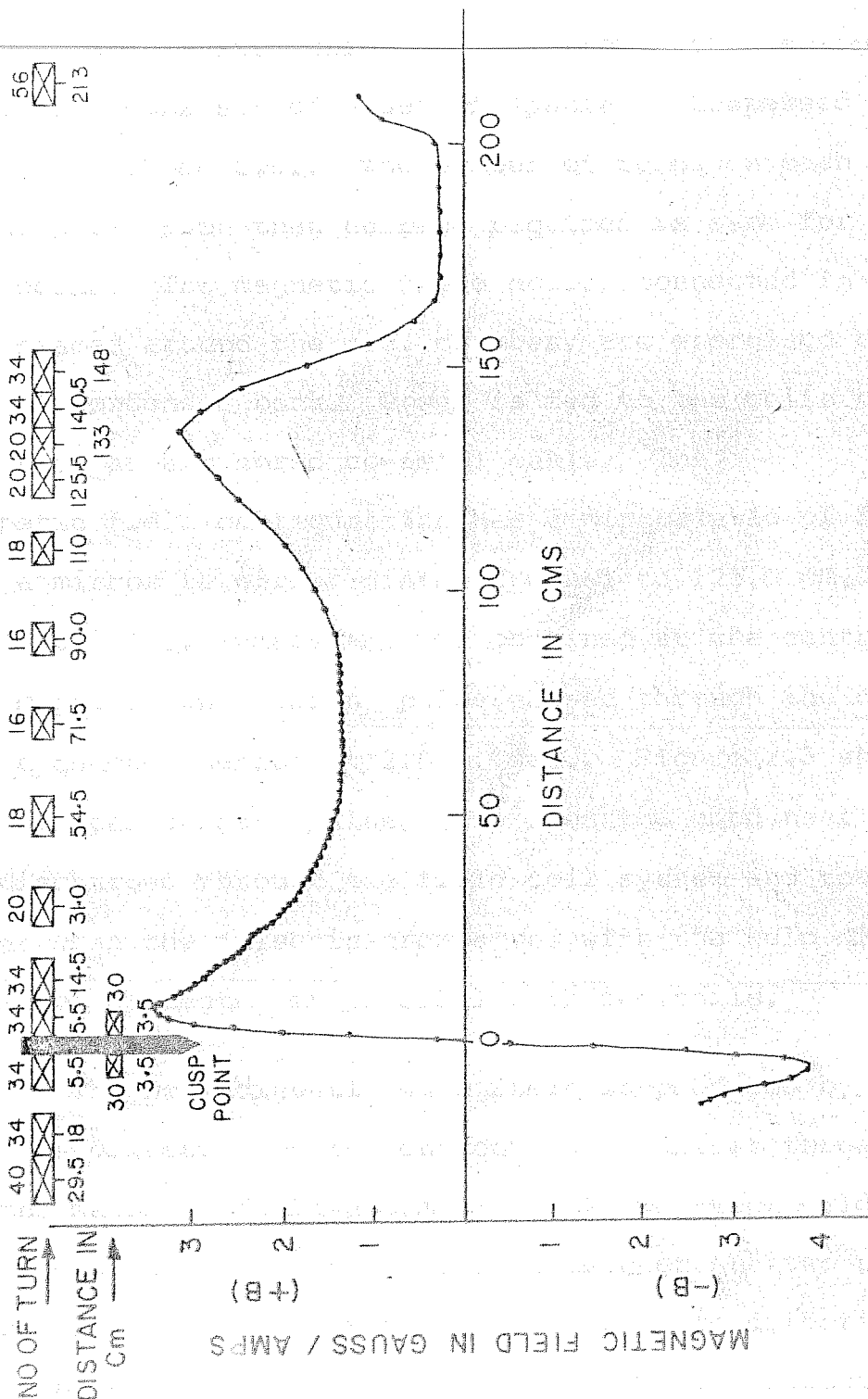


Figure 2.2 Magnetic mirror cum nonadiabatic cusp field profile.

The system which evolved from such a design procedure consists of a set of spatially dispersed pancake coils of 40 cm i.d.. The number of turns in each coil is adjusted such that current required is same for all the coils. The magnetic field coils, connected in series and placed around the s.s. chamber, are energised by a 8.0 KJ condenser bank. Power is fed to the coils by means of an air cored co-axial cable. The magnetic field configuration has a mirror ratio of 2.6 and a mirror to mirror distance equal to 125.0 cm. A field of ~ 1.4 Gauss/Amp. is obtained at the centre of the mirror. The current pulse passed through the coils has a quarter period of 2.0 m. sec.. Figure 2.3 shows two typical current pulses, one when the condenser bank is discharged through the field coil system and the other when the pulse is crowbarred with the help of an ignitron connected in parallel with the coils.

The non-adiabatic cusp field is produced by reversing the direction of the current in the first three coils of the magnetic field assembly. A 25 mm thick mild steel annular plate is introduced between the two sets of coils, carrying currents in the opposite directions and also an additional set of coils is wound directly over the chamber in order to make the cusp strongly

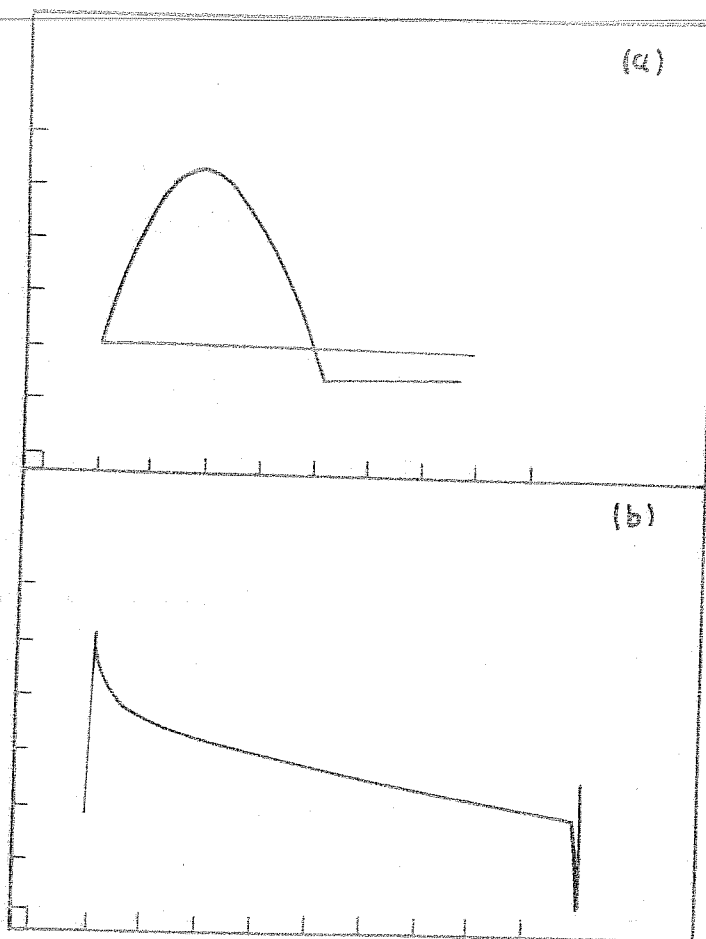


Figure 2.3 Current through magnetic field coils

- (a) without crowbar, vertical scale 100 Amp/div
horizontal scale = 1 msec/div
- (b) when the crowbar circuit is triggered
vertical scale 100 Amp/div, horizontal
scale = 5 msec/div.

non-adiabatic. The resultant transition-width of the cusp is 50 mm (FWHM). The axial profile of the magnetic field was mapped using a Gauss meter when a d.c. current was passed through the coils and with a magnetic probe in case of pulsed currents.

2.3 GAS INJECTED WASHER PLASMA GUN

A modified version of washer gun, in which gas is injected externally, is used as a plasma source. The major advantage of using the gas injected washer gun over the conventional occluded one (Coensgen et al., 1959) are:

- i. There is a control over the quantity of the neutral gas present in the gun.
- ii. The additional trigger pulse is not required for initiation of the discharge.
- iii. The gas injected gun is capable of producing plasmas other than hydrogen or deuterium.

The plasma gun, as shown in figure 2.4, consists of a number of brass and nylon washers with an i.d. 22 mm and thickness 5 mm stacked together alternately. The first washer acts as a cathode and the last washer is connected to the ground through the metallic rods.

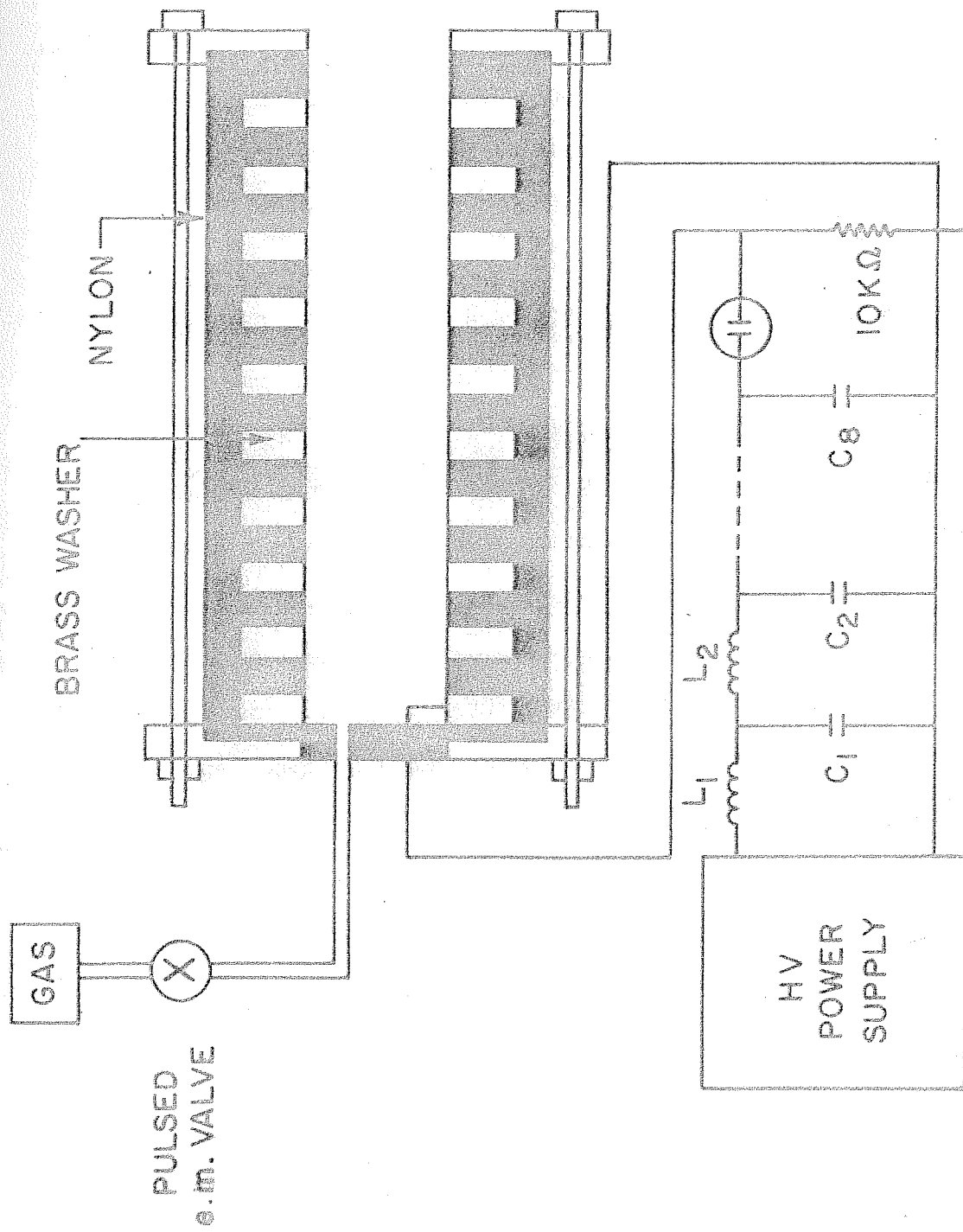


Figure 2.4 Schematic diagram of the gas injected washer

gun. $L = 2.2\mu\text{H}$ $C = 2.4\mu\text{F}$. The impedance compensating resistor is not shown in figure.

The gas to be ionised is let into a nylon plenum with the help of a slow pulsed electromagnetic valve and enters near the cathode. The electromagnetic valve consists of a light aluminium piston contained in a gas manifold sitting over an orifice with an O-ring seal. The sealing is done by the pressure difference between the manifold and the experimental chamber. A small piece of mild steel is attached to the aluminium piston. A coil surrounds the mild piece. A 80 μ F, 1.0 KV capacitor bank is fired through a thyatron to generate a magnetic field in the vicinity of the mild steel and the resultant magnetisation of the mild steel piece lifts the piston to allow the opening of the orifice and entry of the gas into the plasma gun. A typical oscillogram of the ion current in a nude ionisation gauge, kept in the experimental chamber immediately after the gun, (figure 2.5) shows the time behaviour of the gas entering the plasma gun. Detailed description of the plasma gun has been published elsewhere (Jain et al., 1980).

The gun is powered by an eight stage pulse-forming line, consisting of 5.0 μ F low inductance capacitors and 2.4 μ H inductors. A nichrome strip is used in series with the gun for proper impedance matching. The plasma discharge current pulse lasts for about 100 μ sec and for

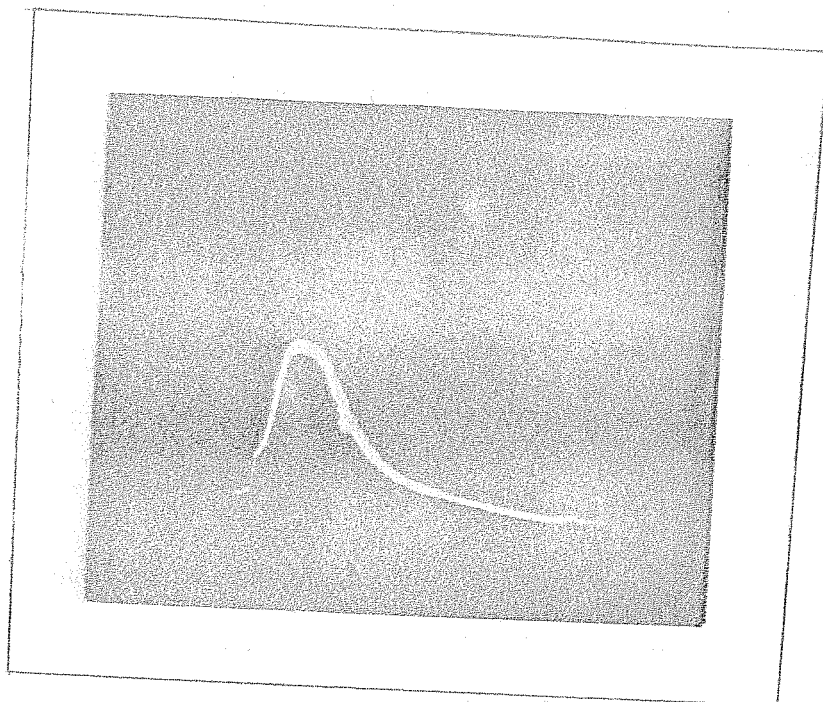


Figure 2.5 Response of a nude ionisation gauge to gas injected by the electromagnetic valve. The gas pressure in the gun peaks at around 2 ms.

an applied voltage of 10 KV, the discharge current is found to be about 3.0 KA.

The experimental study of the plasma produced by this source is done with the help of numerous diagnostics. The plasma velocity is measured by the time of flight technique using four Langmuir probes, placed along the axis of the vacuum chamber. The plasma velocity obtained for different gas species are given in Table 2.1.

The phase shift type 22 GHz₂ microwave interferometer is used to measure the plasma density. As the plasma density varies, the phase of the microwave traversing through it shifts, thus permitting a recording of the temporal density variation. The phase shift is dependent on integrated plasma density while cut-off depends on the peak plasma density. Figure 2.6 shows the recording of the plasma density as measured by the interferometer. The cut-off region corresponds to the density greater than $6 \times 10^{12} \text{ cm}^{-3}$. To obtain the plasma density beyond the cut-off region and also the radial density profile, the Langmuir probe was used. The probe was biased in the range between -100 V to +100 V. The probe current was measured with the help of a current to voltage

Table 2.1

PLASMA VELOCITIES FOR DIFFERENT SPECIES	
<u>Gas</u>	<u>Velocities (cm sec⁻¹)</u>
Hydrogen	1.2×10^6
Nitrogen	8×10^5
Argon	7×10^5

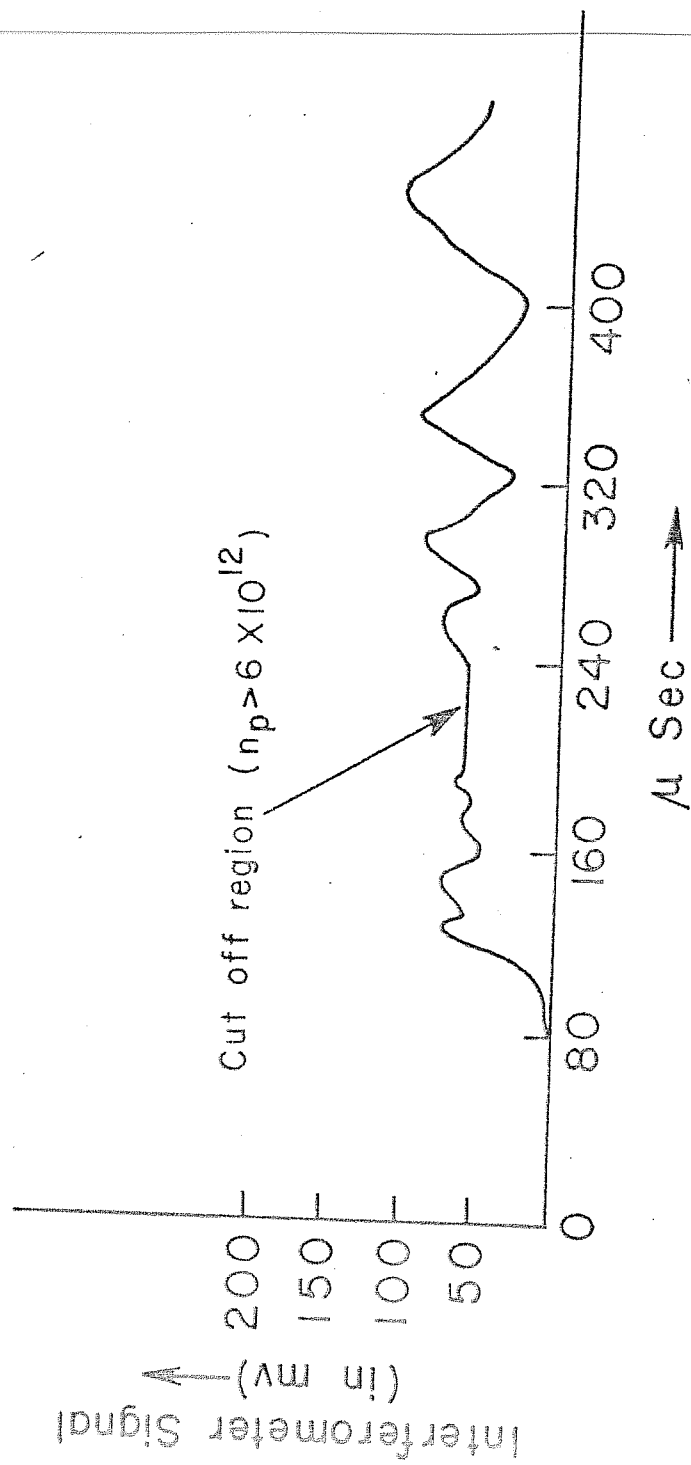


Figure 2.6 A typical signal from the 22 GHz_z microwave interferometer as a function of time.

converter. The observed absence of saturation in the electron current in the probe characteristic is probably due to the fact that the high energy ion flow does not allow the shielding effect of the probe (Segall and Koopman, 1973). Thus, the plasma density was determined from the ion saturation current. The complete temporal profile of the plasma density obtained with the help of the interferometer and the probe is shown in figure 2.7. The peak value is found to be 10^{13} cm^{-3} and is attained at 200 μ sec after the initiation of the plasma discharge at the mirror centre. The radial density profile, obtained with the help of the probe, as shown in figure 2.8, is Gaussian, with an average diameter equal to 5.0 cm.

2.4 RELATIVISTIC ELECTRON BEAM GENERATOR

The basic principle for relativistic electron beam generation is illustrated in figure 2.9. A high voltage power supply charges a Marx generator. On a trigger command, the Marx is erected by switching all the capacitors in series and thus providing the high voltage needed. Next, the stored energy is transferred in less than a microsecond to a pulse forming network that enables a time-compression of the voltage pulse. The beam generation and acceleration occur in a beam

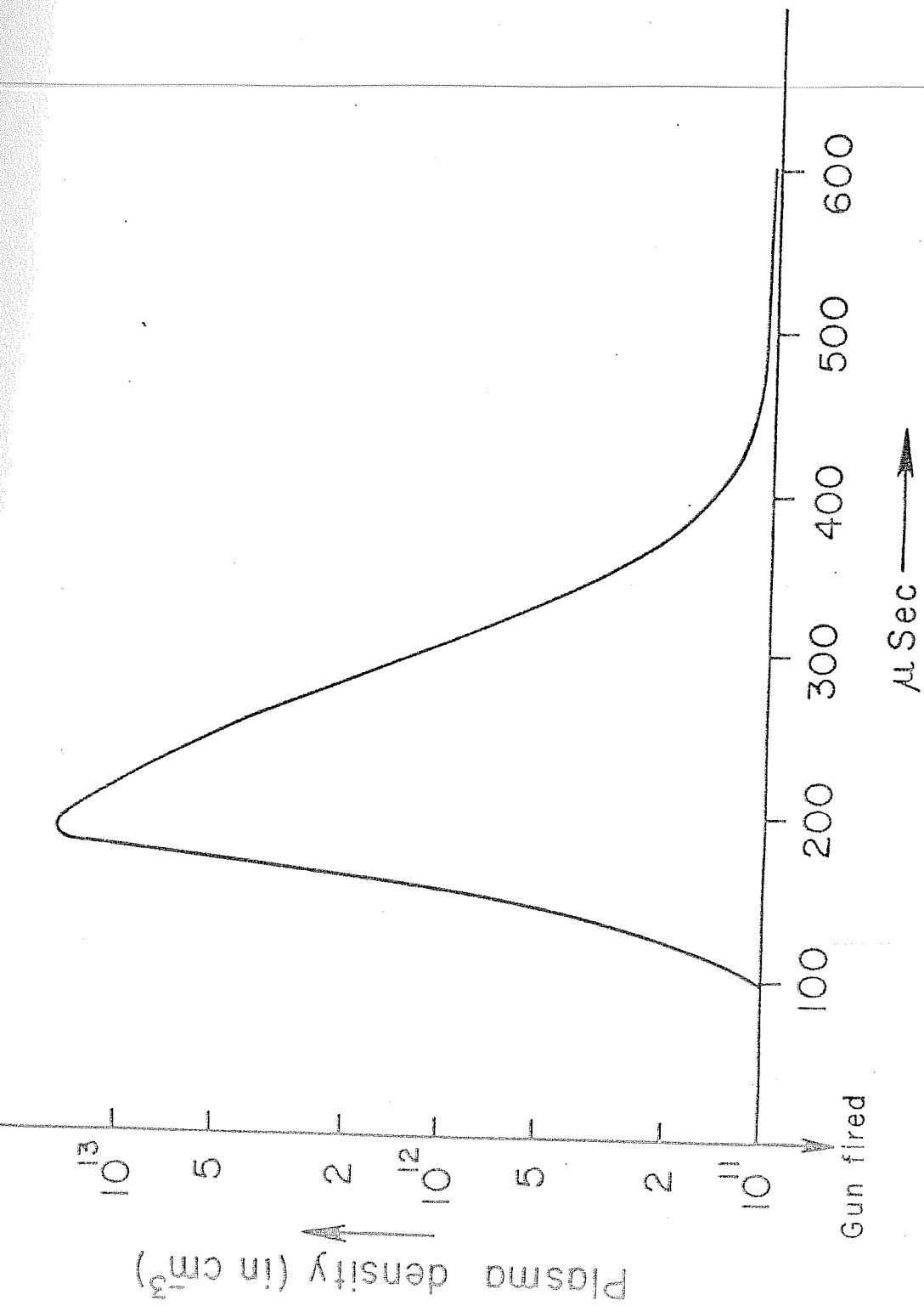


Figure 2.7 Variation of plasma density with time.

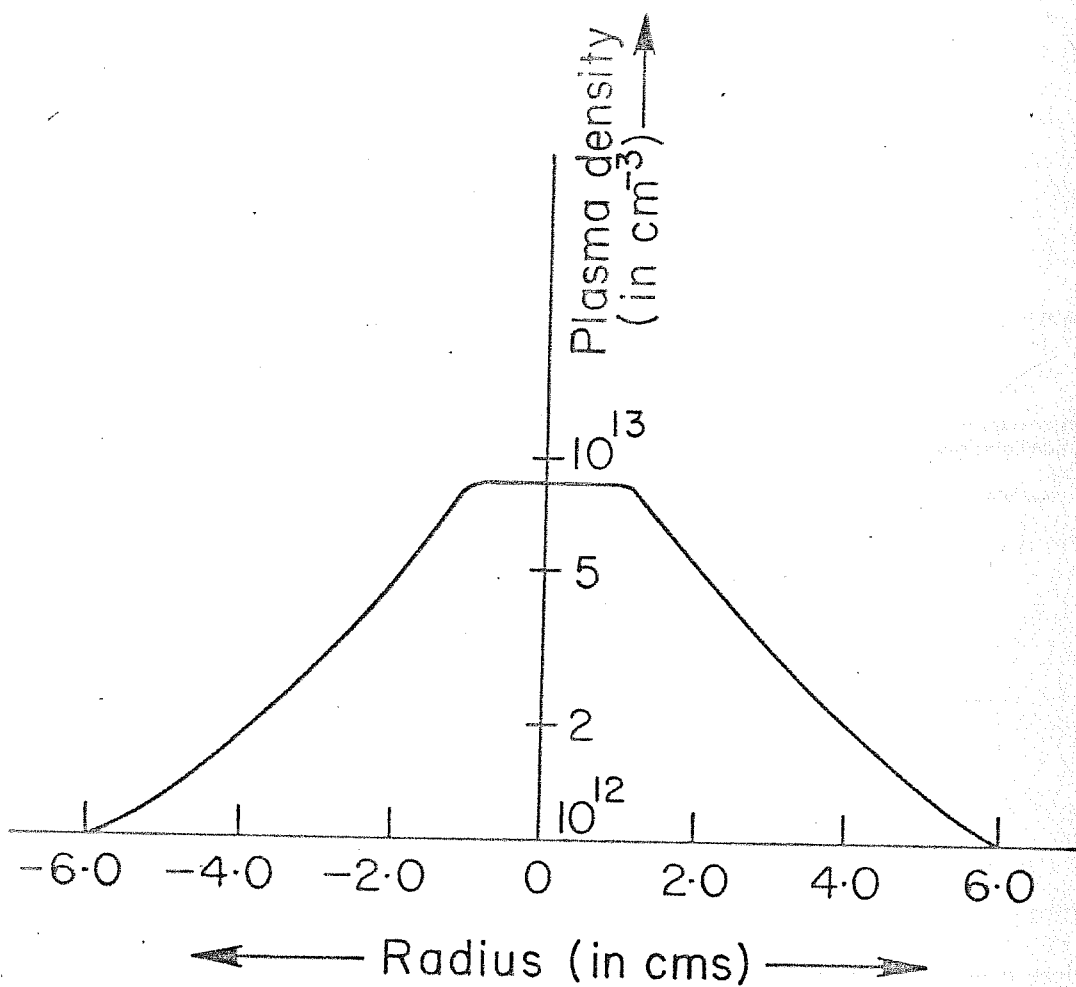


Figure 2.8 Radial distribution of the plasma density.

FUNCTIONAL DIAGRAM OF RELATIVISTIC ELECTRON BEAM GENERATOR

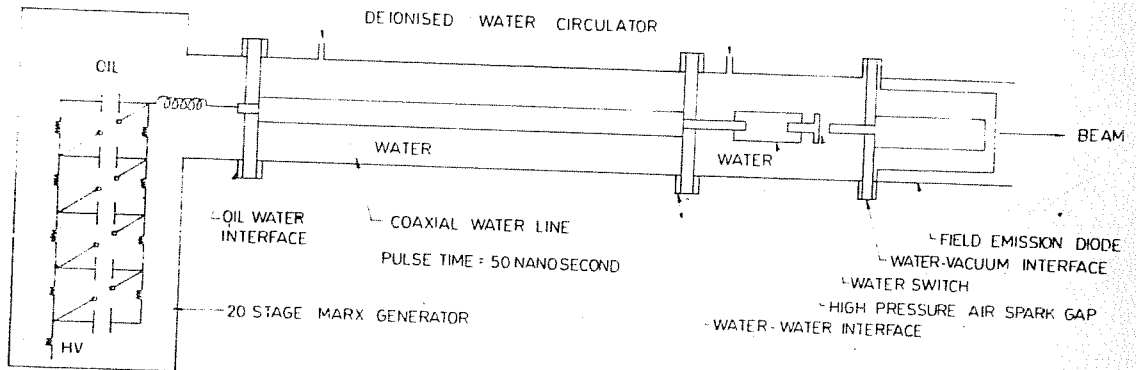


Figure 2.9 Functional diagram of the relativistic electron beam generator.

diode, which is energised by the pulse forming line. The details of the major constituents of the beam generator are described below:

2.4.1 Marx Generator

The basic principle involved is the transient series connection of a number of electrostatic energy storage modules. The capacitors are charged in parallel via the charging resistance in the high voltage leg of the circuit while the other side is connected to the ground via the ground leg resistor chain. The Marx generator is erected by triggering a series of air spark gaps. When this happens, the low impedance spark gaps effectively connect the capacitors in series. The net voltage achieved with the Marx circuit is equal to the charging voltage per stage times the number of stages.

The assembly of capacitors, the spark gap chamber and the charging resistors is immersed in transformer oil. Twenty $0.2 \mu\text{F}$, 50 KV capacitors are mounted on a cloth fibre support and two columns of copper sulphate solution with 40 Kiloohm resistance each are used as charging resistances. The capacitors in the Marx generator are charged by a variable 0-50 KV high voltage power supply, whose input voltage is varied linearly using a variable auto transformer coupled

to a low r.p.m. reversible motor. A high voltage circuit breaker driven by a motor is used to connect the high voltage power supply with the Marx. After the capacitors are charged, this motor disconnects the power supply from the Marx generator to prevent transients, generated during the Marx generator erection, from damaging the power supply.

The twenty spark gap switches, operating in high pressure air, are housed inside a common pressure sealed 1.5 meter long chamber. Each spark gap is made of brass electrodes having a diameter equal to 20 mm, while the electrode gap is 8 mm. A trigger generator in the form of a sliding spark source is used to erect the Marx generator. The source consists of two electrodes, fixed on the plane of a nylon cylinder, with their tips just projecting on the surface of nylon as shown in figure 2.10. The trigger source is mounted about 5 cm away from the first spark gap inside the chamber and is electrically isolated from the Marx generator. When a 6.0 KV pulse is applied between the electrodes, a surface discharge is developed emitting ultra-violet (UV) radiation. This UV radiation photoionises the gas in the gap region of successive gaps and is sufficient to cause switching of all the spark gaps.

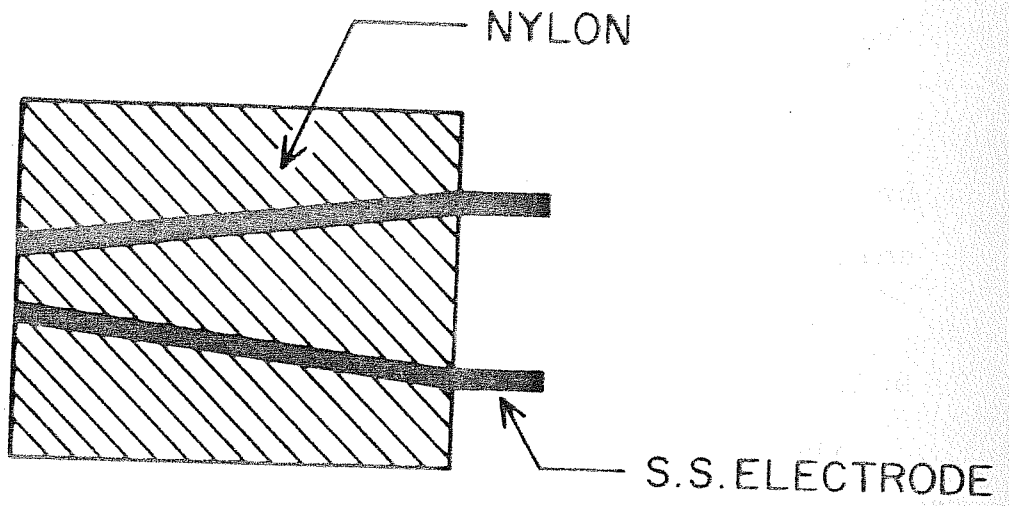


Figure 2.10 Nylon spark initiator.

It has been found that this triggering helps to get the Marx generator erected at a voltage which is 60-70% of the value at which the spark gaps normally fire without the triggering pulse.

An external inductance of 10 μ H is introduced between the Marx generator and the pulse forming line in order to reduce the rate of charging and hence reduce prepulse. The line gets charged to peak value in about 600 n sec. The voltage pulse of the Marx generator which charges the water line is shown in figure 2.11. A corona ring is connected at the output end of the Marx where the pulsed high voltage appears. This is shaped in such a way that large electrical stresses in any preferential direction are avoided. A 20 mm thick perspex flange is used as an interface between the Marx generator and the pulse forming water line.

2.4.2 Co-Axial Water Line

The co-axial water line is the secondary energy storage which shapes and compresses the Marx generator's output pulse. The shape of the output pulse depends on the load which is connected across the water line while the duration of the pulse is decided by its length.

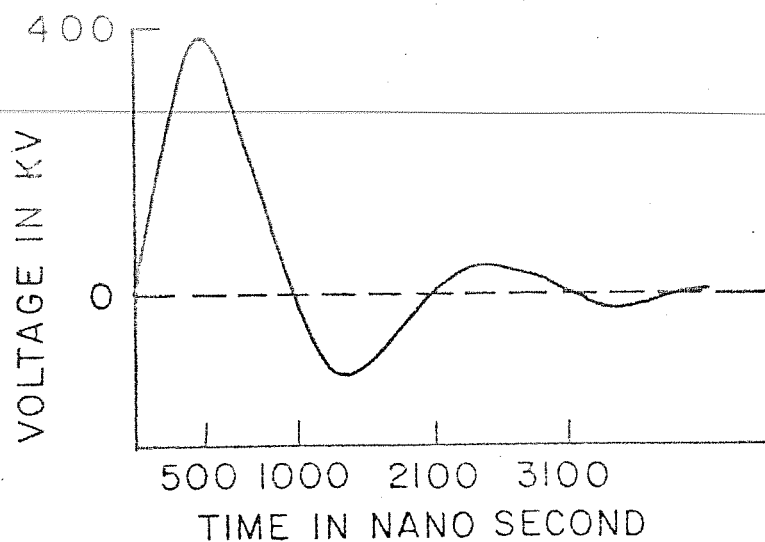


Figure 2.11 Water line charging waveform.

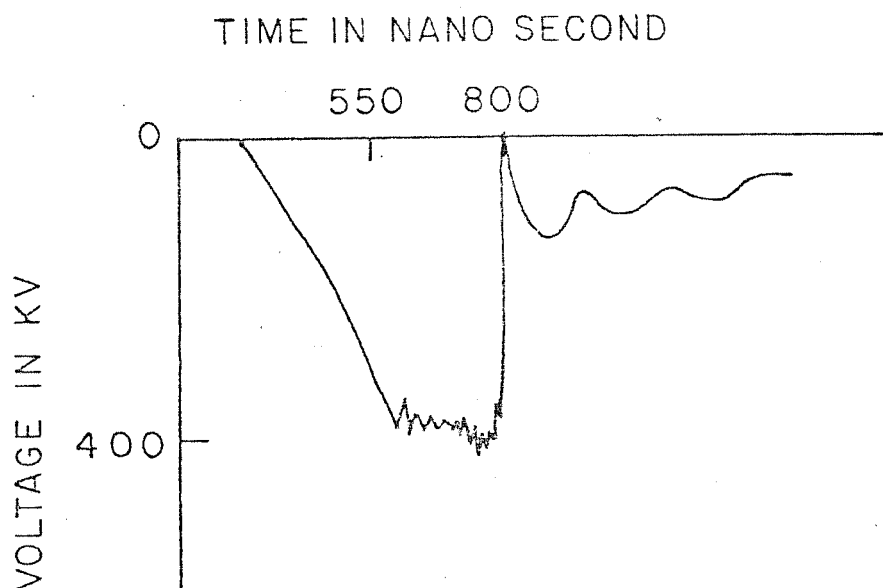


Figure 2.12 Marx voltage when high voltage holding switch fires.

While getting charged, the water line acts as a lumped capacitance but while discharging, it functions in a transmission line mode. The water line produces nearly an order of magnitude decrease in the pulse duration resulting in an increase in the power output. Water, having a high dielectric constant ($\epsilon = 80$) provides a medium, capable of storing energy at a density of 160 Kilojoule/meter³. In addition, the velocity of propagation of an electromagnetic wave through water is about nine times less than that through air, and hence the pulse-forming line becomes quite compact.

The co-axial water line consists of an inner conductor made of stainless steel with a diameter of 15 cm and an outer conductor (ss) with a diameter of 30 cm, thus having a characteristic impedance of 4.8 Ohms. The physical length of the line is 80 cm corresponding to an output pulse duration of 50 nanoseconds when terminated with a matched load. Deionised water with low conductivity is circulated in the coaxial water line. The resistive discharge time for the line in the present geometry is a few microseconds, much longer than the time, the Marx generator takes to charge the line.

2.4.3 High Voltage Holding Switch

The switching of the charged pulse line into the diode requires the reliable firing of a normally insulating gap, which has been achieved in the present set-up by the self-breakdown of a water switch. The water switch consists of two brass electrodes in the form of hemispheres with 30 mm diameter. The gap between the electrodes is adjustable from 0 to 30 mm. The water switch is mounted inside a stainless steel cylinder in which deionised water is continuously circulated. The breakdown strength of water depends upon the time period during which the high voltage exceeds 63% of the breakdown-voltage and the area of the electrodes over which the voltage exceeds 90% of the breakdown fields. The breakdown strength of the water switch calculated from Martin's empirical formula (Nation, 1979) is around 300-400 KV/cm. Figure 2.12 shows the output voltage waveform from the Marx generator when the water switch fires at the peak voltage.

2.4.4 Field Emission Diode

The production of the relativistic electron beam from the voltage pulse requires the use of a high voltage low inductance field emission diode, which can

provide the required high current densities. The diode consists of an annular brass cathode of 40 mm o.d., 26 mm i.d. and in front of it is placed an anode of 6 μ m thick aluminium foil. For a plane parallel diode consisting of a cylindrical cathode of radius R and vacuum gap d to the flat anode, the impedance is given by the Child-Langmuir's relation i.e.

$$Z = 136 \frac{(d/R)^2}{\sqrt{V}}$$

where V is in MV and Z is in ohms.

The aluminium foil, used as anode, is in most cases destroyed after each shot because of the high current densities of the electron beam passing through it. This necessitates the use of a foil-changer which enables the replacement of the anode foil without opening the vacuum system. This foil changer consists of a modified brass flange with various gears, stretcher rings, dispenser and receiver spools fixed on it and is mounted in the anode plane of the diode. A shaft, connected to the gear system, is brought out of the vacuum system, which when rotated changes and stretches the foil without disturbing the vacuum. Foil sufficient for over 30 shots is loaded onto the changer.

2.4.5 Beam Characteristics

The most important parameter of the REB generator is the output beam current. A self-integrated Rogowski coil mounted over the cathode is used to monitor the diode current. The diode current obtained when a 200 KV voltage pulse is applied to the cathode is shown in figure 2.13. The peak current in this signal is 30 Kilo amperes and the duration is about 60 n sec. This value of the diode current is in agreement with the Child-Langmuir relation. The diode currents obtained, are in the 10-30 KA range, by adjusting the cathode-anode gap.

2.5 AUTOMATIC CONTROL UNIT

Since the experiment utilises a number of high voltage energy storage capacitor banks to power various systems such as the Marx generator, pulsed magnetic field coils, plasma gun, pulsed gas inlet valve etc., an automatic system for programmable charging as well as the subsequent sequential discharging of these banks through their respective loads has been used (Lali et al., 1979). The banks are charged linearly through variable auto transformers coupled to low r.p.m. reversible motors. Voltages on the banks are sensed and compared with "Preset" levels and at the moment

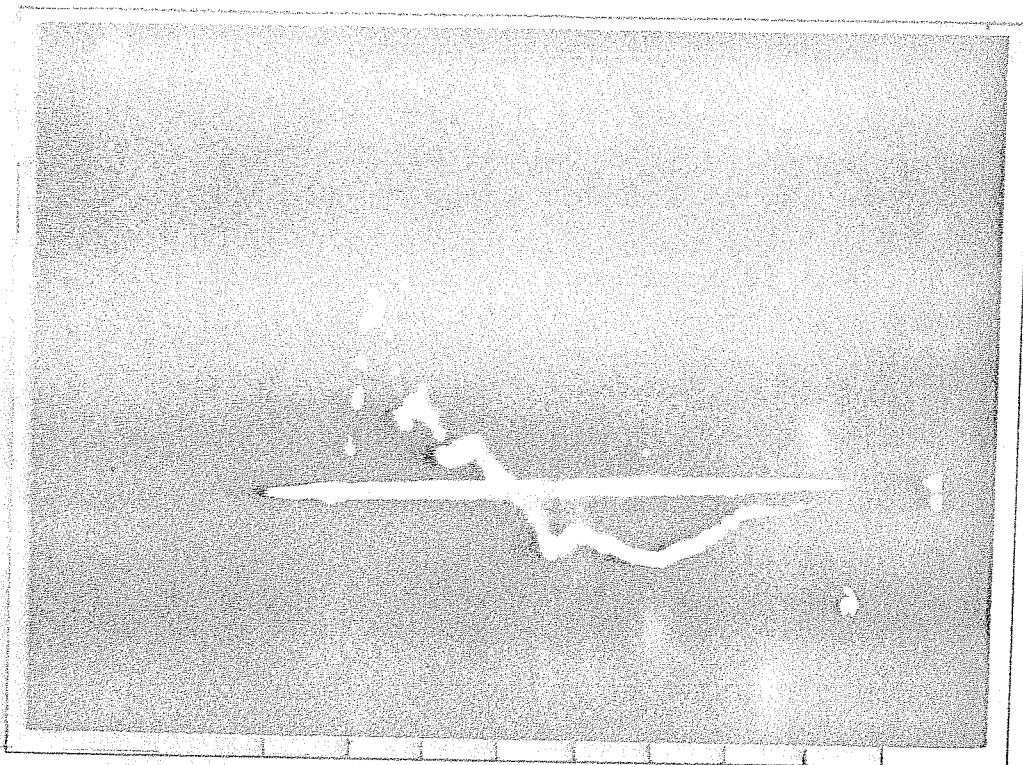


Figure 2.13 Field emission diode current waveform. Peak current is 30 KiloAmperes. Horizontal scale = 100 nsec per division.

of coincidence, the following sequence of events takes place:

- i. The power input to the capacitor banks is cut-off.
- ii. The various control motors are reversed.
- iii. Bank triggering circuits await a triggering pulse.

The sequential triggering of the bank firing circuits in a pre-selected sequence, is accomplished with the help of various digital delay circuits. The delays from 1.0 μ sec. through 9.999 m sec in steps of 1 μ sec. can be selected with the help of front panel thumb wheel switches.

The complete sequence of events is initiated by a single "initiate" command, which starts the charging of various banks. As all the banks charge up to their preset voltages, one of the charging circuits, which is preselected generates a "go" command which results in sequential firing of the banks through their loads and reset various charging circuits. The remote control unit is kept far off from the capacitor banks and associated triggering systems.

2.6 DIAGNOSTICS

Being a pulsed experiment, fast response diagnostics are used to monitor the different experimental parameters. Most of the diagnostic elements are calibrated using a 100 n sec. 40 Amps current pulse generated by a co-axial cable pulse-forming line terminated with a matched load. Details of the various diagnostics used in the present experiment are described below:

2.6.1 Time of Flight Mass Spectrometer

To verify whether the gas injected washer plasma gun is capable of producing plasmas of heavier gases, a time of flight mass spectrometer was constructed and operated in conjunction with the plasma gun (figure 2.14). The mass spectrometer consists of an assembly of two grids separated by 20 mm, one being used as an accelerator and the other as a collector, a meter long flight-tube and a collector at the end of the flight tube. With a knowledge of the energy of the ions accelerated by the grid, the length of the flight-path and measuring the time of flight, the ion species are identified. As the plasma gun is pulsed, the accelerating voltage was kept steady. Experiments were done with hydrogen nitrogen and argon as the ionising gases.

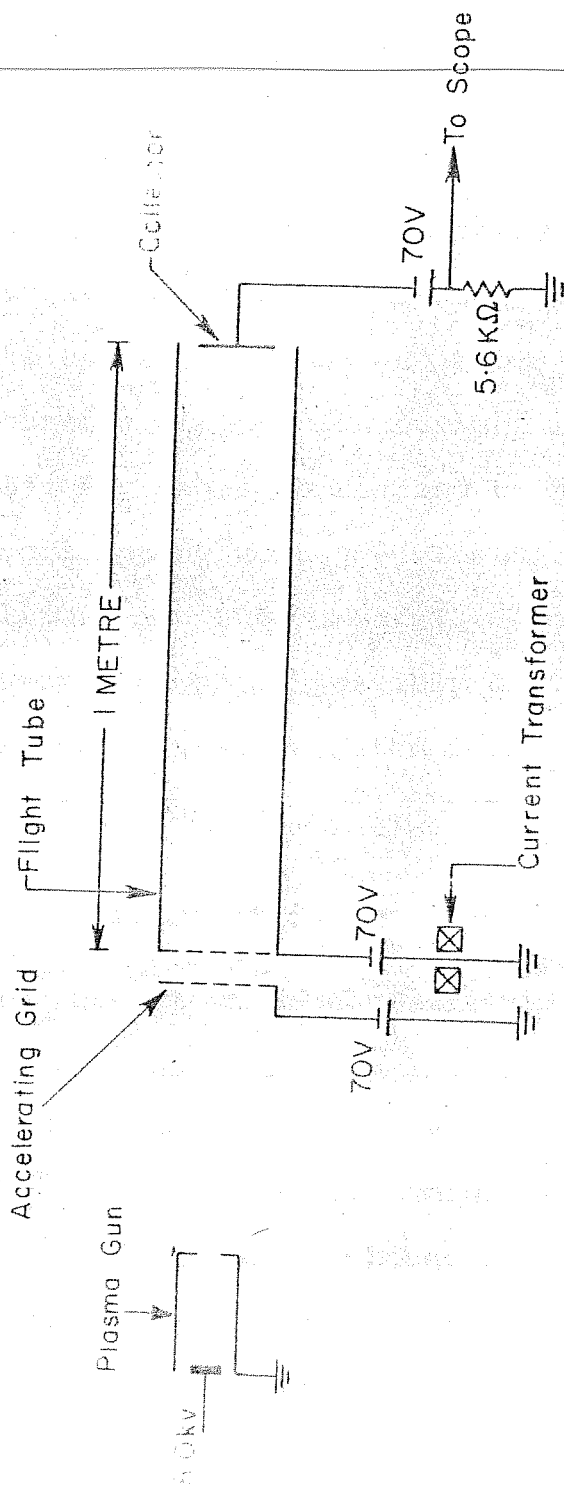


Figure 2.14 Schematic of the time of flight mass spectrometer.

The two traces in figure 2.15 correspond to the currents, registered by the two collectors when argon gas is injected. The first large peak in both the traces appear during the discharge duration ($= 40 \mu\text{sec}$ in this shot) and are not affected by the accelerating voltage. The peaks appearing at 52 and $100 \mu\text{sec}$ respectively in the two traces are the ion current signals. Observed time delay for peaks correspond to argon ion species for known accelerating voltage. The difference in polarity and amplitude are instrumental. The dispersion in time in the second trace is possibly due to the fact that the ions are post-accelerated from a plasma with a finite energy dispersion.

2.6.2. Voltage Divider

The output voltage of the pulsed Marx generator is measured with the help of a linear resistive voltage divider. A schematic of the voltage divider is given in figure 2.16. The voltage monitor consists of three copper electrodes, placed in a perspex container filled with copper sulphate solution. The resistance could be adjusted by changing the concentration of the solution.

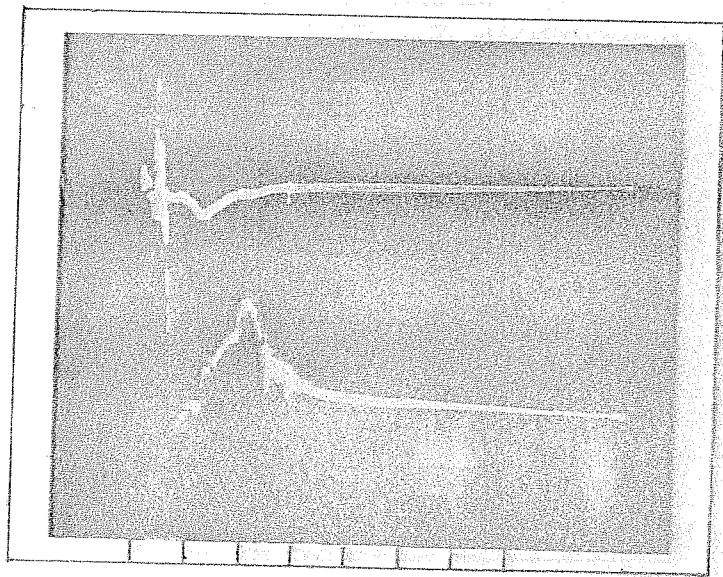


Figure 2.15 Ion currents collected by second grid and the collector of the time of flight mass spectrometer separated by 1.0 meter. The horizontal scale = $50 \mu \text{ sec.}$

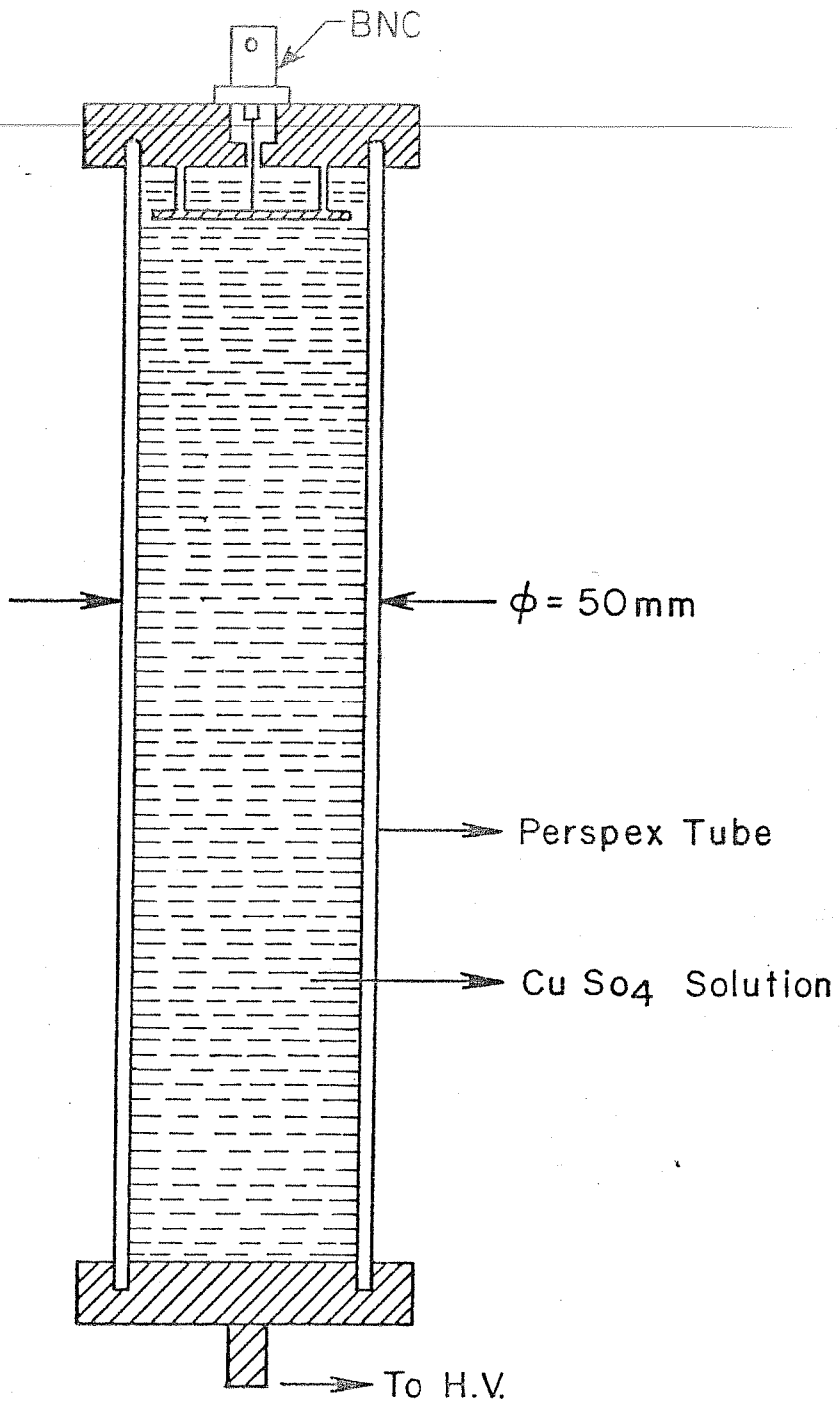


Figure 2.16 Schematic of the resistive voltage divider.

2.6.3. Rogowskii Coil

The diode current is measured with the help of a self-integrated Rogowskii coil, mounted over the cathode shank. The coil is made from copper windings, mounted inside perspex enclosures. The two ends of the coil are connected by a thin wire of negligible resistance. The current through the wire is measured with the help of a current transformer (figure 2.17).

A pair of miniature Rogowskii coils are constructed specifically to determine radial and angular profiles of the net current (beam + return current). Each of them consists of hundred turns of thin copper wire wound on 8.0 mm i.d., 10 mm o.d. toroidal mild steel. These coils are wrapped together to form one loop. One end of the each coil is grounded in such a manner that when one of the coils gives a positive output, the other gives a negative output. Both the coils are terminated by a 50 Ω resistance and the signals are integrated at the oscilloscope and subtracted from each other so that the electromagnetic noise gets nullified while the signal gets doubled.

2.6.4 Faraday Cup

A Faraday cup has been used to determine the

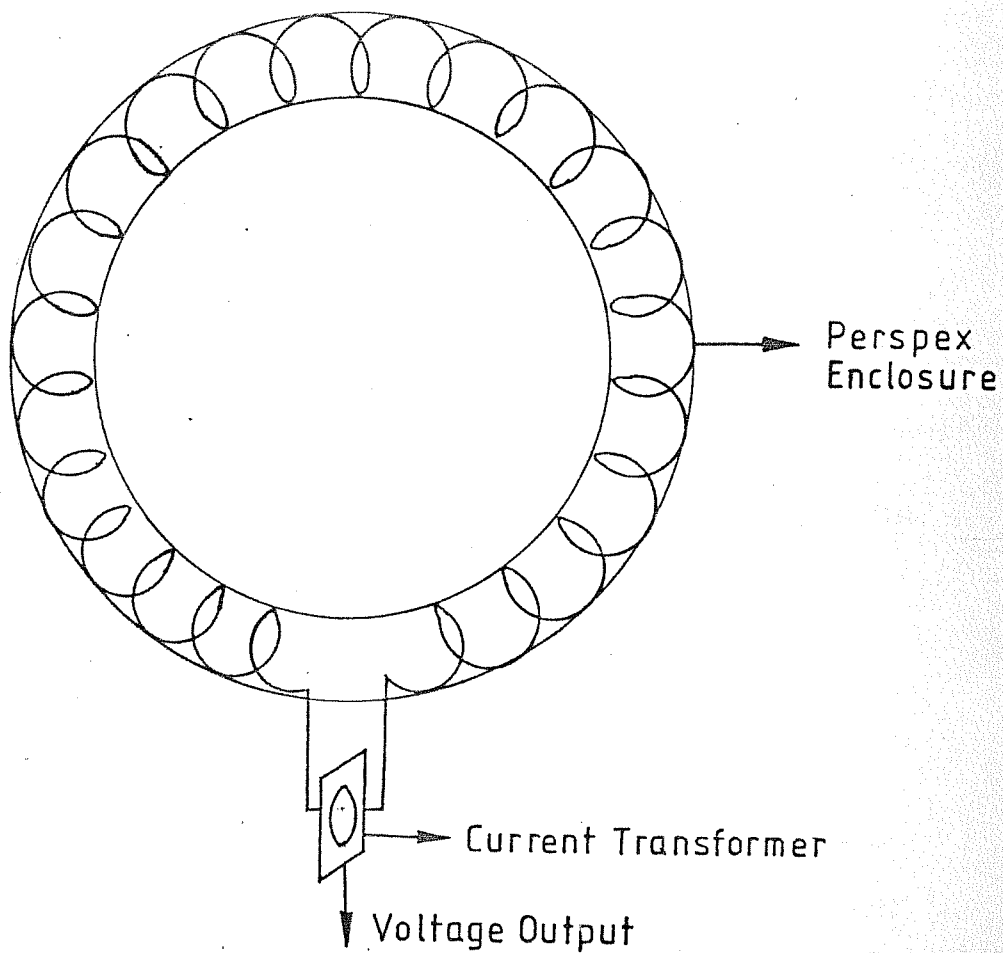


Figure 2.17 Schematic diagram of the self integrated Rogowski coil.

transmission efficiency of the relativistic electron beam through the cusp in vacuum. The Faraday cup is made of aluminium with 60 mm opening and has a graphite disc as the collector. The current collected by the collector is measured with the help of a standard Pearson model current probe. A cross sectional view of the Faraday cup is depicted in figure 2.18.

The inaccuracy in absolute current measurements by the Faraday cup can occur due to secondary emission from the cup and reflection of the relativistic electron beam from the collector. The secondary emission coefficient for graphite is less than 3% (Bruining, 1954) and any currents generated by the secondary emission will be opposed by the relativistic electron beam and hence this effect is insignificant. The use of graphite as the collector minimizes the reflection of high energy electrons due to the low Z of graphite. Further the cup is made hollow and deep, so that a large fraction of the reflected electrons are recaptured by the cup itself, thus minimizing the effect of reflection of the REB.

2.6.5 Electron Beam Probe

To determine the life time and current density of the relativistic electron beam in the mirror in

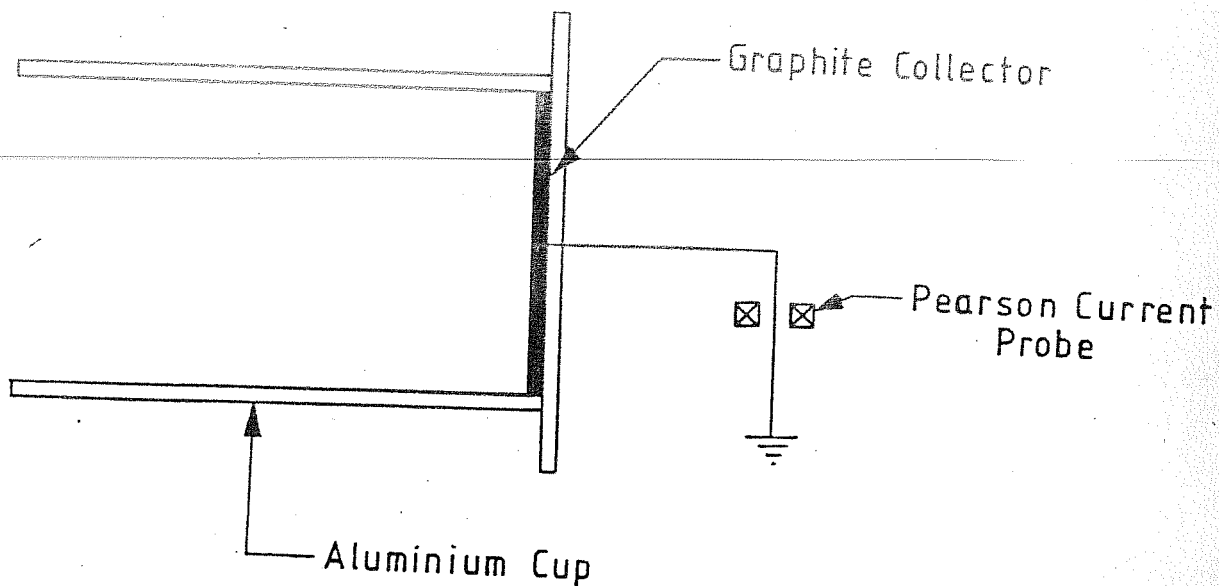


Figure 2.18 Cross sectional view of the Faraday cup.

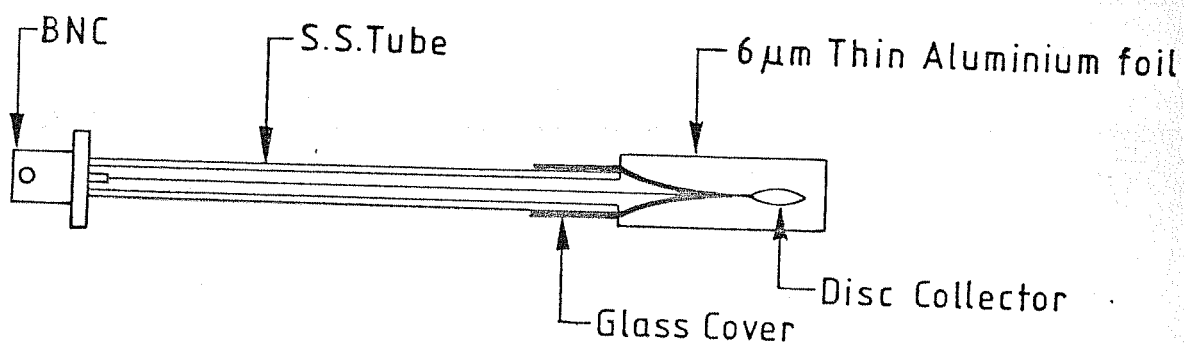


Figure 2.19 A schematic of the electron beam probe.

presence of the plasma, an electron beam probe, capable of collecting preferentially energetic electrons is fabricated. The probe is made of a cylindrical s.s. disc (or wire) of 5 mm diameter covered with a 6 μ m thin aluminium foil (figure 2.19). The thin aluminium foil allows only the energetic electron beam particles to penetrate to the probe, and prevents the collection of plasma electrons. A current transformer is used to monitor the collected current.

2.6.6. Magnetic Probe

The profile of the external pulsed magnetic field along the vacuum chamber is obtained by a millisecond time response magnetic probe. In such a probe the changing magnetic induction causes an induced voltage, proportional to $-d\phi/dt$, where ϕ is the magnetic flux threading the probe. A measure of the field is thus obtained by integrating the induced voltage.

The magnetic probe consists of a 16 mm long, 100 turns coil of 12 mm diameter. The coil was placed inside a glass tube, closed at one end. A 50 m sec passive RC integrator was used for integration of the induced probe voltage. A schematic of the magnetic probe is shown in figure 2.20.

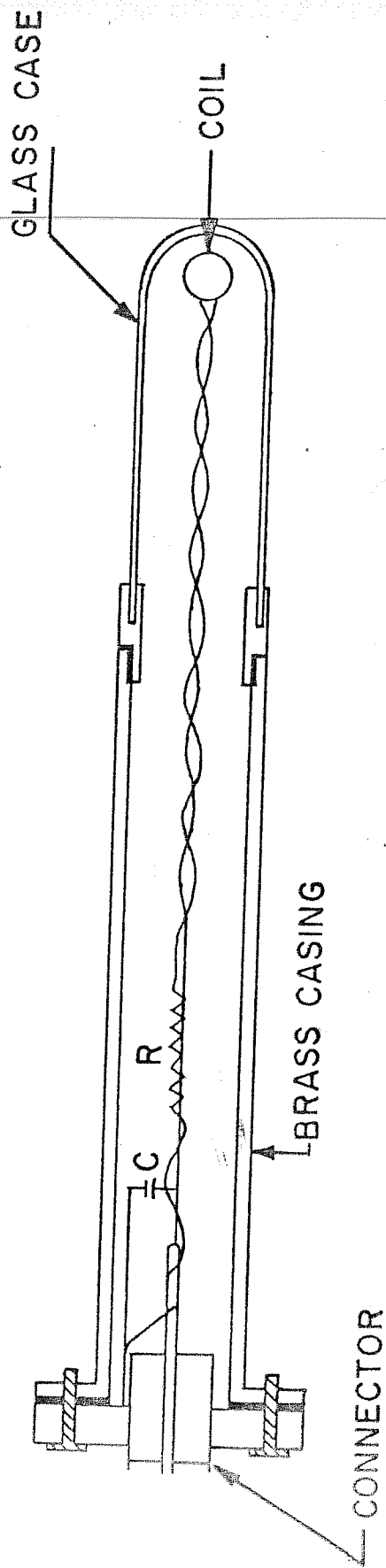


Figure 2.20 A schematic of the magnetic probe.

2.6.7 Diamagnetic loop

For relativistic electron beam propagation and plasma response studies, a number of diamagnetic loops were used in the present experiment. A diamagnetic loop encircling the interaction region measures the change in the magnetic flux created by the beam passage. The voltage induced in the diamagnetic loop of cross sectional area A due to change in the magnetic flux is given by:

$$V_{in} = NA \frac{dB}{dt}$$

Where, N is the number of turns in the diamagnetic loop. When this voltage is integrated with a passive RC integrator, the output voltage is given by

$$V_{out} = \frac{1}{RC} \int V_{in} dt$$

In almost all the rotating REB - Plasma interaction experiments, the diamagnetic loop signals last for a few microseconds while the magnetic skin time for vacuum wall is few tens of microseconds i.e. long compared to the duration of the signal. Hence, the magnetic flux is conserved inside the experimental chamber during this time. By assuming flux conservation, the output of the diamagnetic loop can

be given as (Gerber et al., 1977)

$$V_{out} = \frac{N\pi\Delta B_z}{RC} \frac{R_w^2}{\left(\frac{R_w^2}{R_p^2} - 1\right)} \left(1 - \frac{R_L^2}{R_w^2}\right)$$

where

- ΔB_z is the change in axial magnetic field,
- N is the number of turns in the loop,
- RC is the time constant of integration,
- R_w is the radius of vacuum wall,
- R_p is the radius of Plasma column,
- R_L is the radius of the diamagnetic loop.

Figure 2.21 shows the construction of a typical diamagnetic loop. The diamagnetic loops are fabricated using thin teflon coated wire wound inside a copper tube with 80 mm i.d.. The number of windings was kept at five. The copper tube served as an electrostatic shield with a poloidal cut so as to preclude the formation of eddy currents, which would otherwise oppose the penetration of change in flux into the loop windings. The output of the loops are terminated with a 50 Ω resistance and the signals are integrated by 22 μ sec passive RC integrator at the oscilloscope. One end of the loop and the copper tube are grounded at the oscilloscope in order to avoid formation of any ground loop. The absence of an

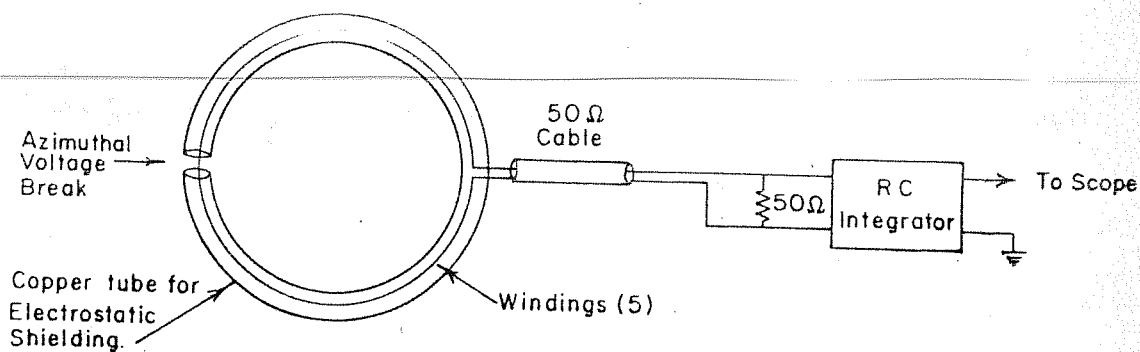


Figure 2.21 Details of diamagnetic loop and passive integrator.

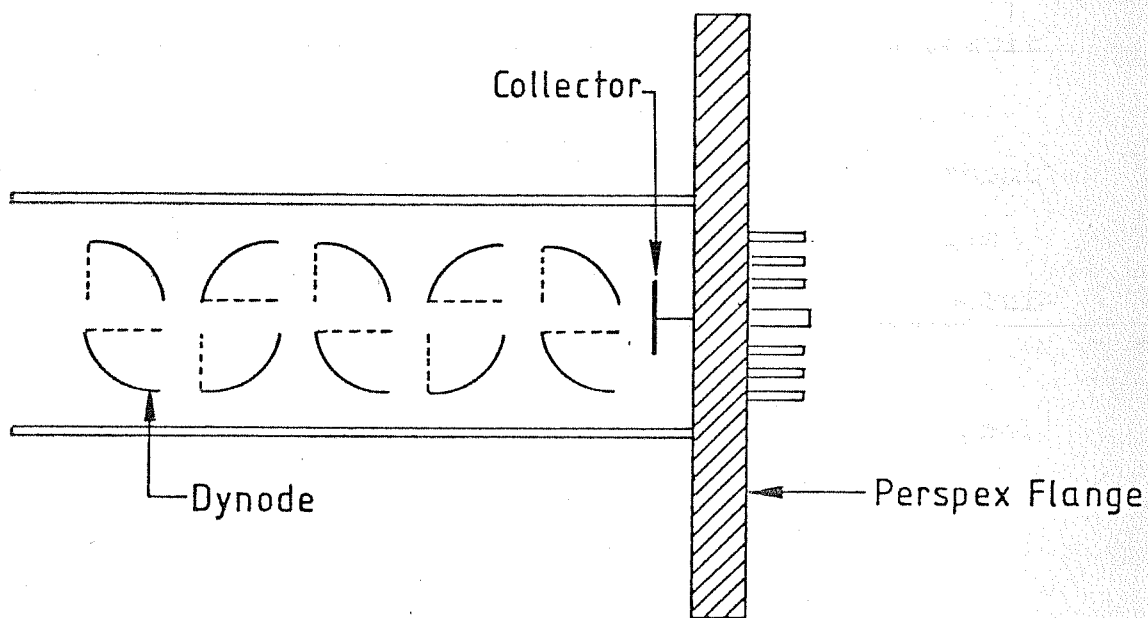


Figure 2.22 The fast particle detector.

electrostatic pick up was confirmed by the reversal of loop signal polarity when the loops were rotated through 180° . The calibration of the loops was done by registering the field in the centre of the 50 mm i.d., three turn coil driven by 35 Amps and 100 nanosecond pulse.

2.6.8 Fast Particle Detector

The acceleration of plasma ions by radial electric fields has been predicted by theoretical models on rotating REB-plasma interaction. An electron multiplier has been used in the present device with an aim to look for these ions or neutral fluxes (which can be produced as a result of charge exchange of ions with background neutral gas). The multiplier has ten stages and a current gain of about 10^6 and is placed in such a way that the fast particles can fall directly on the 1st dynode of the electron multiplier (figure 2.22). The multiplier output is further amplified by a current amplifier and the resultant signal is displayed on the oscilloscope. The sensitivity of the electron multiplier was determined experimentally by measuring its response to a monoenergetic beam of H atoms of known intensity and variable energy.

2.7 GROUNDING AND SHIELDING

Since the experiment involves high current and voltage pulses, proper grounding and shielding of the experimental set-up and associated diagnostics was found to be necessary in order to avoid the electromagnetic noise. For this reason the main experimental set-up and the various diagnostics elements were electrically isolated from each other and a massive copperplate, placed right below the device was used for grounding purpose in order to minimise the length of the grounding connections. The signals were recorded on the oscilloscopes, kept inside a shielded cage and all the cables from the diagnostics to the oscilloscopes were run through a copper tube for proper shielding.

CHAPTER III

GENERATION AND PROPAGATION OF ROTATING REB

3.1 INTRODUCTION

The laminar relativistic electron beam produced by the generator is converted into a rotating beam prior to injecting it into the plasma. This is done according to a simple and different scheme suggested by Schmidt (1962) for the production of a rotating electron beam. According to the single particle orbit calculation, an annular beam of electrons injected into a nonadiabatic cusp magnetic field will emerge out of the cusp with velocity components.

$$V_{||} = V_0 \left[1 - \left(\frac{r_0}{r} \right)^2 \right]^{1/2}$$

$$V_L = V_0 \left(\frac{r_0}{r} \right)$$

Where, V_0 is the initial electron beam velocity before entering the cusp, V_{L1} and V_L are the axial and rotational velocities respectively, r_0 is the radius of the annular beam and r is the electron Larmor radius. The motion of a charged particle injected axially into a cusp geometry is depicted in figure 3.1. Experimental results on the rotation of a laminar hollow REB by the nonadiabatic cusp are briefly presented in this chapter.

Experiments on the injection of a short duration high current electron beam into the nonadiabatic cusp in vacuum have revealed that the beam propagation through the cusp is poor. It has been found that transmission efficiency of the cusp, defined, as the percentage of the number of particles transmitted through the cusp to the total number of particles entering the cusp, is around 10% (Friedman, 1970 a,b; Rhee et al., 1974) i.e. a significant fraction of the beam particles are lost while propagating through the cusp.

Previous experiment performed (Kapetanakis, 1974) to increase the cusp transmission efficiency by filling the cusp and drift tube with neutral gas showed that in

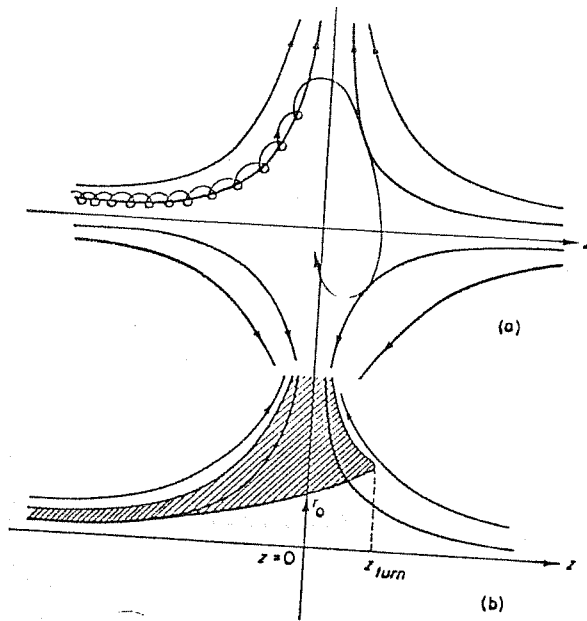


Figure 3.1 Motion of a charged particle injected into a cusp geometry.

the pressure range of 100-1000 milli Torr, 85% of the beam particles emerge out of the cusp. The main disadvantage here is that it is always essential to fill the experimental chamber with the neutral gas which limits the flexibility of the experimental configuration. In beam generators with foilless diodes or grid anodes, this technique would not be feasible since the gas filling, would impair the diode performance. In experiments on beam interaction with magnetic fields, for example, in the studies of intense microwave generation, the neutral gas ionisation and subsequent current neutralisation of the beam bring additional complexities to the problem.

A technique for improving the transmission of intense electron beam through the cusp magnetic field in vacuum is described in this chapter. It has been observed that dielectric tubes help in channeling the beam through hard vacuum, resulting in an improved transmission of the beam through the cusp.

The experiments on the propagation of a rotating relativistic electron beam through a mirror trapped plasma are also described and compared with the predictions of the existing theoretical models.

3.2 EXPERIMENTAL SET UP

The experimental system along with the magnetic field configuration, described in the last chapter, is shown in figure 3.2. During the experiments, the beam parameters were; energy in the range 200-250 KeV, current of the order of 10-12 KA and pulse duration equal to 80 n sec. The experimental chamber was evacuated to a base pressure of 2×10^{-5} Torr. The plasma gun was operated in the density regime 10^{11} - 10^{13} cm⁻³ during the study of the rotating REB propagation in the plasma, but was switched off while carrying out experiments on beam rotation and cusp transmission.

Perspex tubes of three different diameters (50, 70 and 95 mm) were used as drift tubes during the study of transmission efficiency. The perspex tube placed immediately after the anode foil, extends through the cusp plane to the other side up to 20 cm. The thickness of the perspex tubes was so chosen, that it was nearly ten times the range of the energetic electrons.

The electron beam flux as a function of time, before and after the cusp was determined with the help of the Faraday cup. The life time and current densities of

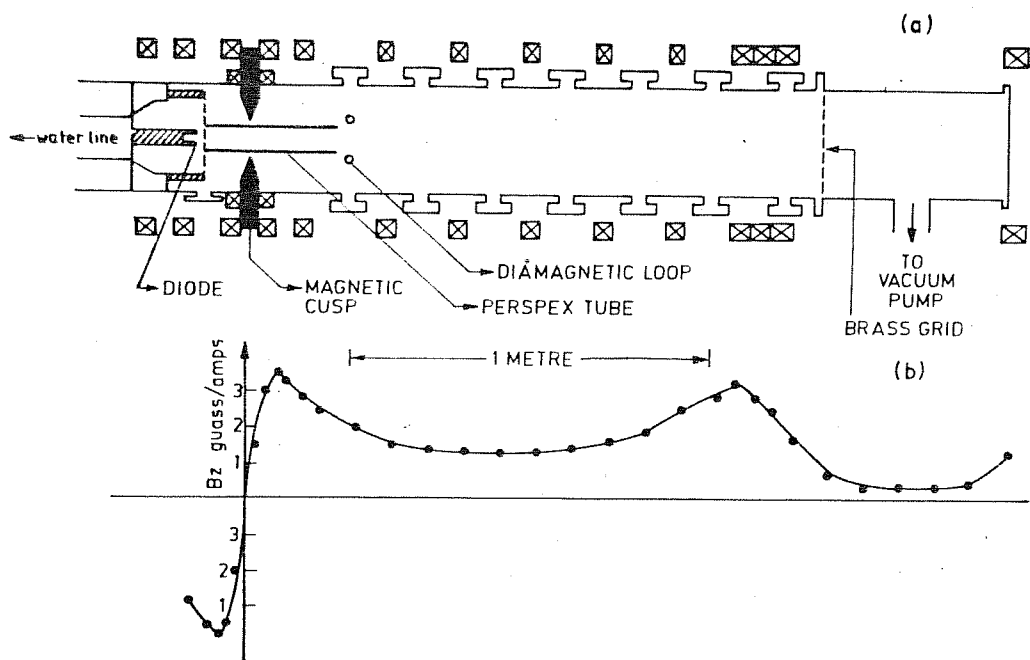


Figure 3.2 (a) Schematic drawing of the experimental system
 (b) External magnetic field configuration

the rotating electron beam in the mirror were measured by an electron beam probe. The diamagnetic loop measures the reduction in the magnetic flux ΔH , resulting from the rotation of the electron beam in vacuum. This magnetic flux ΔH , can be written as (Friedman, 1970 b)

$$\Delta H = -\left(\frac{2Ne}{r}\right)\beta_{\perp} \dots\dots\dots (3.1)$$

Where $\beta_{\perp} = v_{\perp}/c$, N is the number of electrons per unit length and r is the radius of gyration. The ratio of rotational to axial velocity of the electron beam can be obtained if in addition to ΔH , the total number of electrons emerging out of the cusp is also known. The total number of electrons emerging out of the cusp can be written as

$$Q = \int \frac{I dt}{e} \dots\dots\dots (3.2)$$

Where I is the axial component of the beam current after the cusp. The equation (3.2) can be rewritten as:

$$Q = \int N v_{\parallel} dt$$

Using equation (3.1), we have

$$Q = \int \frac{\Delta H r c}{e} \frac{v_{\parallel}}{v_{\perp}} dt$$

$$\frac{v_{\perp}}{v_{\parallel}} = \frac{\Delta H r c}{2 Q e} \Delta t \dots\dots\dots (3.3)$$

Where Δt is a characteristic time describing the duration of the diamagnetic loop signal. Thus with the

knowledge of the amplitude and time duration of the diamagnetic signal as well as the number of particles crossed the cusp, the average value of rotational to the axial velocity ratio can be obtained.

3.3 EXPERIMENTAL RESULTS

3.3.1 Passage of REB through Cusp Magnetic Field

During these experiments, the beam generator was switched on 2 milli seconds after the magnetic field capacitor bank was discharged i.e. when the magnetic field has reached a peak value. This ensures that the external magnetic field remains constant during the beam propagation through the chamber, which last for a few nanoseconds. A typical diode current signal is shown in figure 3.3.a.

Figure 3.3.b. shows the signal of the diamagnetic loop kept at a distance of 22 cm from the cusp, when the magnetic field was 800 Gauss at the mirror point. A reversal of the polarity of the signal registered, when the loop is rotated through 180° , confirmed that the observed signal was not due to electromagnetic noise. As mentioned that the diamagnetic loop measures the induced magnetic field because of the beam rotation in vacuum. Thus, the observed finite loop signal shows that the relativistic electron beam starts rotating

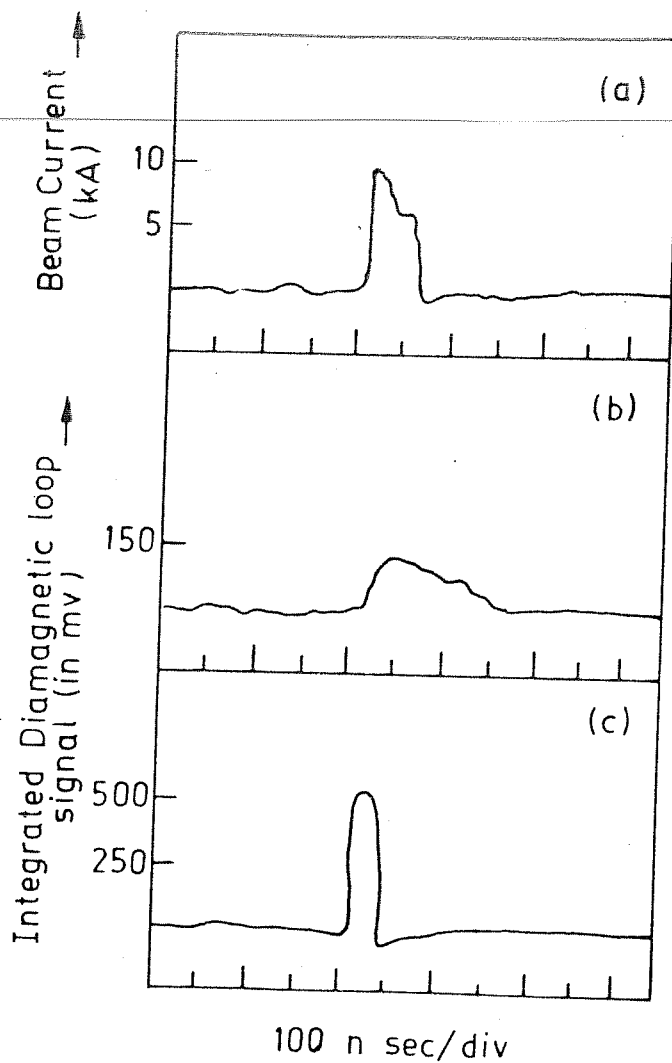


Figure 3.3 (a) Diode current signal measured using a self integrated Rogowski coil
(b) Diamagnetic signal for beam propagated in vacuum
(c) Diamagnetic loop output for beam propagation using 5.0 cm diameter perspex tube.

after the cusp or in other words nonadiabatic cusp converts a part of the beam axial energy into a rotational one.

To determine the value of $(V_{\perp}/V_{||})$, the total number of beam particles transmitted through the cusp was monitored with the help of the Faraday cup. The Faraday cup was mounted 22 cm, away from the cusp point inside the vacuum, such that it intercepts the entire beam cross section. Figure 3.4 shows the Faraday cup signal for the same experimental parameters as in the case of the diamagnetic loop measurements. An integration of the Faraday cup signal with respect to time and a further division by electronic charge (equation 3.2) shows that the total number of particles transmitted through the cusp is 3×10^{13} , which amounts to roughly 8% of the beam particles, produced by the beam generator. The average value of $V_{\perp}/V_{||}$ obtained, for $\Delta H = 5$ Gauass, $\Delta t = 200$ n sec as shown by the diamagnetic loop signal and $Q = 3 \times 10^{13}$, is found to be 1.8.

The dependence of the electron beam flux transmitted through the cusp magnetic field on the externally applied magnetic field is shown in Figure 3.5. It is seen that the cusp transmission nearly remains constant

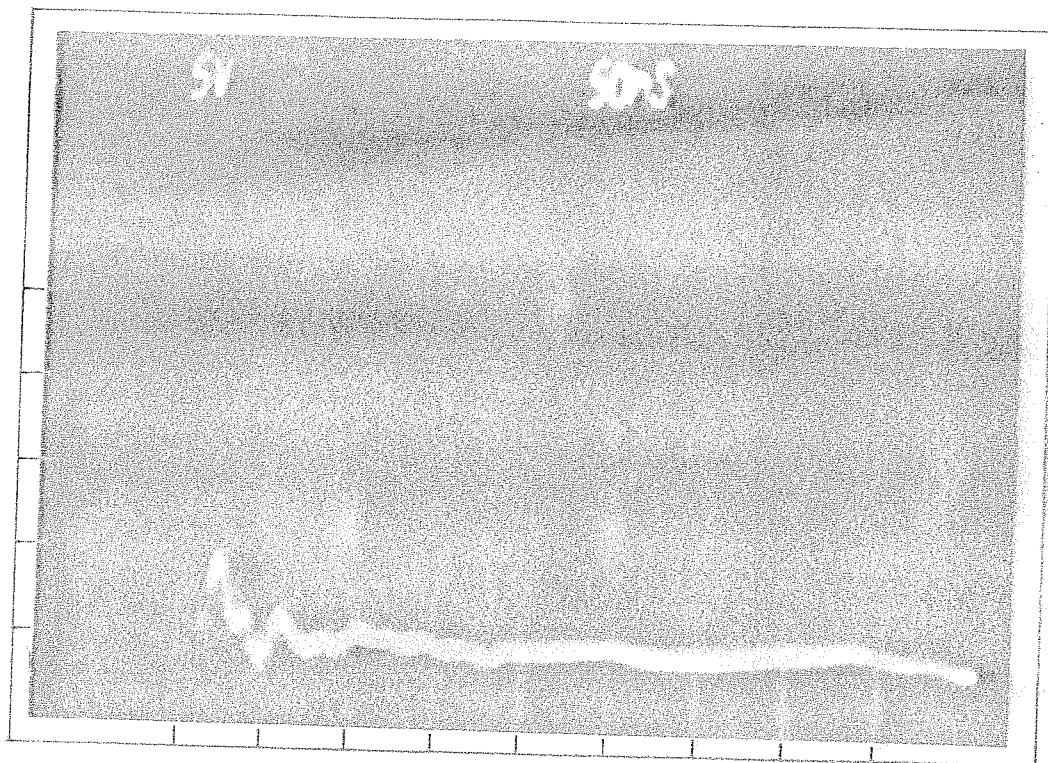


Figure 3.4 Faraday cup signal for intense beam propagation in vacuum. Horizontal scale = 50 ns/div., Vertical scale = 5 V/div.

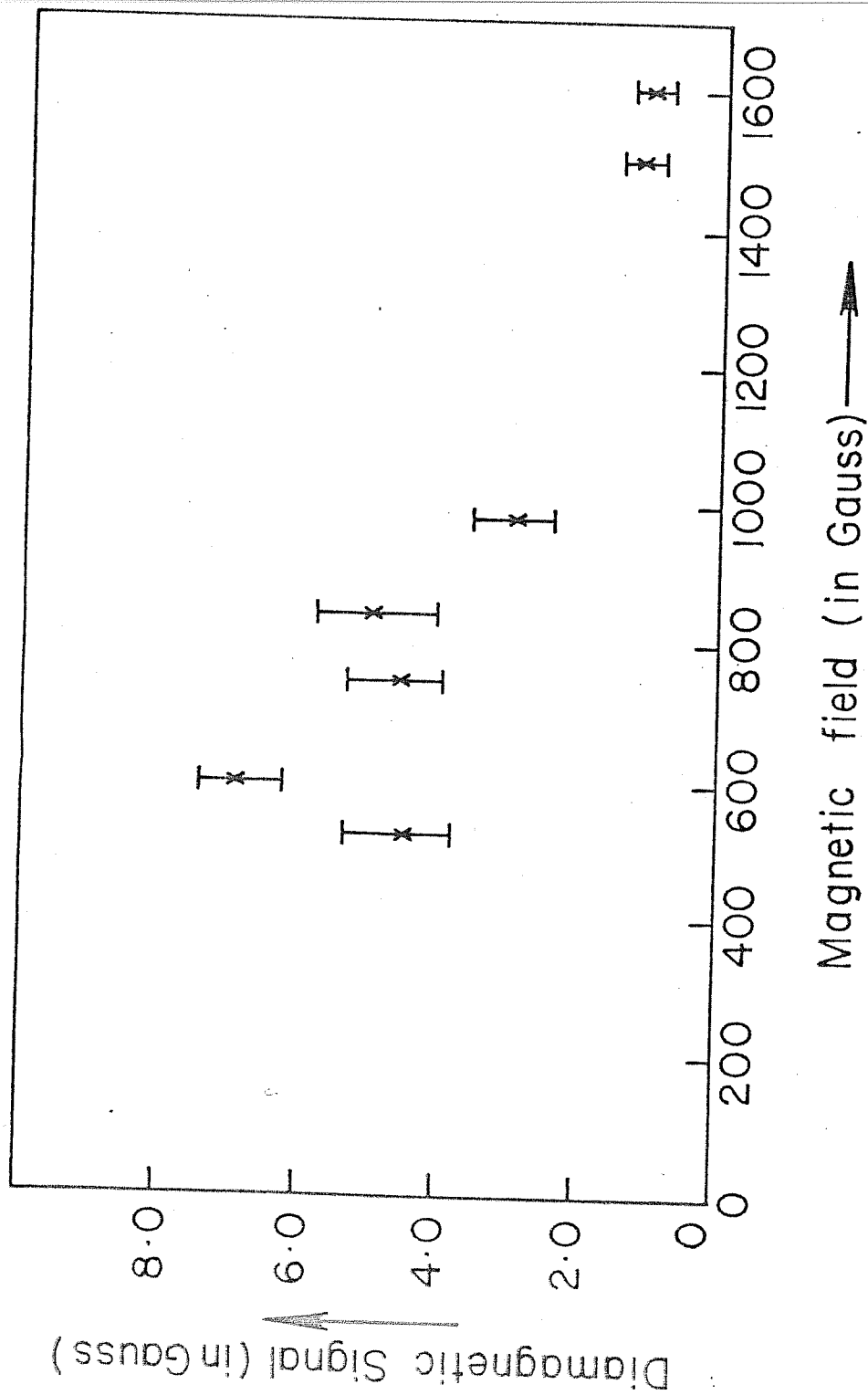


Figure 3.5 Variation of diamagnetic loop signal with external magnetic field in vacuum.

up to 840 Gauss and a further increase in the field results in a reduction of cusp transmission.

3.3.2 Enhancement of Cusp Transmission in Vacuum

As observed in the last section, the transmission efficiency is found to be 8% in vacuum. Experiments were performed with dielectric tubes in the drift region to study their influence on the beam transmission in vacuum. Figures 3.4 and 3.6 show the observed Faraday cup (placed at the end of the tube) signals without and with the perspex tube of 50 mm i.d.. It is evident that the transmitted electron beam flux through the cusp increases substantially in the presence of the perspex tube. The enhancement of the cusp transmission with the introduction of the perspex tube is also registered by the diamagnetic loop (figure 3.3 c). An increase in the transmission over the vacuum value by a factor of 2.5 results by 50 mm i.d. perspex tube (John and Jain, 1981).

During these experiments, it was noticed that the first shot after pumpdown from the atmospheric pressure always shows a significantly large transmission efficiency, and during the subsequent shots the transmission efficiency continuously decreases

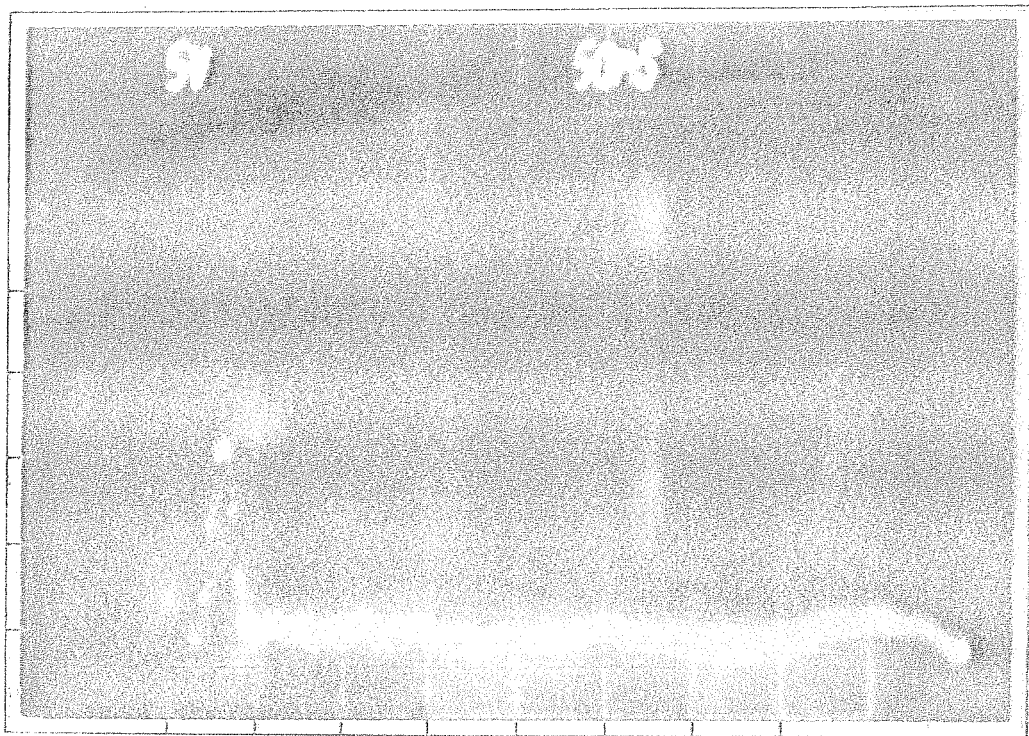


Figure 3.6 Faraday cup output with a conditioned 5.0 cm diameter perspex tube as a beam guide.
Horizontal scale = 50 ns/div., Vertical scale = 5 V/div.

reaching a stable value. This is represented in figure 3.7, where the diamagnetic loop output is plotted against the shot number. The time duration between two consecutive shots is about a few minutes, which is typically the time taken to recharge the Marx generator and to pump out the gas load introduced into the vacuum system. The enhanced diamagnetic loop and Faraday cup outputs, depicted in figures 3.3 c and 3.6 respectively were obtained after the conditioning of the tube by several shots.

The study of the percentage transmission efficiency of the cusp with perspex tubes of different diameters shows that (figure 3.8) the beam transmission increases with tube diameter and then attains a saturation. The maximum enhancement obtained by the introduction of the dielectric tube corresponds to four times the vacuum value. The ordinate in figure 3.8 represents a diamagnetic loop output normalised with respect to the vacuum value and in all the cases the perspex tubes were conditioned by firing a few initial shots.

3.3.3. Rotating Electron Beam Propagation

A series of measurements have been made in order

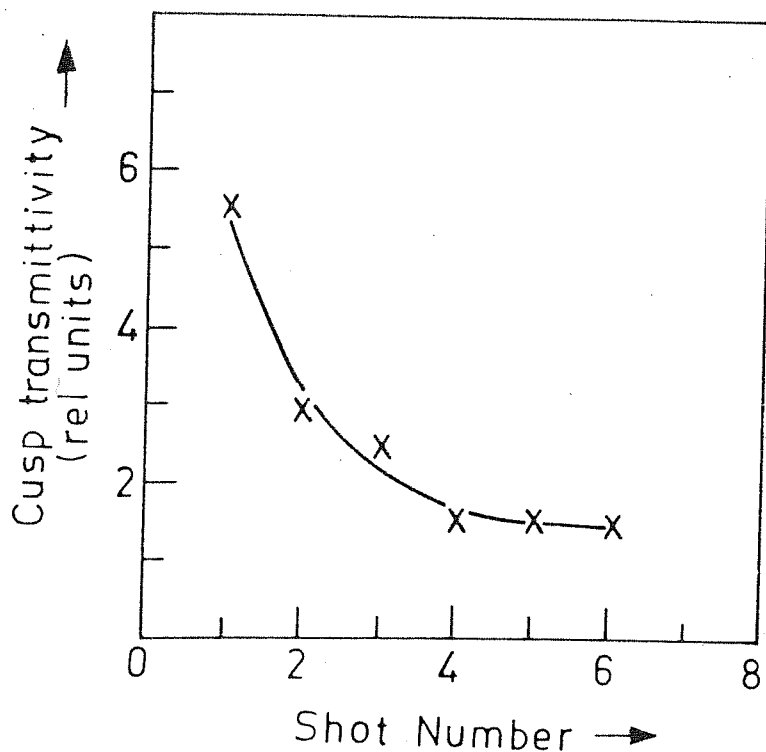


Figure 3.7 Variation of the cusp transmittivity with shot number after the pumpdown from atmospheric pressure. Diameter of the perspex tube used is 5.0 cm.

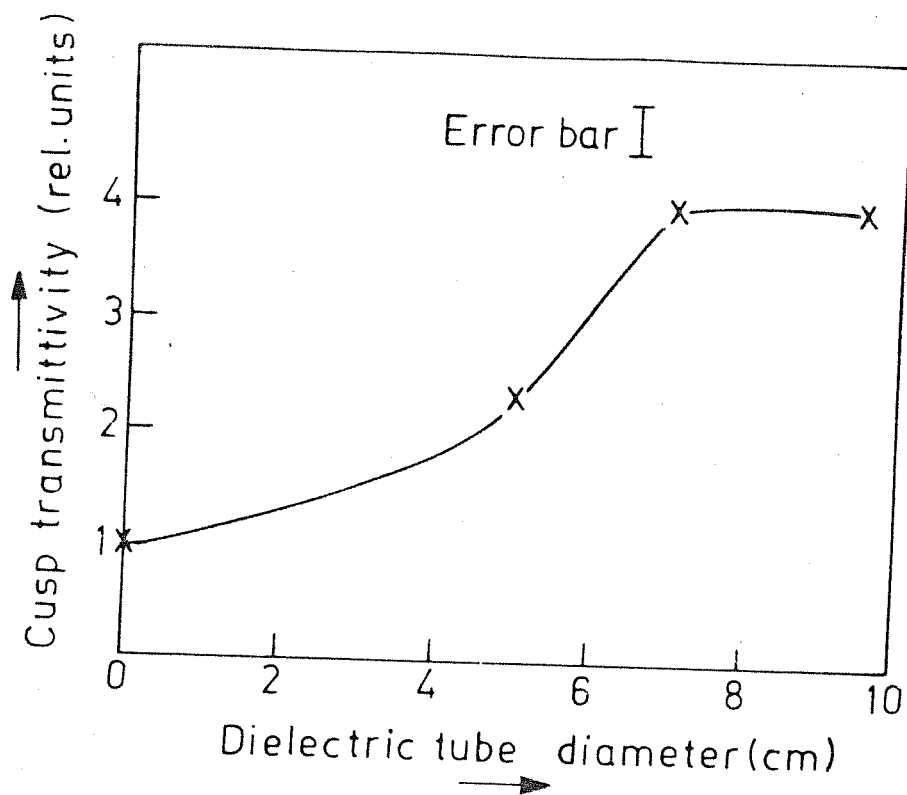


Figure 3.8 Variation of the diamagnetic loop output with perspex guide tube diameter. In all the cases the tube was conditioned with a number of shots.

to study the propagation of a rotating relativistic electron beam through a plasma. These studies were carried out using an array of identical diamagnetic loops placed at different axial distances, two electron beam probes, one placed at 25 cm and the other at 105 cm from the cusp, a witness plate and a Faraday cup. When the beam was fired in vacuum (2×10^{-5} Torr), the diamagnetic loops, the Faraday cup and the witness plate registered the beam only up to a distance of 25 cm from the cusp. At distances longer than 25 cm, all these diagnostic elements recorded no appreciable signal, thus suggesting that in vacuum, the rotating electron beam does not travel an appreciable distance inside the mirror.

During the study of the rotating beam propagation through plasma, the chamber was first filled with hydrogen plasma (density $\approx 10^{12} \text{ cm}^{-3}$) produced by the plasma gun. The beam is fired into this plasma and the signals from different diamagnetic loops were registered on the oscilloscope. The studies show that in this case all the diamagnetic loops including the one placed outside the second mirror (figure 3.9) register the rotating beam induced signals. An electron beam probe placed at the mirror minimum region, used to

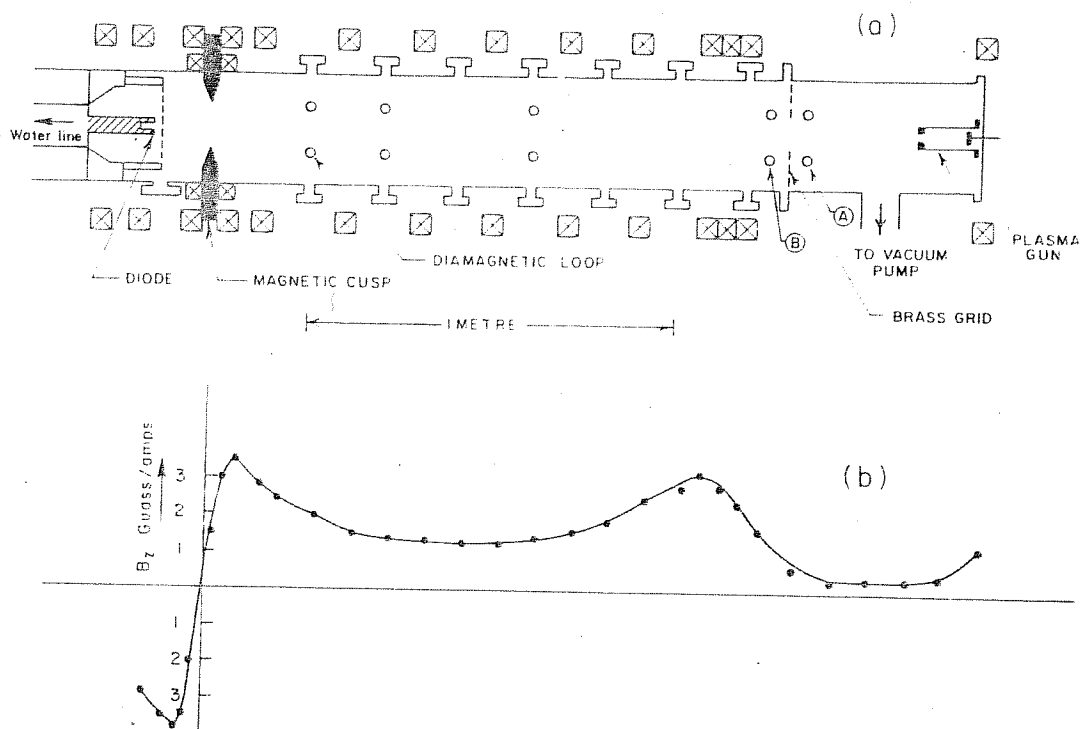


Figure 3.9 Schematic of the experiment showing the location of the diamagnetic loops.

determine the life time of the beam in the mirror, shows (figure 3.10) that a substantial part of the beam induced signal lasts for only 100 n sec which is comparable to the beam pulse length, although the overall extent of the signal is about 250 n sec. From these observations we conclude that the presence of plasma has led to an efficient propagation of the beam all along the chamber or in other-words the rotating electron beam is not stopped by either the plasma or the mirror field.

A relatively large rotating electron beam induced magnetic field ($\Delta B/B_0 = 0.7$) is observed with the help of the diamagnetic loop B (See figure 3.9), located near the end brass grid as compared to the signals recorded at other axial position, as shown in figure 3.11 a. The measured signal lasts for only 300 n sec and does not have the characteristic of an induced return current. This is attributed to the piling up of the rotating beam particles near the brass grid after traversing through the plasma. This is further confirmed by the diamagnetic loop A placed at the other side of the grid, which registers a comparatively small signal, as is seen from figure 3.11 b.

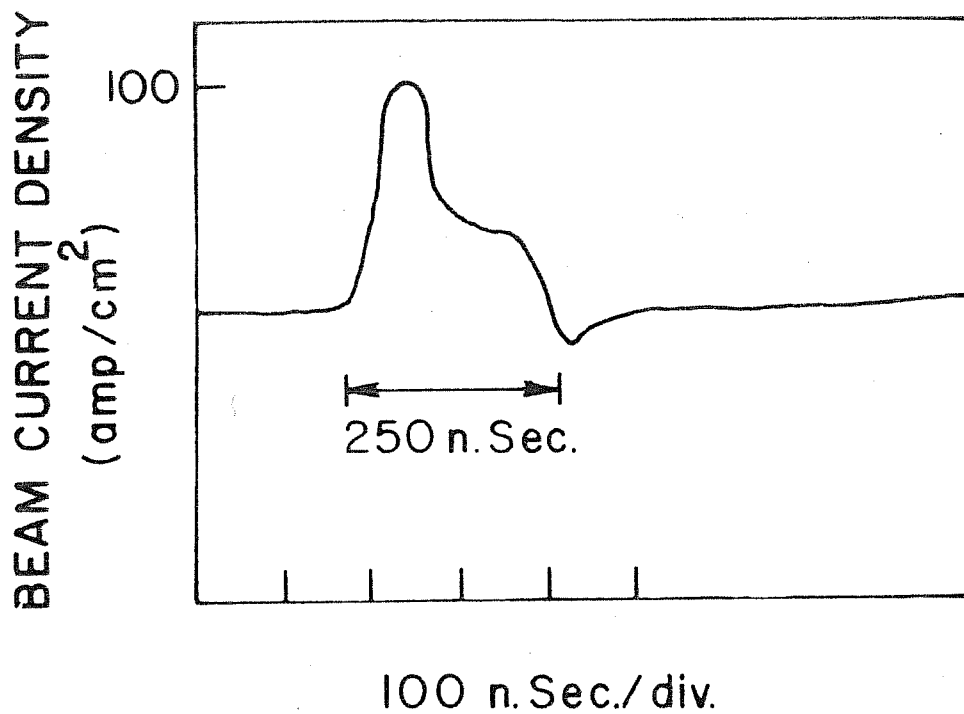


Figure 3.10 The electron beam current density, measured with an electron beam probe at the mirror center.

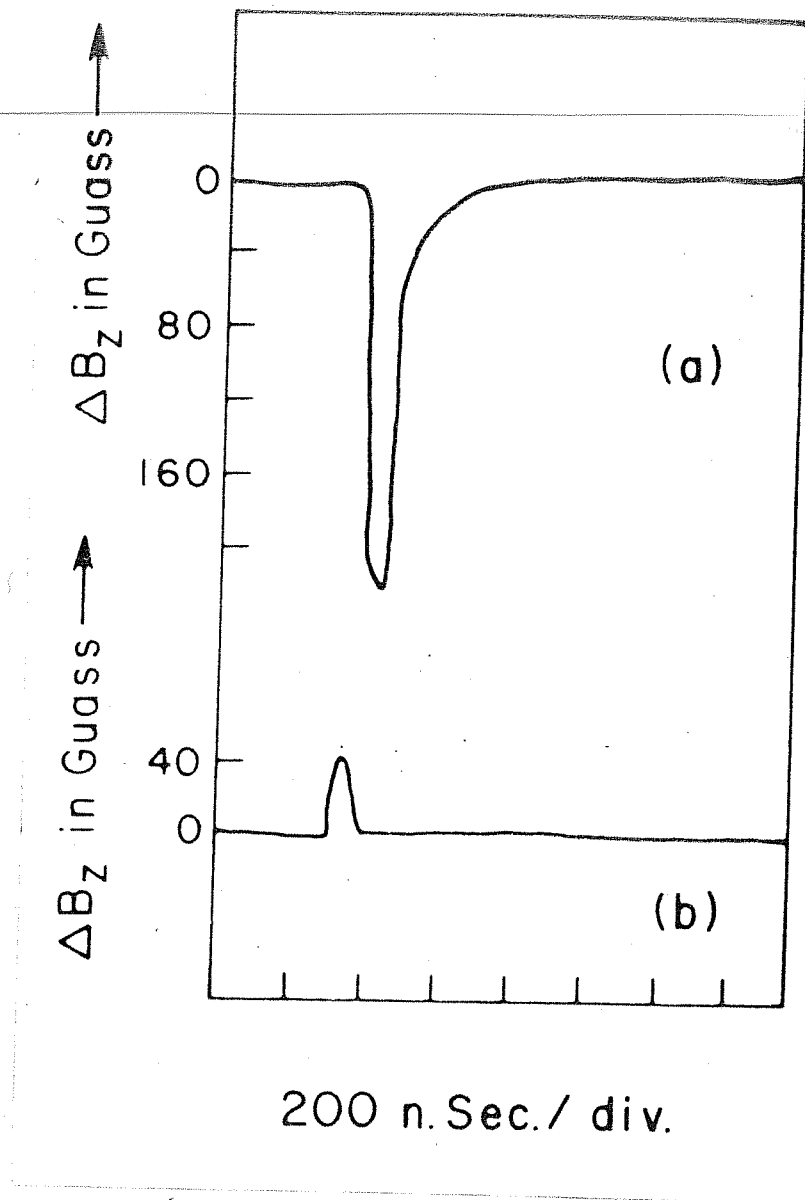


Figure 3.11 The diamagnetic loop signal measured

- (a) at the inner side of the grid with loop B
- (b) at a point outside the grid with loop A.

The percentage of the axial energy lost by the rotating electron beam while traversing the plasma is determined with the help of signals from two identical electron beam probes placed at distances of 25 and 105 cm from the cusp. Figure 3.12 depicts the recorded oscillogrammes of the probe signals. From these, we find that the beam has lost at least 80% of its axial energy while traversing a meter long column of plasma. Further, the radial profile of the beam current obtained with the help of the electron beam probe at the mirror minimum shows that the beam is localised at the radial distance of 2.0 cm from the axis. This indicates the absence of any macroscopic beam instability.

3.4 DISCUSSION

3.4.1 REB Rotation

As per Schimdt's orbit calculation, an intense electron beam traversing the cusp magnetic field experiences a $J_z \times B_r$ force, where J_z is beam's axial current density and B_r is the radial magnetic field. As a result of this force, part of the axial energy of the beam will be converted into rotational energy. Further, the calculations show that above a particular value of the magnetic field for a given

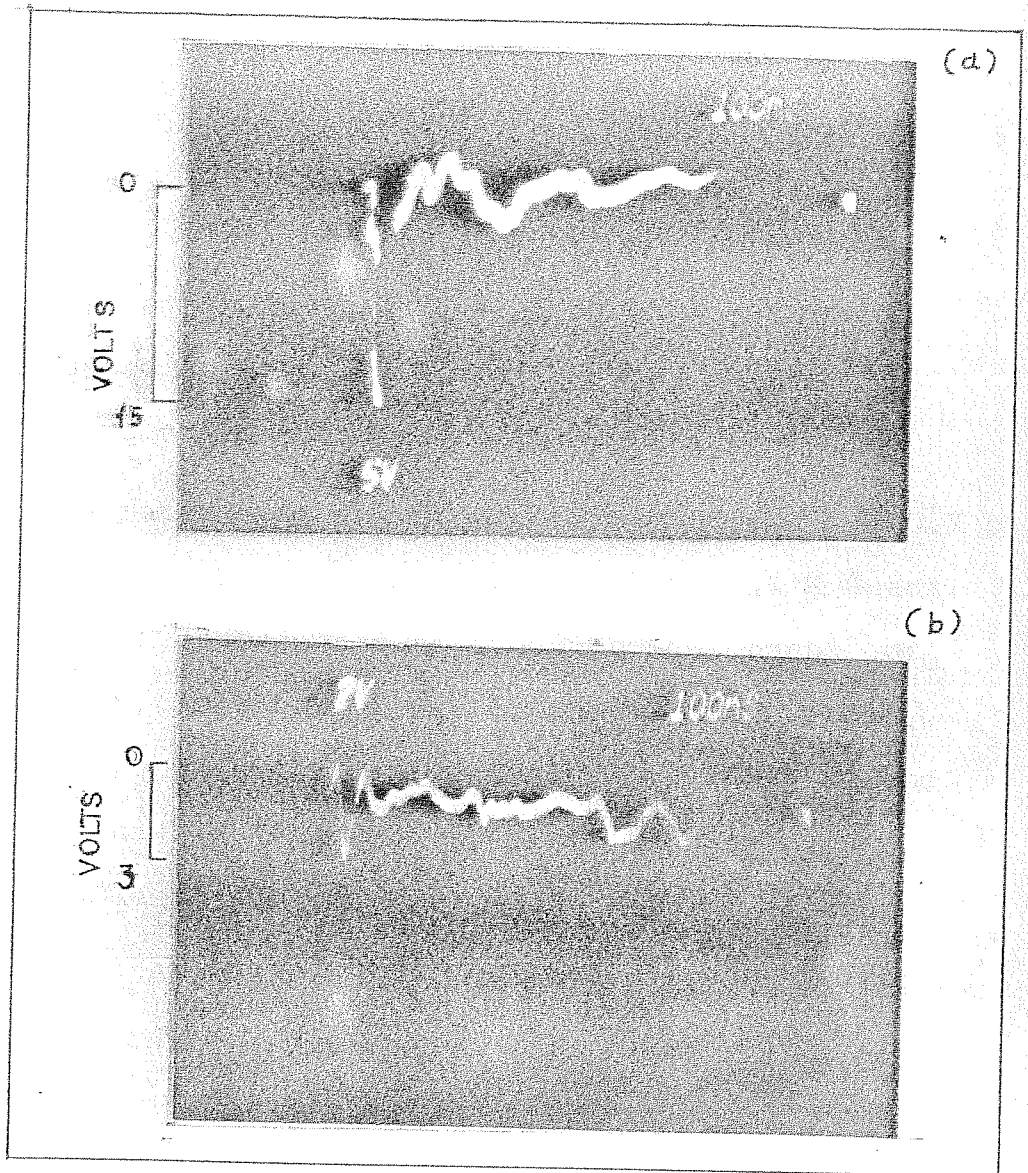


Figure 3.12 The oscillogramms of the electron beam probe output obtained at axial distances
 (a) $Z = 20.0$ cm (b) $Z = 105.0$ cm, from the cusp.

energy and radius of the beam, the beam does not propagate across the cusp magnetic field. This critical value of the magnetic field is given by

$$B_{\text{crit}} = \frac{\gamma m V_0 c \gamma}{e R} \dots\dots\dots(3.4)$$

in homogeneous region of the cusp field.

Here

R is beam radius

V_0 is beam's initial velocity

γ is relativistic mass factor.

For parameters in our experiments i.e. $V_0 = 0.7 c$, $R = 1.6 \text{ cm}$, $\gamma = 1.4$, the B_{crit} is equal to 1.1 K Guass. The experiments, conducted to study the dependence of transmission through the cusp on the magnetic field (figure 3.5) however, show a gradual decrease in the transmission when the magnetic field is increased above 840 Guass.

The difference between the experimentally observed and theoretically calculated critical magnetic field can be visualised by examining the assumption made while obtaining equation 3.4. It has been assumed that the electron beam particles are injected parallel to external magnetic field i.e. they do not have any azimuthal velocity to start with. But in case of an electron beam, injected with a finite initial $V_{\theta 0}$

the equation 3.4 needs a modification. In this case, the critical magnetic field is given by (Kapetanakis, 1974)

$$B_{\text{crt}} = \frac{m \gamma c}{q R} \left[(V_0^2 + V_{\theta 0}^2)^{1/2} - V_{\theta 0} \right] \dots \dots \dots (3.5)$$

It is seen from equation 3.5 that B_{crt} is smaller for a beam having finite initial azimuthal velocity in comparison with that of a beam with zero $V_{\theta 0}$. The initial azimuthal beam velocity could have resulted from the scattering of the beam by the anode foil having a finite thickness.

3.4.2 Cusp Transmission Enhancement

The principal mechanism responsible for low efficiency of particle transmission through a cusp magnetic field in vacuum is related to the collective effects, taking place in the vicinity of the cusp. As the beam electrons approach the cusp, they start gaining rotational velocity at the cost of a reduction in their axial energy. Due to this loss of axial energy at the cusp region, there will be an accumulation of the beam particles. This in turn builds up a space charge potential hill in the vicinity of the cusp and this potential hill scatters the beam particles, resulting in a loss of particles in the cusp.

The presence of a dielectric tube in the cusp region enables a considerable reduction of the loss of particles due to this space charge effects while passing through the cusp. The mechanism by which the enhanced transmission efficiency obtained, is as follows:

The beam is initially space charge limited and so the beam head strikes the side walls of the perspex tube. The charges accumulated on the surface of the dielectric tube could generate electric fields having a large component along the tube surface. These electric fields cause a surface breakdown resulting in a thin surface layer of the perspex getting sublimated or the adsorbed gas in the dielectric getting released and ionized, forming a background plasma in the tube. The plasma electrons would be repelled from the beam column, following the beam head, due to electrostatic repulsion, leaving behind stationary positive ions, which charge neutralise the rest of the beam and thus enhancing the transmission through the cusp.

The observation of a higher transmission efficiency with dielectric tubes during the first few shots and a subsequent decrease in the transmission to a stable value is in agreement with the experimental observations with laminar beams (Little et al., 1975).

This phenomena is attributed to desorption and ionisation of wall adsorbed gases by the beam. It should, however, be noted that in the present experiment, the background pressure is of the order of 10^{-5} Torr and the monolayer formation time for most of the atmospheric gases is of the order of 10^{-2} seconds. For water vapour, however, this time is much more than an hour. The time lag between two consecutive shots during the experiments was generally of the order of a few minutes. Thus it is most likely that water forms the bulk of the absorbed wall molecules and that the walls are not recharged between the consecutive shots to contribute significantly to the enhancement of the transmission after the first few shots.

Since the diameter of the perspex tubes were chosen to be larger than the final electron Larmor radius, one would expect the transmission efficiency to be independent of tube's diameter. However, experimental (Rhee and Destler, 1974) and numerical (Friedman, 1971, Bora and John, 1981) studies of single particle transport through a nonadiabatic cusp have shown that there is a radial translation of the particles at the cusp plane. Although it is difficult to estimate the radial translation due to the beam electric field,

it should be an enhancement over the single particle translation. Thus, it is likely that due to this radial translation, some of the rotating beam particles could be getting intercepted by the dielectric tube with the smallest diameter. This would explain the increase in the transmission with larger diameter tubes and a saturation in the transmission when the diameter is increased beyond a certain value.

3.4.3 Propagation Characteristics

Molvig and Rostoker's (1977 a) magnetic diffusion model has predicted the generation of angular return currents in addition to the usual axial return current. They have shown that the subsequent decay of these counter-flowing plasma currents can produce an efficient retarding force on the beam. The stopping length of the rotating beam thus calculated is:

$$\lambda_s = \frac{1}{2} \frac{n_p}{n_b} \left(\frac{v_{||}}{c} \right)^3 \frac{\gamma}{v_e}$$

where n_p is the plasma density, n_b is the electron beam density, $v_{||}$ is the axial plasma velocity and γ is the relativistic mass factor.

The collision frequency ν_e is a difficult parameter to measure during the interaction. Hence, it has been determined by comparing the rising part of

the observed diamagnetic loop signal with that of numerical calculations using a diffusion model (for details see next chapter). The value of v_e thus obtained is 10^7 sec^{-1} . For $n_p = 10^{13}$, $n_b = 10^{11}$, $v_{||} = 10^{10} \text{ cm/sec}$, $\gamma = 1.4$, the stopping length turns out to be a few meters, much longer than the length of the vacuum chamber, as confirmed by the experimental results.

The accumulation of the rotating electron beam near the end brass grid could be explained in the same way as in the case of E layer trapping using resistive rings in the ASTRON machine. It has been shown by Nebenzahl (1973) that a rotating electron beam, passing through a resistive ring, induces an azimuthal current in the ring and the fields produced by the induced currents interact with the beam electrons. The energy dissipation as heat in the resistive ring is at the cost of beam's axial energy alone while rotational energy of the beam remains unchanged. In the present experiments, when the rotating electron beam approaches the brass grid, angular counter currents are induced in the conducting grid. These induced currents interact with the beam and as a result the beam slows down and a piling up of the beam particles occurs.

CHAPTER IV

MAGNETIC RESPONSE OF THE PLASMA

This chapter describes the response of the mirror trapped plasma to the passage of a rotating relativistic electron beam through it. The spatial and temporal evolution of the two components of the return current - axial and azimuthal - have been extensively studied. The role of the mirror magnetic field in the evolution of these currents and their subsequent decay is also investigated. Numerical calculations of the plasma response to the rotating beam using a magnetic diffusion model are carried out and further, a comparison is made with the experimentally observed results.

4.1 EXPERIMENTAL SET-UP

The schematic of the experimental set-up along with the various diagnostics deployed and the magnetic field configuration are depicted in figure 4.1. The ranges in which the various experimental parameters were varied are listed in Table 4.1. Normally, the experiments were conducted with a hydrogen plasma of density $\approx 10^{12} \text{cm}^{-3}$ at the mirror minimum and with a magnetic field of 800 gauss at the mirror points. Diagnostics used during the experiments were a miniature Rogowskii coil, an electron beam probe and an array of spatially dispersed diamagnetic loops. In addition, an electron multiplier was used as a detector for fast radial ion or neutral flux.

The sequence of the experiment is as follows: Initially the pulsed electromagnetic gas valve is activated. After a delay of 3.0 msec, when the gas density in the plasma gun reaches its peak value, the gun is fired. The magnetic field condenser bank is discharged 2.0 millisecond prior to the gun, so that the magnetic field reaches its peak value at the time of plasma gun firing. The beam generator is put into operation 300 μ sec after the firing of the plasma when plasma density in the mirror minimum becomes equal to

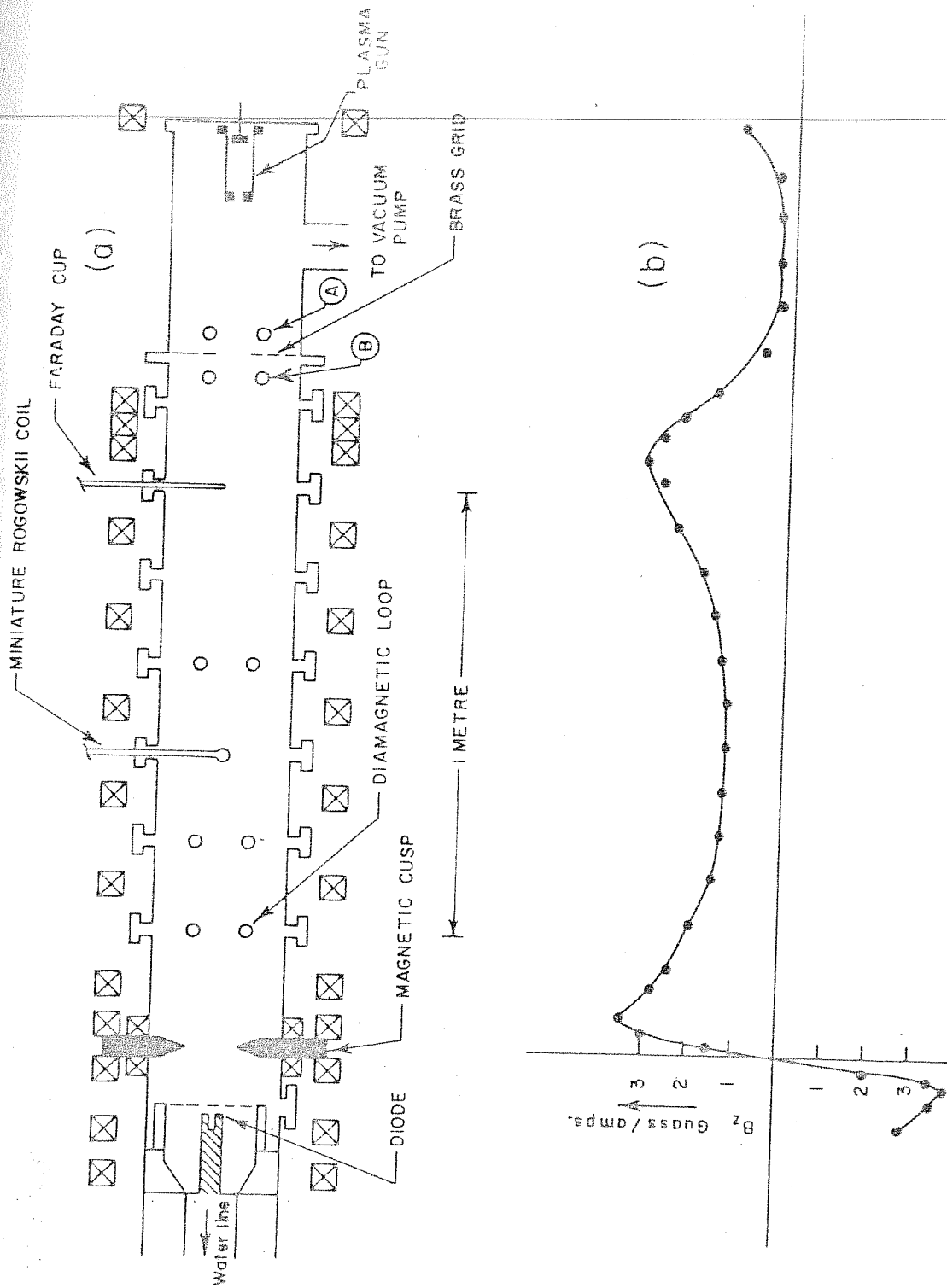


Figure 4.1 Schematic of the experimental set-up along with key diagnostics and magnetic field configuration.

Table 4.1

Experimental parameters for the rotating electron beam-
plasma interaction experiment

Beam Energy	200 - 250 KeV
Beam current	10 - 15 KA
Beam Parallel velocity	$= 10^{10}$ cm/sec
Beam perpendicular velocity	$= 1.8 \times 10^{10}$ cm/sec
Beam outer radius	$= 2.0$ cm
Beam annular thickness	$= 0.7$ cm
Magnetic guide field at mirror point	500 - 1500 gauss
Plasma temperature	5 - 10 eV
Plasma density	$10^{11} - 10^{13}$ cm ⁻³

10^{12} cm^{-3} . The signals from the various diagnostic elements are recorded with the help of Tektronix storage oscilloscopes situated inside a shielded room and triggered by the diode current signal.

4.2 EXPERIMENTAL RESULTS

4.2.1 Net Axial Currents

A miniature Rogowskii coil deployed at 65.0 cm from the cusp plane and at a radial distance of 20 mm from the axis, was used to measure the net currents. It's axis was oriented parallel to that of the system so as to enable it to register the axial component of the net currents. Pulse duration of the rotating relativistic electron beam injected into the plasma column of density 10^{12} cm^{-3} was 100 nanoseconds, as shown in figure 4.2 a. Figure 4.2 b depicts a typical net axial current monitored by the Rogowskii coil. A positive signal corresponds to currents, flowing in the same direction as that of the beam propagation. In the figure, the net axial current peaks at 100 n sec, with a current density equal to 100 Amps/cm^2 . It is also seen that a substantial part of this current lasts for nearly 300 nsecs, much longer than the beam duration. This indicates that after 100 nsec, the signal registered

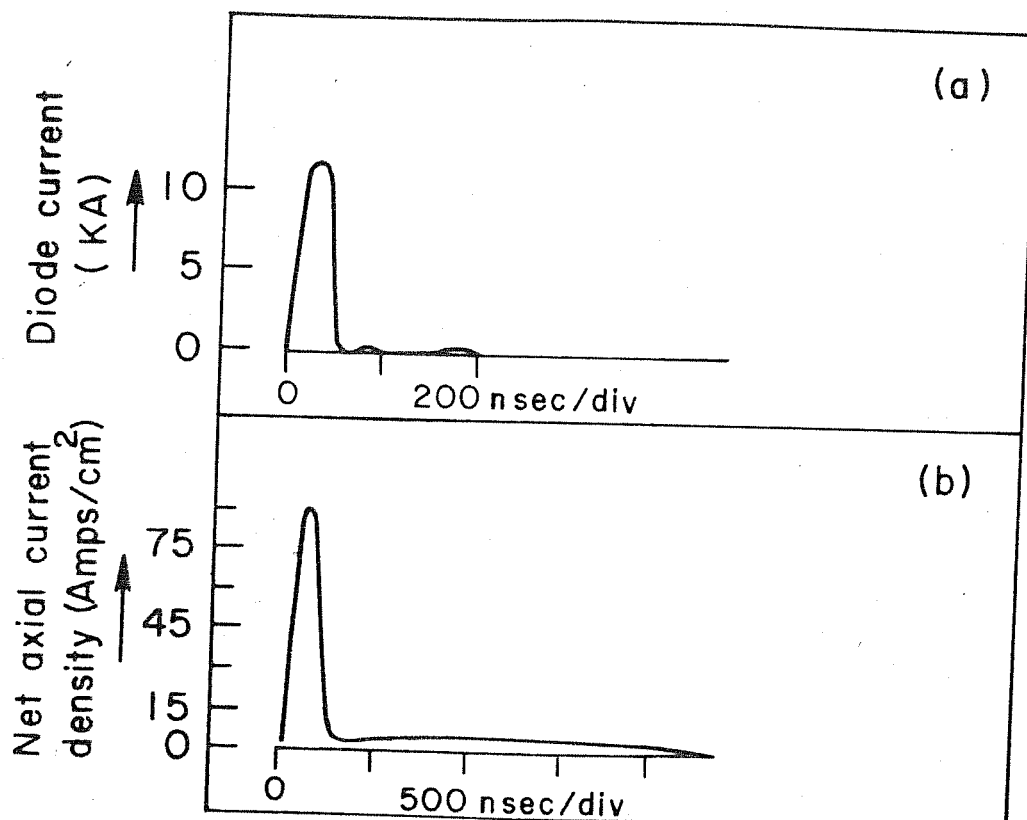


Figure 4.2 (a) A typical beam current signal
(b) Net axial current density as function
of time obtained at 20 mm radial position,

by the Rogowskii coil is caused by the axial return currents established in the system by the beam passage.

The radial profile of the net axial current was obtained by moving the Rogowskii coil along the radius. Figure 4.3 shows the radial dependence of peak values of the signals registered by the Rogowskii coil. The net axial current has a maximum value at a distance of 20 mm away from the axis. In addition some finite current also exists at distances of 90 mm away from the axis. This suggests that the axial return current is localised at distance of 20 mm away from the axis. It was observed that the time evolution of the net axial current does not change significantly along the radius.

4.2.2. Net Azimuthal Currents.

During the net azimuthal current measurements, the experimental parameters were maintained in the same range as in the case of net axial current measurements. The Rogowskii coil was placed 65.0 cm away from the cusp plane and at a radial distance of 20 mm from the axis. The Rogowskii coil was placed such that it's axis was perpendicular to that of the system. Figure 4.4 shows the time evolution of the net azimuthal current registered by the coil for three different time scales.

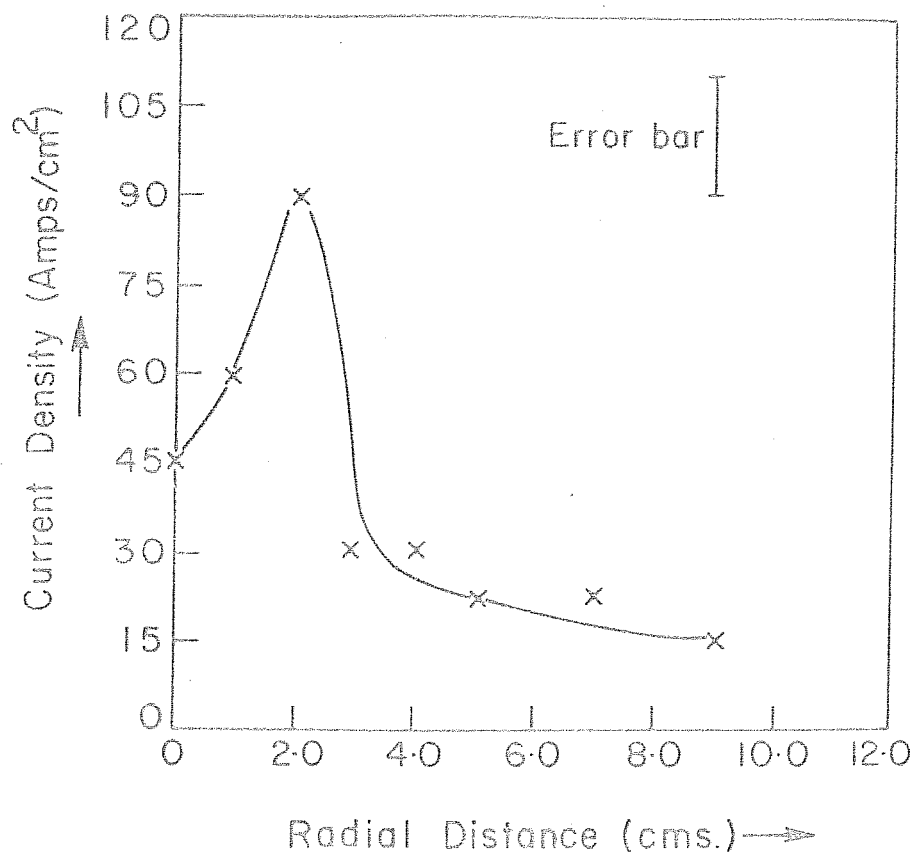


Figure 4.3 Radial profile of the net axial current density.

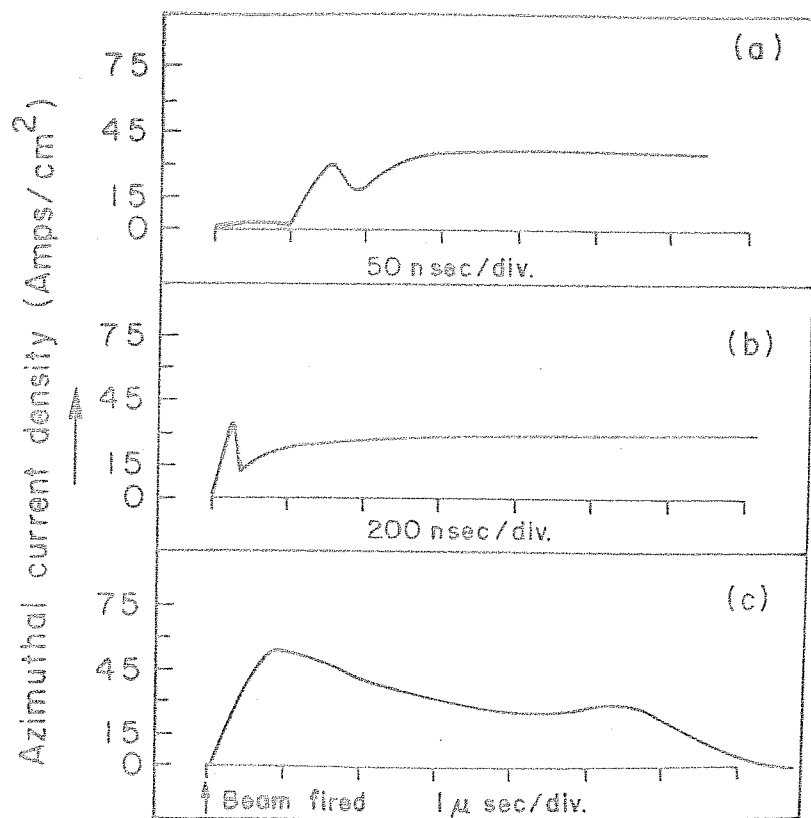


Figure 4.4 Time evolution of the net azimuthal current.

A positive signal in this case corresponds to a net azimuthal current flowing in the same direction as that of the beam rotation. The net azimuthal current appears only 50 nsec after the firing of the beam and attains a peak value of 60 Amps/cm^2 . The absence of any appreciable current signal during the first 50 nsec, indicates that azimuthally the beam is current neutralised to a good extent. The later part of the net azimuthal current signal is due to the azimuthal return current induced by the rotating electron beam. The net azimuthal current signal lasting for nearly $6 \mu\text{secs}$ shows a diamagnetic behaviour throughout. From the temporal profile, we observe that the net azimuthal current goes through a second maximum after a time delay of $4.5 \mu\text{sec}$ from the first maxima. In order to verify whether the observed maxima are due to the existence of any natural mode, the experiments were repeated varying the plasma density and the magnetic field. However, it was observed that the time difference between the two peaks remains unaltered in the density range $10^{11} - 10^{13} \text{ cm}^{-3}$ and in magnetic field range 500 - 1200 gauss. This rules out the possibility of the observed oscillatory behaviour being connected with any mode of the plasma. As in the case of the net axial current, the net azimuthal current is also

localised at a radial distance of 20 mm from the axis, as seen from the figure 4.5.

A comparison of figure 4.4. with 4.2 b shows that the net axial current builds up faster and also decays more rapidly, compared to the net azimuthal current, which rises slowly and decays at a still slower rate. Further, the amplitude of the net axial current is more than that of the net azimuthal current, however, the decay time of the former is shorter by an order of magnitude.

In order to study the net currents flowing in the intermediate positions, the Rogowskii coil placed at 20 mm from the axis in the mirror minimum region was rotated in steps of 30° from $\Theta = -90^\circ$ to $\Theta = +90^\circ$, where Θ is the angle between the system axis and the Rogowskii coil axis. For each position, four to five shots were fired and the average peak amplitude and the signal decay time (defined as the e folding time) are plotted against the angle Θ as shown in figures 4.6 and 4.7 respectively. The net current signal increases initially when the angle Θ is increased from $\Theta = -90^\circ$, reaches a maximum value at $\Theta = 0^\circ$ and decreases when Θ is increased to $+90^\circ$. On the other hand, the decay time of the signal shows a reverse tendency i.e.

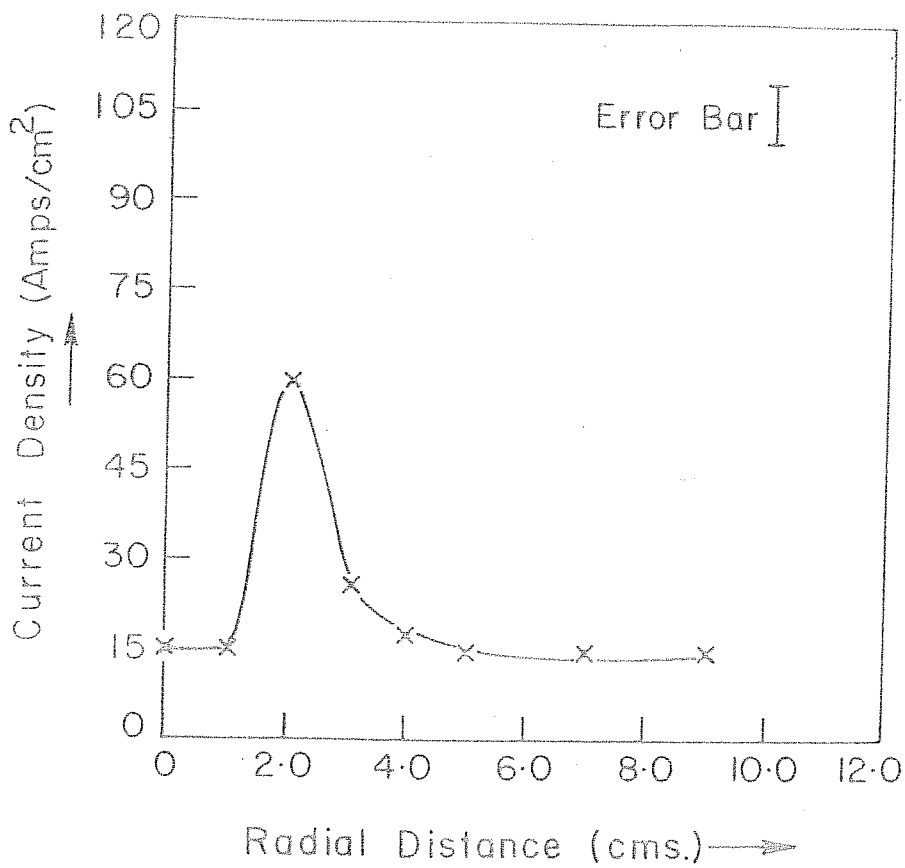


Figure 4.5 Radial distribution of the net azimuthal current density.

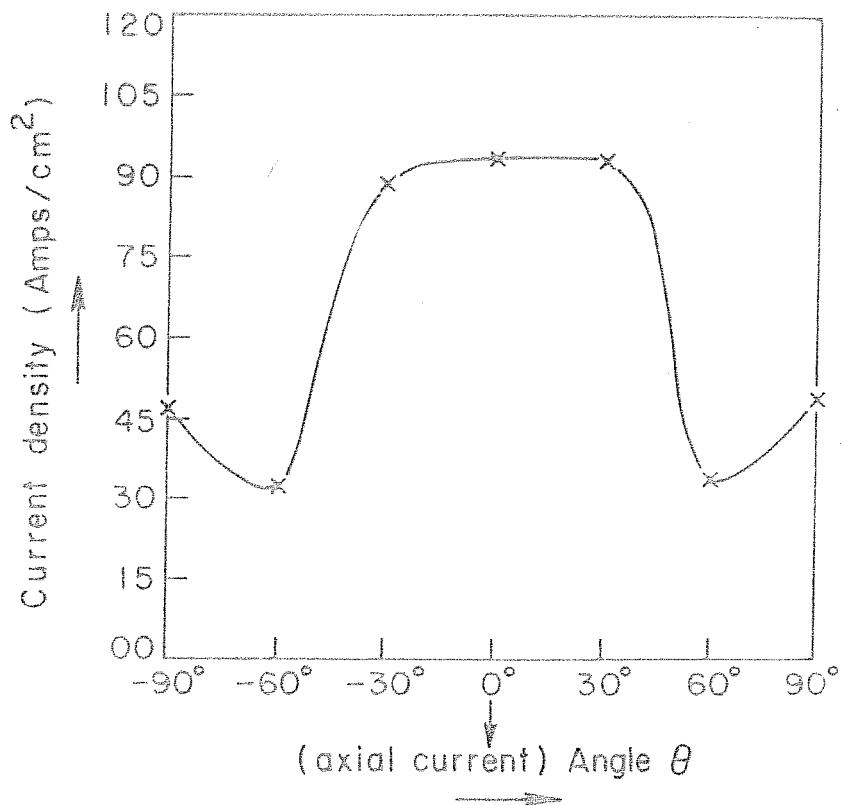


Figure 4.6 Net current density vs. Angle θ

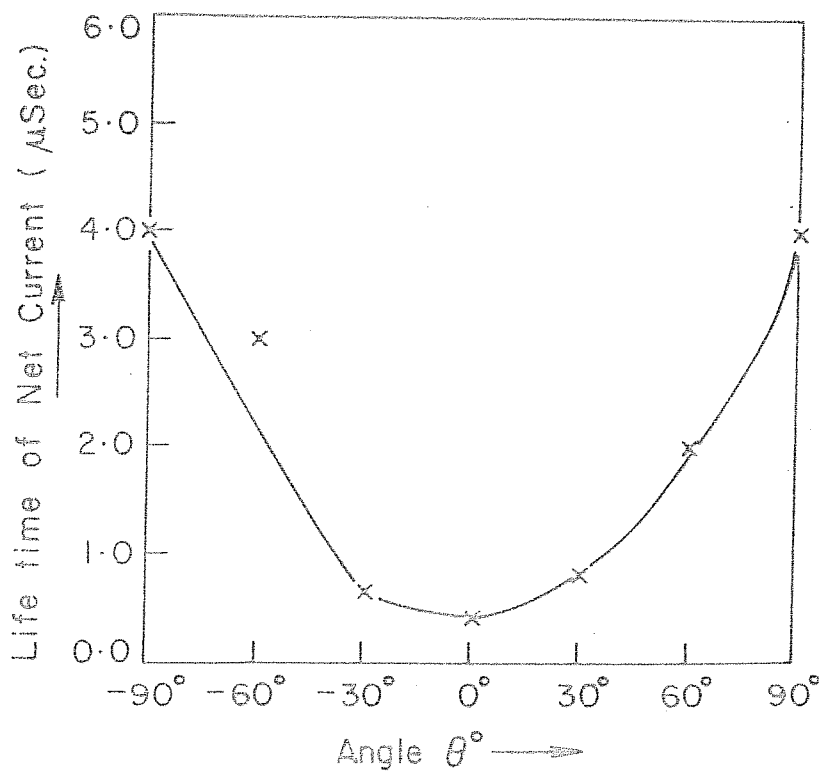


Figure 4.7 Dependence of the decay time of the net current on the angle θ

a minimum . around $\Theta = 0^\circ$. It is seen from these figures that the signal amplitude and the decay time show a symmetric behaviour around $\Theta = 0^\circ$.

4.2.3 Induced Axial Magnetic Field

Knowing the net azimuthal current density at various points along the radius, the radial profile of the induced axial magnetic field ΔB_z is obtained, as shown in figure 4.8. We see from this figure that the induced axial magnetic field is diamagnetic up to a distance of 25 mm from the axis, having a peak value of 140 gauss. This value of ΔB_z , obtained in the mirror minimum region corresponds to a reduction of external magnetic field by 45%. The induced axial magnetic field changes polarity i.e. becomes paramagnetic after a distance of 25 mm from the axis. The peak paramagnetic field observed is found to be very small as compared to the diamagnetic field.

4.2.4 Trapped Return Current Layer

The diamagnetic loops, placed at different axial distances along the path of the beam within and outside the mirror region, were used to study the spatial dependence of the induced axial magnetic field. The output from each loop was recorded on the storage oscilloscope

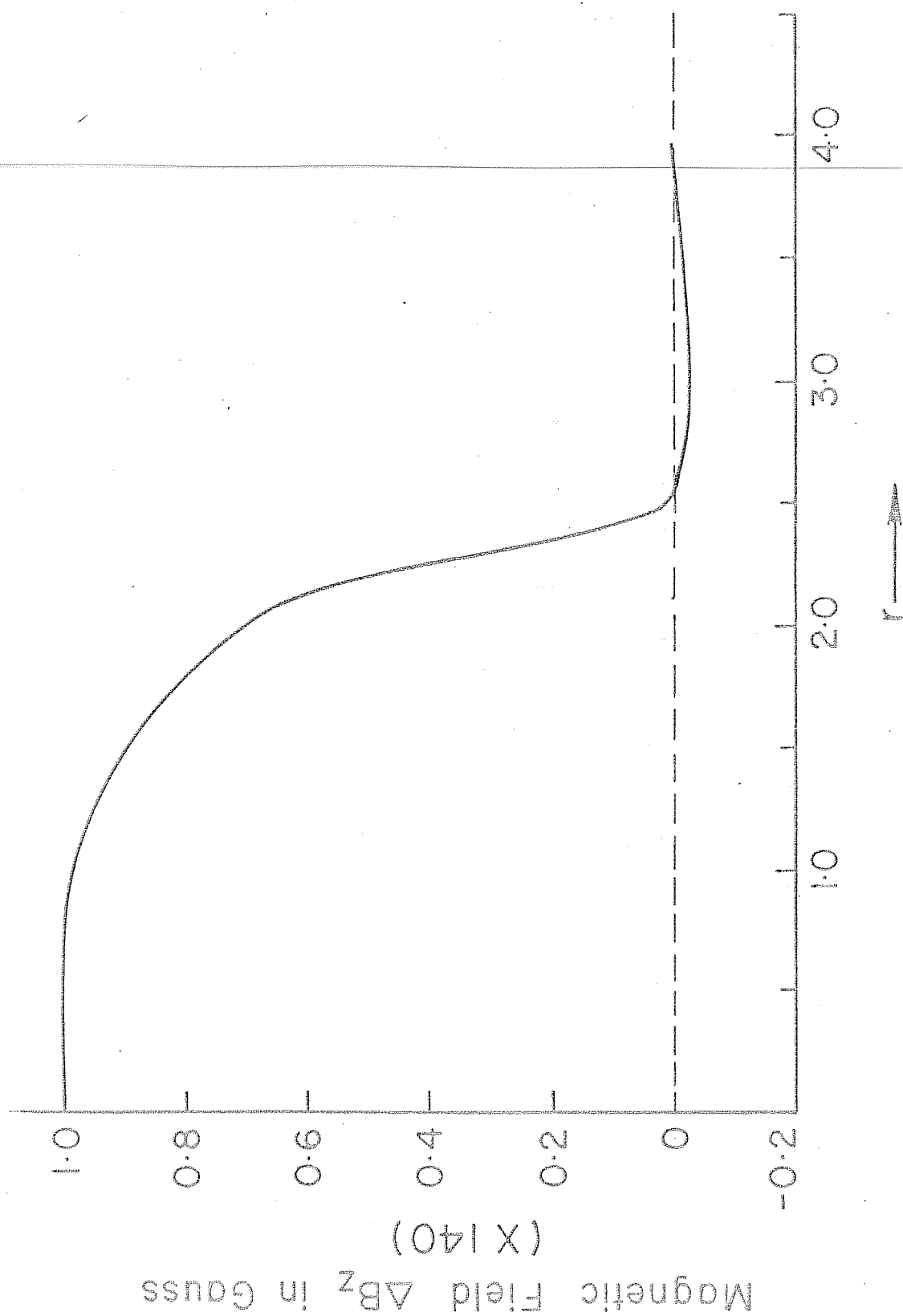


Figure 4.8 Radial profile of the induced axial magnetic field.

as a function of time and later combined together to obtain the spatial and temporal dependence of the magnetic perturbations. The shot to shot variations, common in the intense pulse beam experiments, were taken care of by using the signal from the loop, located at the mirror centre, as a standard. The magnetic perturbations at the center of the mirror region reaches its maximum value in 100 nsecs and then decays slowly (figure 4.9). The peak value of the induced axial magnetic field intergrated over the area of the loop as recorded by the diamagnetic loop was found to be 42 gauss. For the plasma densities in the range 10^{11} - 10^{13} cm⁻³, the signals from the diamagnetic loops do not show any oscillatory behaviour, in agreement with the earlier experimental observations (Kapetanakis et al. 1973, Roberson 1978).

The signal registered by the diamagnetic loop could have been caused by three different processes. It can be (i) due to the trapped particles of the rotating electron beam (ii) a result of plasma heating or (iii) due to the magnetic field generated by the net azimuthal return current. As it was already explained in the last chapter, the significant part of the rotating electron beam current lasts only for about 100 nsecs in the mirror

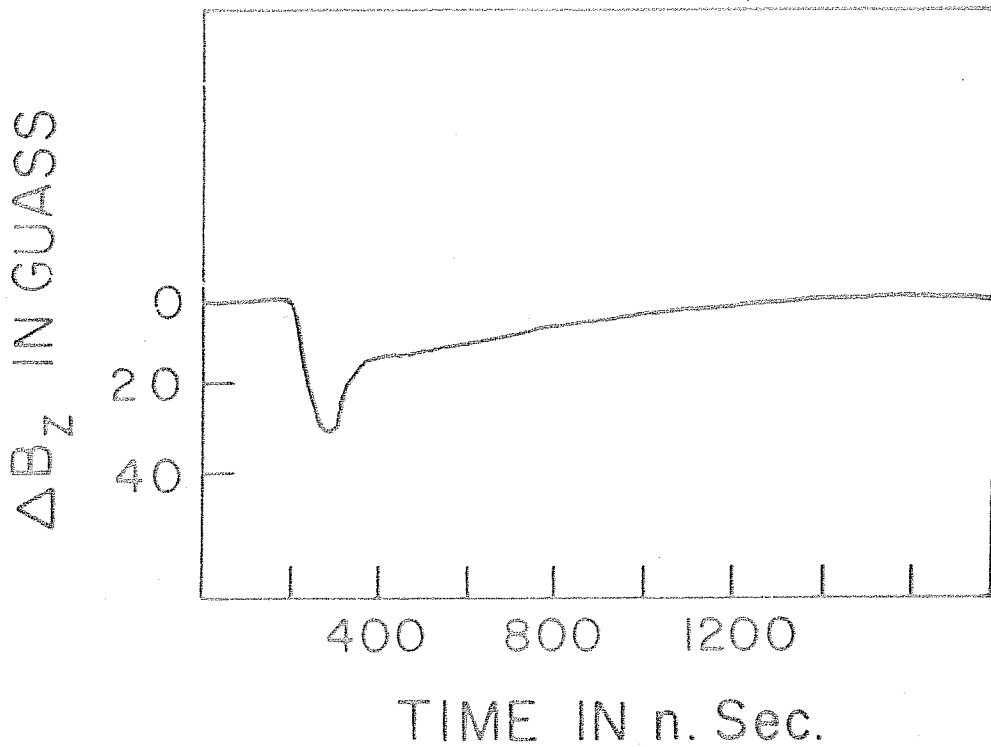


Figure 4.9 A typical diamagnetic loop output showing the magnetic perturbation at the mirror center as a function of time.

region and therefore the rotating electron beam particles cannot be contributing in a significant manner to the loop signal. A further verification of this conclusion was made by introducing the diamagnetic loop and the electron beam probe which drain off any trapped beam particle, simultaneously in the interaction region. The absence of any change in the diamagnetic loop signal even in the presence of the electron beam probe, rules out the possibility of the diamagnetic loop signal being caused by any trapped beam particles.

As seen from section 4.2.2, there are significant currents flowing in the azimuthal direction, which in turn produces an induced magnetic field in the axial direction. With the help of the radial profile of this induced axial field as shown in figure 4.8, we have calculated the contribution to the loop signal due to the azimuthal current alone. The contribution to the loop signal by the azimuthal currents was calculated by integrating the induced axial magnetic field ΔB_z over the area of the loop. The calculated integrated induced magnetic field comes out to be equal to 36 gauss, which is 85% of the registered diamagnetic loop signal. This shows that most of the loop signal is caused by the net azimuthal current.

The rest of the signal, unaccounted by the azimuthal currents, is attributed to the heating of plasma by the rotating electron beam. The value of $nk(T_e + T_i)$, calculated from these considerations is found to be $\sim 3 \times 10^{15} \text{ eV/cm}^3$. The above calculations, showing the contribution of the azimuthal return currents to the signal registered by the diamagnetic loop, clearly indicates that the interpretation of the diamagnetic signal as being solely due to the plasma heating is incorrect as has been done in the earlier rotating electron beam-plasma interaction experiments (Kapetanakis et al. 1973, Roberson 1978).

The signals obtained from the various spatially dispersed diamagnetic loops, show the following significant aspects (figure 4.10); During the rotating electron beam passage, the entire plasma column shows a diamagnetic behaviour caused by the azimuthal return current. In about 100 nanoseconds after the beam injection, the observed signals all along the chamber start decreasing. After 300 nanoseconds, the diamagnetic loop signal at the cusp plane and at the end brass grid, both the points being situated outside the mirror region, reduces to zero, while the diamagnetic loop signals in the mirror region are still significant. The signals in the

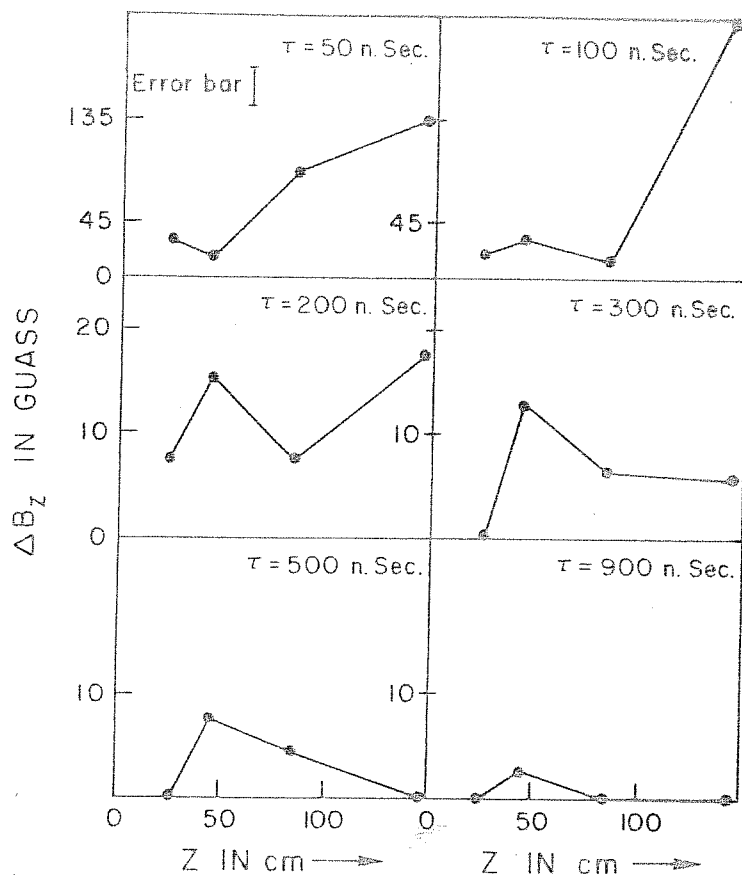


Figure 4.10 The spatial behaviour of magnetic perturbation at different intervals of time. The horizontal axis represents the distances marked from the cusp plane. The mirror center is at 70 cms, the grid wall is at 155 cms.

mirror region last for times of the order of a micro-second. Experiments conducted with an axially movable diamagnetic loop show that the region, where the diamagnetic loop signals persist for a long time, is about 60 cm long and is situated symmetric about the midplane of the mirror i.e. between the two mirror points. From these experiments we conclude that the azimuthal return currents, produced by the beam passage through the plasma, get decoupled from the two ends of the chamber and persist in the centre of the mirror, thus forming a mirror trapped return current layer. As time progresses, the spatial extent of the return current layer starts reducing i.e. the layer starts shrinking axially.

The dependence of the azimuthal return current on the plasma density was studied, by firing the beam generator at different time delays with respect to the plasma gun discharge, thus corresponding to different plasma densities. The plasma density attains a peak value of 10^{13} cm^{-3} at time delay of $200 \mu \text{ sec}$. For delays smaller or larger than $200 \mu \text{ sec}$, the plasma density decreases. From figure 4.11, we observe that with a decrease in the plasma density, the strength of the azimuthal current also decreases. The value of

the induced axial magnetic field obtained from the diamagnetic loop signal is about 48 gauss at $n_p = 10^{13} \text{ cm}^{-3}$ and 8 gauss at $n_p = 10^{11} \text{ cm}^{-3}$. Further, the dependence of the diamagnetic loop signal on the external magnetic field at the mirror center was also studied. As shown in figure 4.12, the loop signal peaks at a value of ~ 900 gauss at the mirror point which corresponds to the observed cusp cut-off magnetic field, for 200 keV REB in vacuum.

4.2.5. Scaling Laws for Azimuthal Return Current Decay

An important aspect of the rotating electron beam-plasma interaction studies is the investigation of the process by which the azimuthal return current decays. A series of experiments were conducted to study the decay behaviour of the observed diamagnetic loop signal, at the mirror center, under different experimental conditions. The decay time of the loop signal is found to be independent of plasma density in the range $5 \times 10^{11} - 10^{13} \text{ cm}^{-3}$ and the external magnetic field in the range 600 - 1200 gauss. It is observed that in the case of hydrogen plasma the diamagnetic loop signal decays in about $1.2 \mu\text{sec}$.

According to Chu and Rostoker's magnetic diffusion model, the net space charge established in the

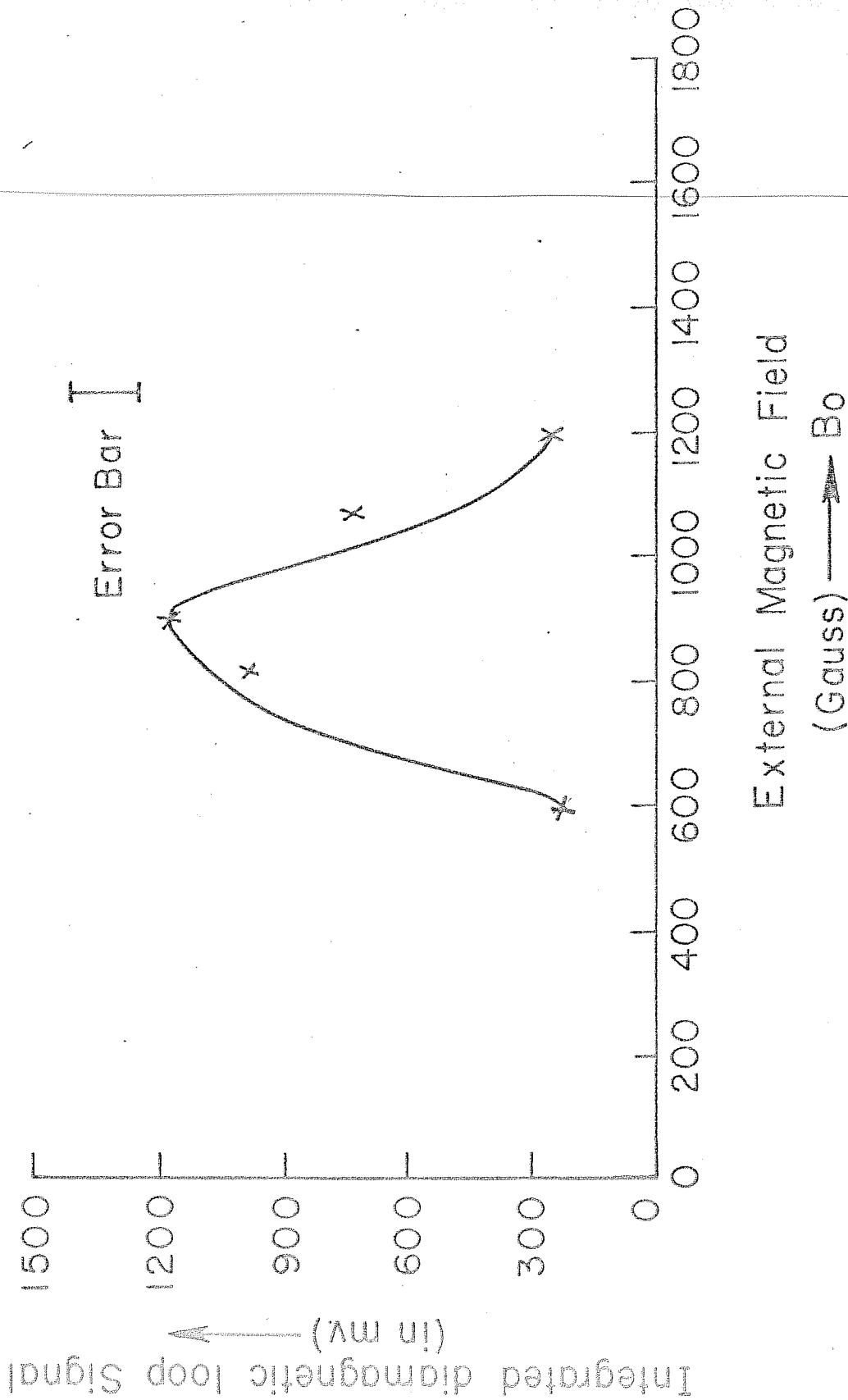


Figure 4.12 Dependence of the peak diamagnetic loop on the external magnetic field. The horizontal axis represents the field at the mirror point.

radial direction sustains the azimuthal return current. This space charge, however, is subject to neutralisation by the radial flow of plasma particles, which can result in the decay of the azimuthal return current. Because of the low collision frequency in comparison to the cyclotron frequency, the plasma electrons drift azimuthally rather than flowing radially under the influence of the radial electric field E_r . On the other hand the ions, little affected by the magnetic field may get accelerated in the radial direction, thereby shortening E_r . In this case, the decay time of the azimuthal return current should depend upon the ion mass. In order to verify whether the azimuthal return currents are caused by E_r , experiments were performed with different gases in the plasma gun. The weak dependence of the decay time of the loop signal with plasma ion mass is seen, as is evident from Table 4.2. The maximum value, of decay time for hydrogen plasma is 1.2μ sec whereas for argon and neon plasma, it is 0.7μ sec.

Since the experimental observations show that the azimuthal return current layer persists in the mirror for a time much longer than the beam pulse duration, experiments were conducted to study the effect of the mirror magnetic field on the decay time of these return currents. For this purpose the magnetic mirror near

Table 4.2

Observed decay time of the diamagnetic loop signal for
different plasma species

<u>Plasma</u>	<u>Decay time (μ sec)</u>
Hydrogen	1.2
Nitrogen	1.0
Argon	0.7
Neon	0.7

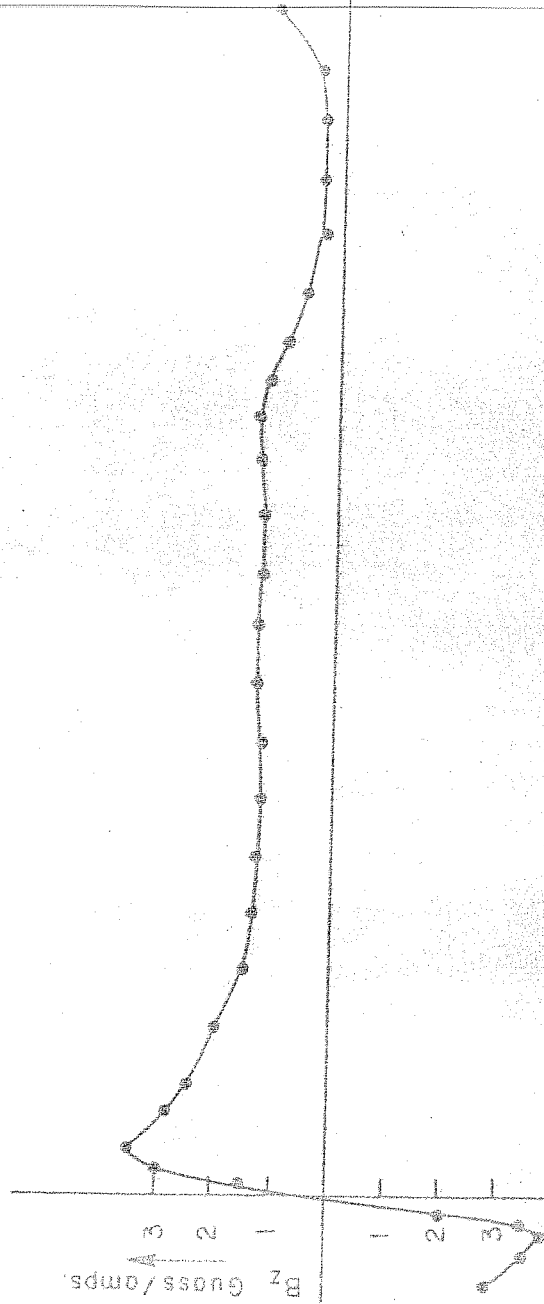


Figure 4.13 Magnetic field configuration with reduced mirror ratio near the plasma gun end.

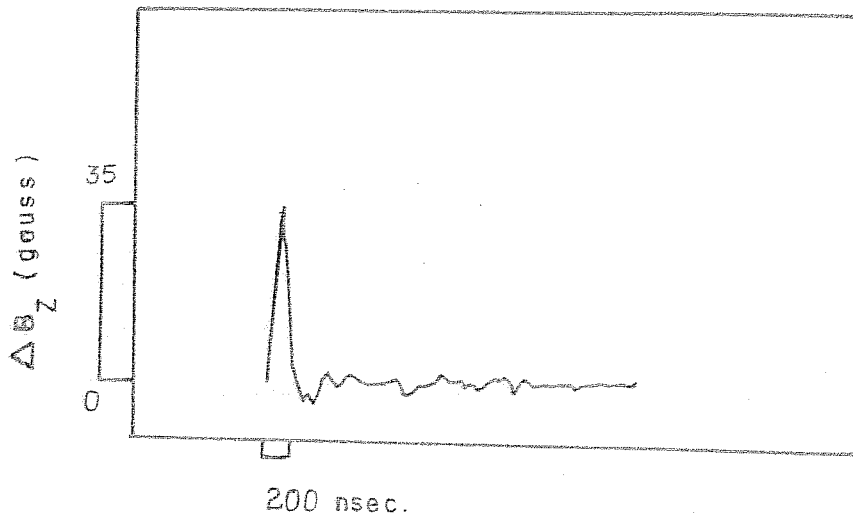


Figure 4.14 The output from a diamagnetic loop located at the mirror center, when mirror field near the gun was lowered.

the plasma gun was lowered by shorting a few coils of the magnetic field assembly, as shown in figure 4.13. When the magnetic mirror ratio on the gun side was lowered from 2.6 to 1.2, it was observed that the decay time of the diamagnetic loop signal reduced to 200 nsec (figure 4.14) from 1.2 μ sec. The rapid decay of the diamagnetic loop signal observed with the reduced mirror ratio clearly shows the important role of the mirror field in trapping the azimuthal return currents.

4.3 NUMERICAL STUDIES ON THE MAGNETIC RESPONSE OF THE PLASMA.

A numerical study of the magnetic response of the plasma to the rotating relativistic electron beam has also been carried out using a magnetic diffusion model. Since radial plasma oscillations are not observed in the present experiment, the use of a diffusion model is justified.

The beam current has been modeled as an infinitely long, thin annular current sheet of radius 20 mm embedded in a cylindrical plasma column of radius 40 mm. Following assumptions have been made to simplify the calculations.

- i. The system is infinitely long and axisymmetric i.e.

$$\frac{\partial}{\partial \theta} = \frac{\partial}{\partial z} = 0 \quad \dots\dots(4.1)$$

- ii. Displacement current is neglected.
- iii. The azimuthal current density $J_{\theta}(\gamma, t)$ in the plasma is proportional to the azimuthal component of the electric field by the relation

$$J_{\theta}(\gamma, t) = \sigma^* E_{\theta}(\gamma, t) \quad \dots\dots(4.2)$$

Where σ^* is an effective conductivity which is independent of space and time.

The return and net azimuthal currents which are proportional to E_{θ} and B_z respectively, are obtained by solving diffusion equation for vector potential A_{θ} , obtained from Maxwell's equation and Ohm's law i.e.

$$\frac{\partial}{\partial \gamma} \frac{1}{\gamma} \left(\frac{\partial}{\partial \gamma} \gamma A_{\theta} \right) - \mu \sigma^* \frac{\partial A_{\theta}}{\partial t} = 0 \quad \dots\dots(4.3)$$

and then introducing A_{θ} into equations

$$B_z = \frac{1}{\gamma} \frac{\partial}{\partial \gamma} \gamma A_{\theta}$$

$$E_{\theta} = - \frac{\partial A_{\theta}}{\partial t}$$

The integrated signal from a diamagnetic loop enclosing the plasma column and having 80 mm diameter is obtained by integrating the magnetic field B_z over the plasma cross section. Details of the procedure adopted to obtain the solution of equation for A_{θ}

is given in the paper by Striffler and Kapetanakis (1975). A beam current pulse $I(t)$, resembling the one observed in the experiment (figure 4.15) is used while solving diffusion equation 4.3.

4.3.1 Numerical Results

The azimuthal electric fields E_θ is plotted as a function of time for various values of plasma conductivities t_d ($\sim \mu \sigma a^2$ where μ is permeability, σ is plasma conductivity and a is plasma radius), in figures 4.16 and 4.17 at four radial positions. In these figures, t_d and t are normalised with respect to the beam current pulse duration τ . At $R = 2.0$ cm which corresponds to the beam radius, we observe that for low plasma conductivities, there is a large induced electric field during the rise and fall of the beam current pulse. The amplitude of E_θ decreases rapidly with an increase in conductivity. There is a change in the direction of E_θ and hence, that of the return current, when the beam leaves the system. The negative values of E_θ correspond to the flow of azimuthal return currents in a direction opposite to that of the beam rotation and vice-versa for positive values.

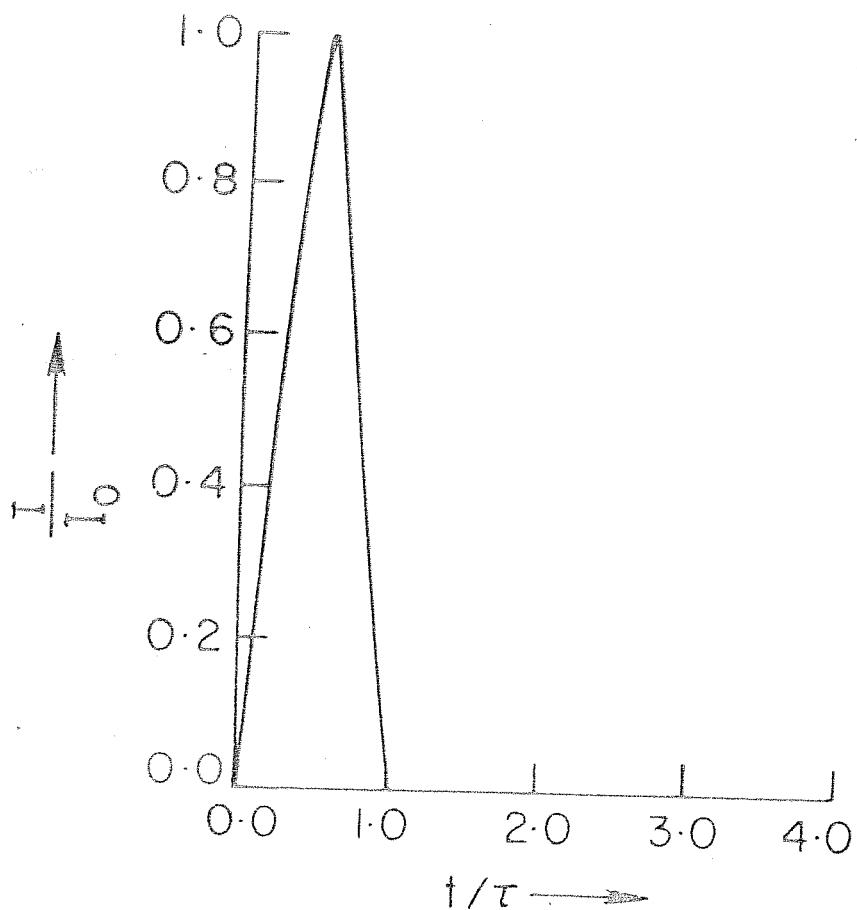


Figure 4.15 The beam current pulse waveform used for obtaining the numerical response.

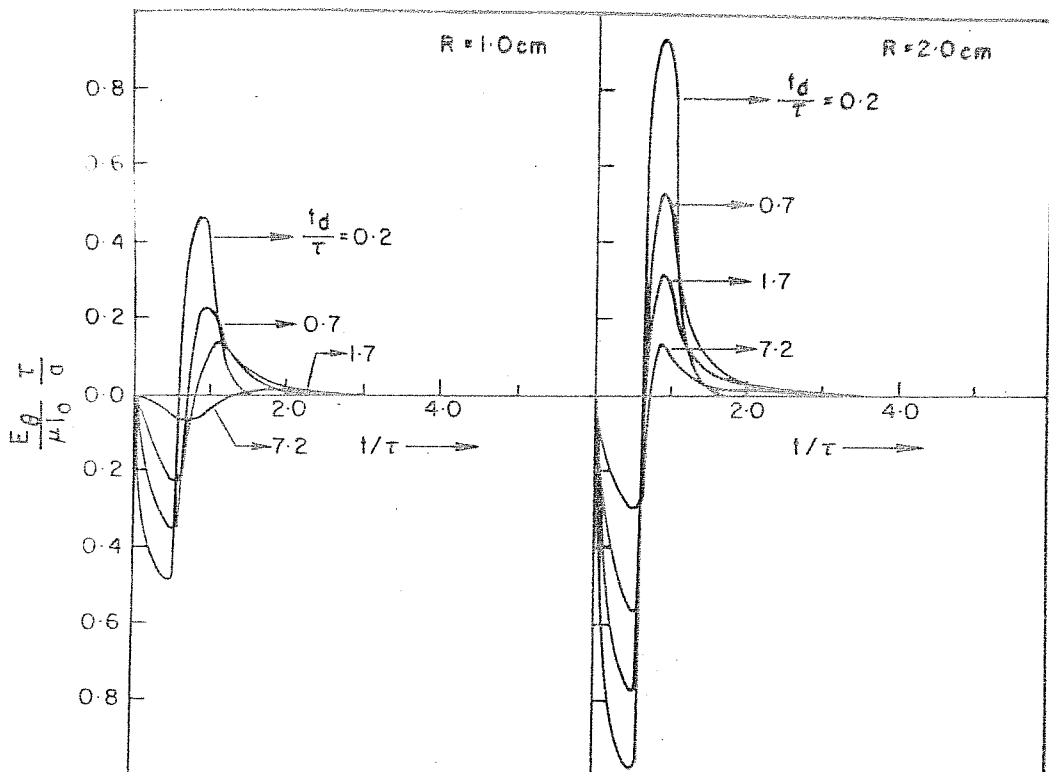


Figure 4.16 Azimuthal electric field as function of time for different conductivities within the beam radius.

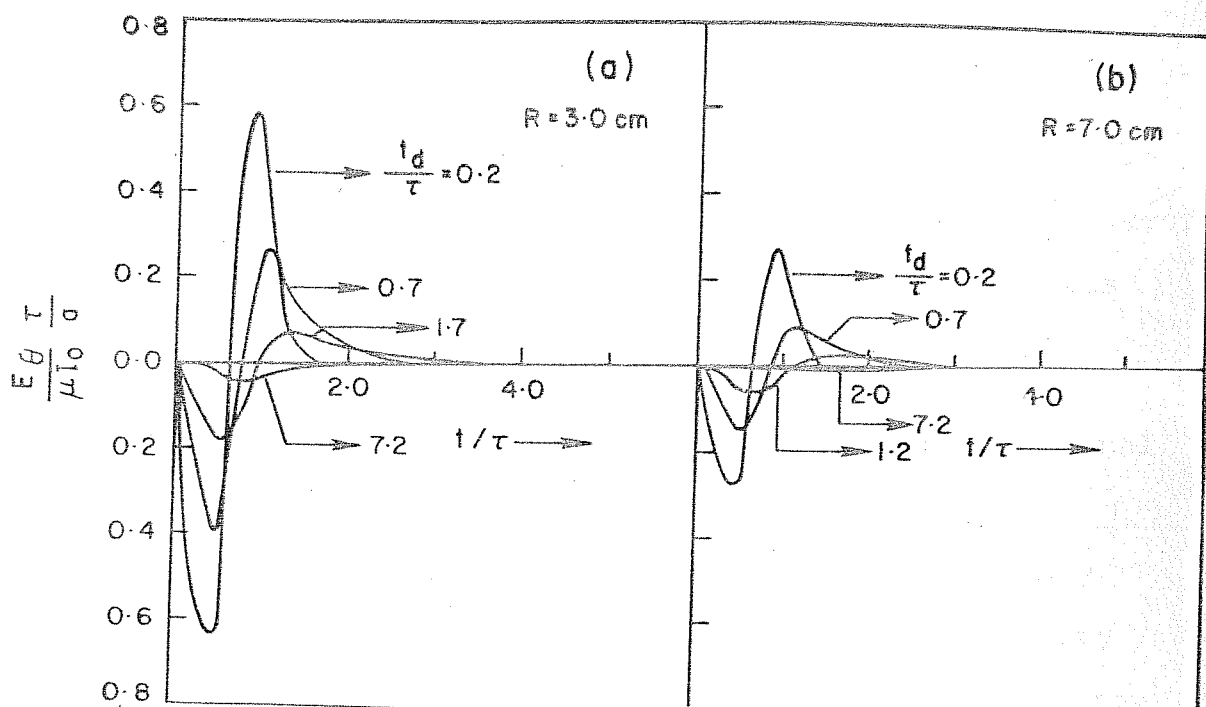


Figure 4.17 Azimuthal electric field as function of time for different conductivities outside the beam radius.

The time dependence of E_{θ} , obtained for various values of R and conductivities t_d , shows that, unlike the case at $R = 2.0$ cm where the E_{θ} reaches the maxima at the same instant of time for different values of conductivity, at other radial positions the maxima appear with increasing time delay with an increase in the conductivity. It is also observed from figure 4.18 that when the conductivity is increased to higher values, E_{θ} and as a result the azimuthal return current gets localised mainly to the radial position of the beam.

The induced axial magnetic field B_z proportional to the net azimuthal return current is plotted as a function of time for various values of t_d along the axis, as shown in figure 4.19. For zero conductivity the magnetic field is identical in shape to that of the beam pulse. The amplitude of B_z decreases with an increase in the conductivity. When the conductivity is increased above certain value, we notice that the maximum of the magnetic field occurs after the beam pulse is over. The decay time of the induced magnetic field also increases with an increase in the conductivity. At $R = 1.0$ cm, the magnetic field is always diamagnetic as in the case, at the axis. However, at positions beyond the beam radius, for

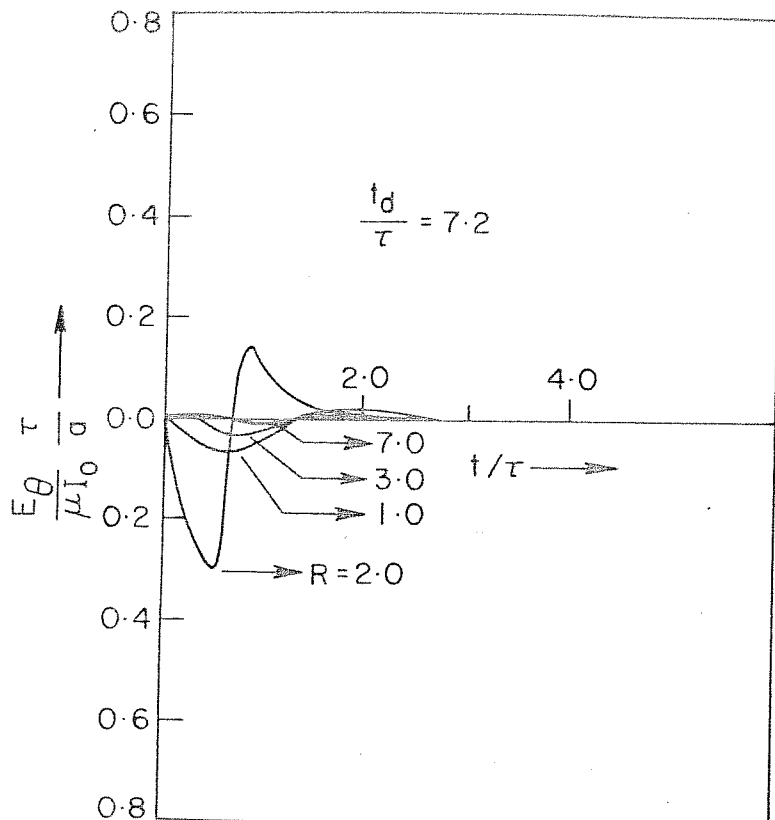


Figure 4.18 Temporal variation of the azimuthal electric field for different radius.

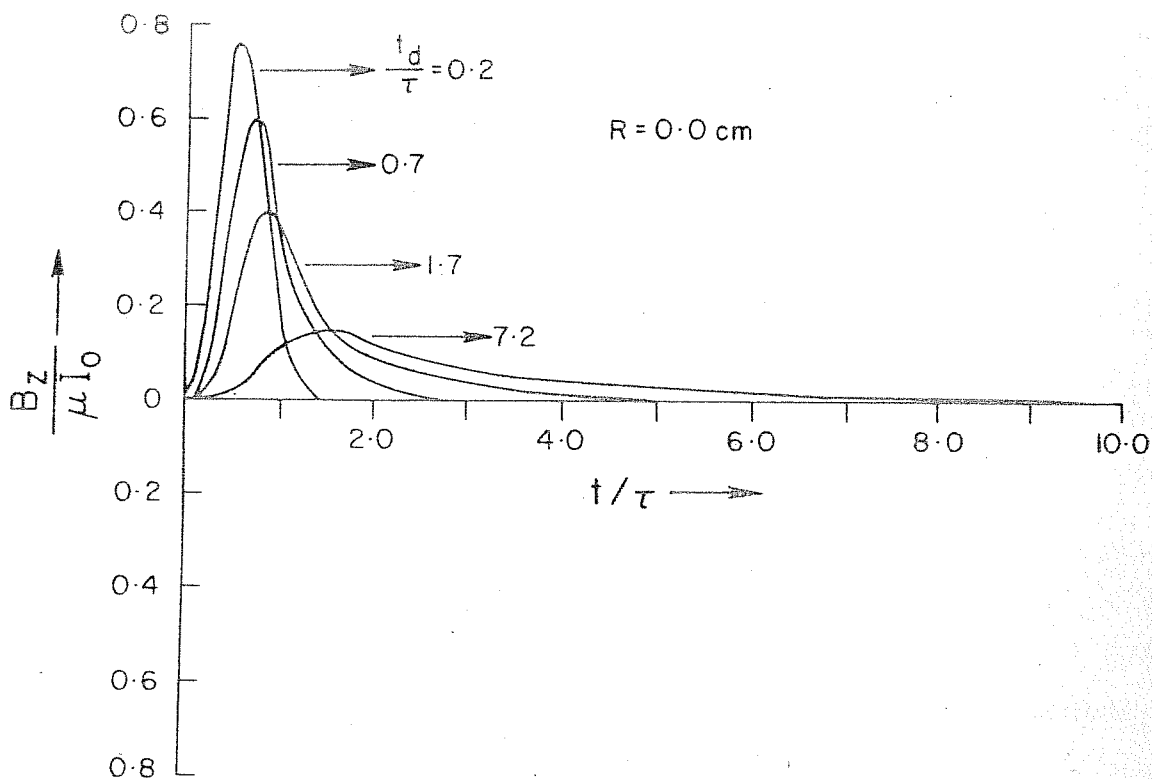


Figure 4.19 Induced axial magnetic field at the axis

example at $R = 3.0$ cm, the magnetic field is paramagnetic during a substantial portion of the beam pulse and becomes diamagnetic during the falling time of the pulse, as shown in figure 4.20.

In figure 4.21, the normalised output of a diamagnetic loop, enclosing the plasma column, is plotted as a function of time for different plasma conductivities. The peak amplitude of the loop signal decreases with an increase in the conductivity. On the other hand, the decay time of the loop signal is found to increase with the conductivity.

4.3.2 Comparison with Experimental Results

A comparison of these results with the experimental observations shows a qualitative agreement at radial positions between the axis and the beam radius i.e. both numerical simulation and the experiment show a diamagnetic behaviour. However, for positions more than 20 mm radially away from the axis, there is a distinct difference, while the experiments show a paramagnetic behaviour, the numerical results predict a paramagnetic behaviour only during the initial stages which continues up to the moment when the beam leaves the system and at later instants exhibits a diamagnetic behaviour.

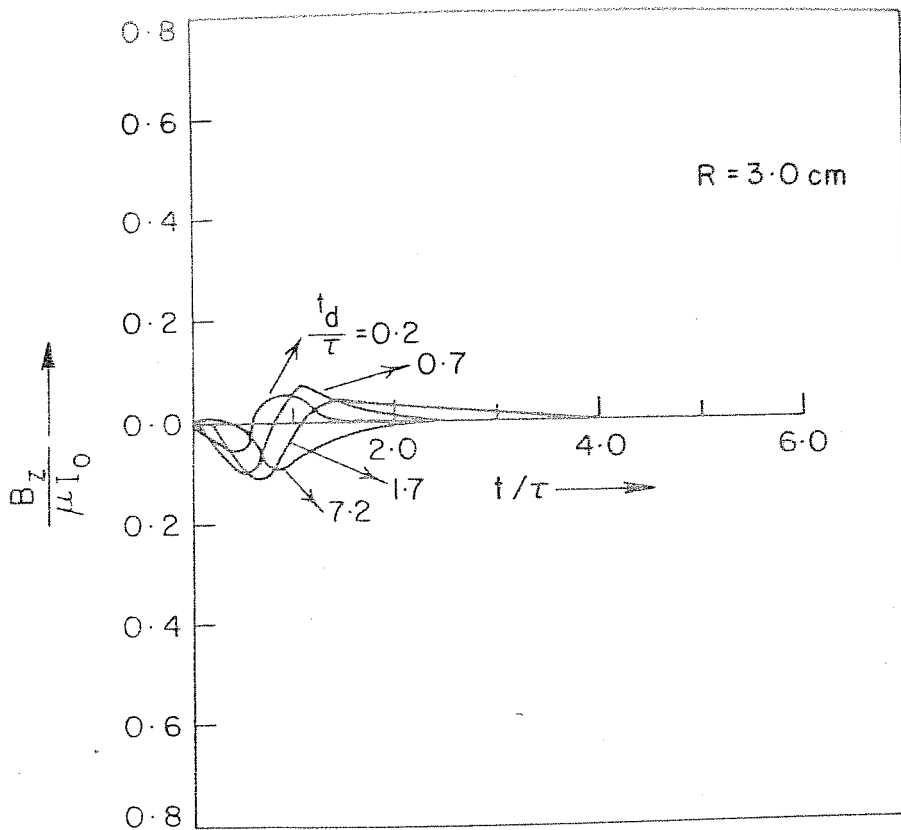


Figure 4.20 Induced axial magnetic field's time profile at 30 mm radius.

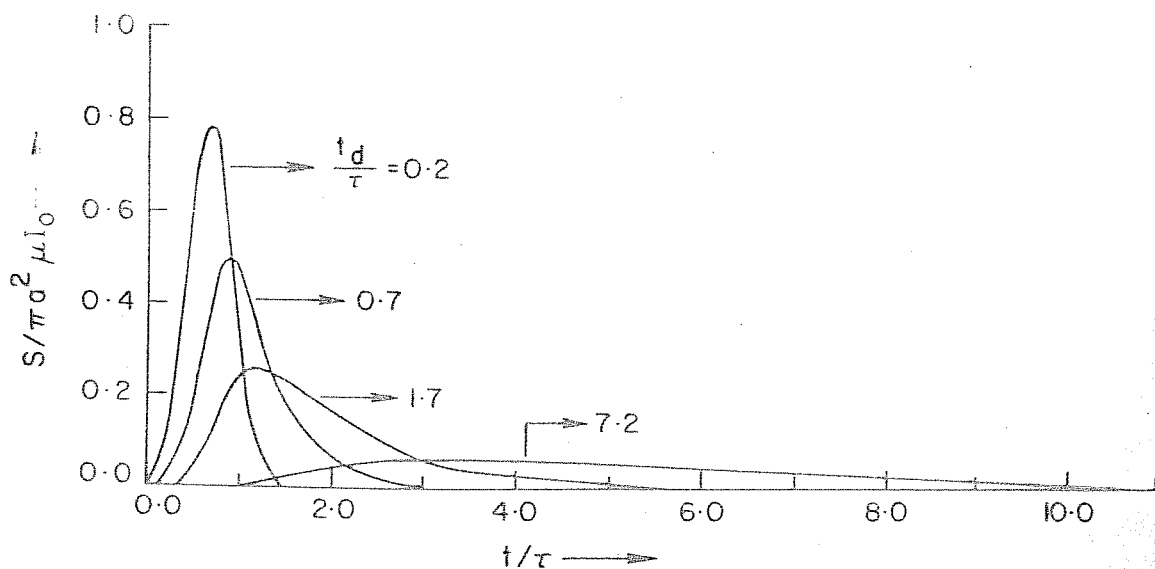


Figure 4.21 Integrated diamagnetic loop signal Vs. time with plasma conductivity as a parameter.

For computing the net azimuthal current density and the output of a diamagnetic loop, in the present calculation, we have used the various experimentally measured beam and plasma parameters, except the plasma conductivity. Due to the uncertainty in the determination of the plasma conductivity, it was obtained by a comparison of the rising part of the observed diamagnetic loop signal with the numerically calculated curves. The net azimuthal current density at $R = 20$ mm, as numerically calculated is found to be 80 Amps/cm^2 whereas the experiments have shown it to be equal to 60 Amps/cm^2 . Further, the diamagnetic loop signal as calculated from the numerical simulation, is equal to 48 gauss, as compared to observed value of 36 gauss.

4.4 DISCUSSION

4.4.1 Return Currents

There are two different theoretical models existing on return current processes, as mentioned in the first chapter. The model of Berk and Pearlstein (1976) deals with the physical conditions, necessary for the generation of axial and azimuthal return currents. This model considers the plasma as a slab, which is homogeneous in the Y-Z direction and spatially

varying in the X direction with conducting walls at $x = \pm L$. The response of the plasma to the beam current having τ_r as the rise time, has been determined. It has been shown that the axial return current arises only when $\tau \ll \tau_d$, where τ is the beam pulse duration and τ_d is the magnetic diffusion time given by $\frac{4\pi\sigma L^2}{c^2}$ where σ is plasma conductivity. In the present experiment, τ is equal to ≈ 100 nsecs and initially the electron temperature $T_e \approx 5-10$ ev, which corresponds to $\tau_d = 1.0$ msec, thus satisfying the condition $\tau_d \gg \tau$ for axial return current generation.

As per Berk and Pearlstein's model the necessary condition for the azimuthal return current generation is $\tau_r \ll L/V_A$, where V_A is the Alfvén velocity. The rise time of the beam current is ≈ 40 nsecs and at the mirror minimum, the external magnetic field is 300 gauss, thus giving a value of L/V_A equal to 200 nsecs (for $n_p = 10^{12} \text{ cm}^{-3}$, $L = 15.0$ cm), so satisfying the necessary condition for the azimuthal return current generation.

The magnetic diffusion model by Chu and Rostoker (1974) and Molvig and Rostoker (1977a) deals with the physical mechanism responsible for the generation of axial and azimuthal return currents and also the effect

of decay of these currents on the rotating beam itself.

The assumptions made in the model are: (i) the plasma electrons are magnetised while ions are not (ii) plasma collision frequency is independent of space and time (iii) annular thickness of the rotating electron beam is larger than plasma skin depth. It has been shown that when these conditions are satisfied, the axial return current results due to the induced electric field E_z and due to the rotation of the electron beam, electric field E_θ and as a consequence of $E_\theta \times B_z$ drift of electrons, E_r are created. The radial electric field E_r , leads to an azimuthal return current through the $E_r \times B_z$ drift of plasma electrons. However, in cases when plasma ions are also magnetised, the dominating mechanism for the generation of azimuthal return current is of the resistive type i.e. $J_\theta = \sigma E_\theta$.

For the initial experimental parameters $T_e = 5-10$ ev, $n_p = 10^{12} \text{cm}^{-3}$, the electron and ion collision frequencies are equal to 10^6sec^{-1} and 10^4sec^{-1} respectively. The electron and ion cyclotron frequencies at the mirror minimum are 5×10^9 and 3×10^6 respectively. Thus, in the present experiment, both electrons and ions being magnetised, the azimuthal return current will be driven dominantly by azimuthal

electric field E_θ rather than by $E_r \times B_z$ drift of electrons. Experiments were conducted for further verification whether $E_r \times B_z$ is the mechanism for the generation of the observed return currents. An electron multiplier placed in the system to register any fast ions or charge exchanged neutral fluxes which should be a natural consequence if E_r is generated as per the model, did not detect any ion or neutral particles. The experiments conducted to verify the dependence of the diamagnetic loop signal decay on the mass of the plasma ions also did not give the expected dependence if E_r was being generated as per the model. The above considerations lead us to the conclusion that in the present experiment $E_r \times B_z$ is not the mechanism for the generation of the azimuthal return current.

4.4.2 Absence of Gross Plasma Oscillation

As was mentioned earlier, the rotating electron beam induced diamagnetic signal does not show any gross oscillatory behaviour of the plasma in the density range 10^{11} - 10^{13} cm^{-3} . Similar results have been reported by Kapetanakis et al (1973) and Roberson (1978). In these two experiments, only above 3×10^{13} cm^{-3} plasma density, magnetosonic modes were observed. Further, the theoretical model predicts

that the magnetosonic mode will be critically damped if (Movig and Rostoker, 1977 a)

$$\nu_e^2 \geq 4 \omega_{LH}^2 \left(1 + \frac{\omega_p^2}{k^2 c^2} \right) \quad \dots\dots(4.4)$$

Where

ν_e is the plasma collision frequency

ω_{LH} is the lower hybrid frequency

ω_p is the plasma frequency

$K = \frac{LH}{a}$, a is the beam radius

It is evident from the expression 4.4 that the magnetosonic mode will be critically damped at low plasma density while oscillations can be excited only above a certain plasma density, as is confirmed by the present and earlier experiments.

4.4.3 Decoupling and Shrinking of Return Current Layer

The present experiment has shown that the azimuthal return current layer, generated by the beam passage through the plasma, decouples itself from the ends of the chamber and persists inside the mirror after the beam has left the mirror. This phenomenon has not been observed in any of the earlier experiments. The main difference between the earlier and the present experiment is that all the earlier experiments have been performed in uniform magnetic

fields, with the field lines extending axially and in contact with the end walls. In this configuration the axial drift of the electrons under the influence of the induced E_z would short out the electric fields, necessary to sustain the azimuthal return currents. In the present experiment, the presence of the mirror fields would inhibit the easy electrons flow to the walls. This is confirmed in the present experiment, in which the 1.0 μ sec long diamagnetic signal is observed only with the mirror field, and when the mirror ratio is reduced, the same signal decays in 200 nsec.

The observed shrinking of the azimuthal return current layer in the axial direction could be explained by the laws of electrodynamics, whereby the pondermotive force acting on a current carrying conductor will always be such that it will tend to increase the inductance of the conductor. Applying this analogy to the present experiment, the azimuthal return current layer, as a result of the pondermotive force acting on them, contracts axially.

4.4.4. Decay Characteristics

As mentioned earlier, in the present experiment $E_r \times B_z$ is not the driving mechanism for the azimuthal return current, thus ruling out any decay due to the

shorting of radial electric fields by the ions. The trapping of the return current layer by the mirror, as observed in the experiment, shows that the decay is not due to losses at the end walls. As a third possibility we have considered the resistive decay of the cross field current by either classical or turbulent process.

According to classical consideration, the azimuthal return current should decay as L/R , where L and R are inductance and resistance of the plasma respectively. However, the return current is observed to decay at a rate ($\sim 1.0 \mu \text{ sec}$) much faster than the calculated value ($\sim 1.0 \text{ msec}$), thus implying an anomalous resistivity of the plasma. Since, the condition $V_d \gg V_{\text{the}} \gg C_s$ (V_d and V_{the} are plasma electron drift and thermal velocities, C_s is ion sound velocity) is satisfied in the present experiment, the beam can excite ion acoustic or Buneman turbulence, resulting in enhanced plasma resistivity. For the case of a return current initiated ion acoustic turbulence, the decay time is given by (Sandel, 1973)

$$\tau_d = 100 \left(\frac{C_s}{V_d} \right) \omega_{pi}^{-1}$$

where ω_{pi} is the ion plasma frequency. For our case, τ_{cl} thus calculated is ≈ 1 nsec i.e. three orders of magnitude smaller than the observed value. Similarly, calculations taking into account Buneman turbulence (Okamura et al, 1977) show that τ_{cl} is around a few nanoseconds. Thus, observed value of the decay time lies in between the classical and the one calculated from ion acoustic or Buneman turbulence.

CHAPTER V

CONCLUSION

Experimental studies on interaction of rotating relativistic electron beam with a plasma trapped in a magnetic mirror has been carried out. Determination of the response of the plasma to the rotating beam as well as propagation studies of the rotating beam through the plasma are the main objectives of the experiments described in preceding chapters. In addition, injection of the intense electron beam in vacuum and plasma filled non-adiabatic cusp magnetic field has also been investigated.

The conclusions drawn from the present investigation are:

1. Space charge neutralisation of the rotating relativistic electron beam is necessary for its propagation up to an appreciable distance. The propagation of the rotating beam to distances more than 150.0 cm is observed in the presence of plasma of density $10^{11}-10^{13} \text{ cm}^{-3}$.
2. The rotating electron beam loses a significant fraction of its axial energy while propagating through the plasma. No macroscopic beam instability is observed during its propagation through the plasma.
3. An improvement in the beam transmission through the cusp configuration is observed, in the presence of a dielectric tube in the cusp region. The maximum transmitted flux is enhanced by a factor of four compared to vacuum value, due to space charge neutralisation of the beam by background plasma, created by the electrical breakdown of the tube surface.
4. The response of the plasma to the rotating electron beam is of magnetic diffusion type, when the plasma density lies in the range $10^{11}-10^{13} \text{ cm}^{-3}$. In this density regime, no radial oscillations of the plasma are observed.

5. The rotating electron beam induces axial and azimuthal return currents in the plasma. The life time of the azimuthal return current is longer by an order of magnitude as compared to that of the axial return current, and these return currents are localised at the beam radial position. The experimental results indicate that the azimuthal return current is of resistive nature rather than of drift type.

6. In earlier experiments, the diamagnetic loop signal was attributed to plasma heating. However, the present experimental studies show that by and large the azimuthal return current diamagnetism contributes to the loop signal, rather than plasma heating. Thus interpreting the loop signal as due to plasma heating is not correct in the rotating electron beam-plasma interaction experiments.

7. The observed spatial and temporal variations of the azimuthal return currents have shown that the return current layer is trapped in the magnetic mirror. After the beam passage, the finite azimuthal return currents are localised in a region about 60.0 cm within the mirror and symmetric around the mirror centre.

8. At the mirror centre, the diamagnetic loop signal decays rapidly in absence of the mirror field. The non-occurrence of the long azimuthal return current decay without the mirror shows that the magnetic mirror field plays an important role in the formation of the trapped return current layer.

9. The observed azimuthal return current decays at a rate much faster than what the classical decay should be but is slow as compared to the rate estimated from ion acoustic or Buneman turbulence.

10. Numerical results of a magnetic diffusion model for the response of the plasma to the rotating electron beam, are in general agreement with the experimental observations.

5.1 SCOPE FOR FUTURE RESEARCH

The experimental results of the present investigation provides the basis to carry out further detailed experimental and theoretical work, in order to acquire a more complete and thorough understanding of the interaction of the rotating relativistic electron beam with plasma and the beam propagation through the cusp magnetic field. The research work need to be carried out in the future are enumerated as follows:

(1) Injection of intense electron beam into a cusp magnetic field in the presence of a dielectric drift tube have shown a significant increase in the beam transmission through the cusp. The observed phenomena is interpreted as due to the presence of a background plasma, created by the electrical breakdown at the tube surface. To determine whether the above predicted physical process is responsible or not for the observed enhancement, a more systematic experimental investigation is being planned to be carried out.

(2) Theoretical models have revealed that the collision frequency plays a crucial role in determining the response of the plasma to the rotating electron beam. When collision frequency is large enough, magnetic diffusion is the dominant process whereas the rotating electron beam excites magnetosonic modes in a collisionless plasma. In the experiments reported so far, no measurements on the collision frequency are available. Nor is it known how response of the plasma to the rotating electron beam depends upon the collision frequency.

(3) Another aspect which would be interesting topic for future research work is the physical mechanism

responsible for the azimuthal return current generation.

The present experiment indicates that the driving mechanism responsible for the generation of the azimuthal return currents is azimuthal electric field, however more experimental work needs to be done to identify the exact process.

(4) A rise in the interaction strength of the rotating electron beam with plasma is observed with an increase in the plasma density, in the regime 10^{11} - 10^{13} cm⁻³. The question arises as to how the rotation of the electron beam results in an increase in the energy transfer efficiency from the beam to the plasma at higher plasma to beam density ratios, in contrast to the case of a linear beam - plasma interaction. Experimental investigation needs to be carried out in a wider plasma density range to establish the scaling for energy transfer efficiency from the rotating electron beam to the plasma.

(5) As has been concluded from the present experiment that the diamagnetic loop signal is dominantly caused by the azimuthal return currents, indicating that the above diagnostic is not reliable for plasma energy measurements in the rotating electron beam - plasma interaction experiments. Therefore the plasma energy

needs to be determined by more sophisticated diagnostics such as Thomson scattering and charge exchange analyser. These diagnostics will also be of help to determine the distribution of the beam energy to ion and electron components of the plasma.

(6) The observed decay of the azimuthal return current could not be explained by either classical analysis or by ion acoustic or Buneman turbulent process, thus indicating the necessity of a new theoretical model on return current decay.

(7) In the magnetic diffusion model used for numerical simulation, the beam is regarded as a specific current source, immersed in the plasma and the interaction is turned on at $t = 0$. Such a model neglects the details of the diode and the cusp field regions, the entry of the beam into the plasma and the effect of the conducting boundary. Determination of the plasma response to the rotating electron beam using a more realistic model would be an added justification for comparing numerical results with experimental observations.

REFERENCES

- Alfvén H., 1939 Phys. Rev. 55 425
- Altyntsev A.T., Eskov A.G., Zolotovskii O.A.,
Koroteev V.I., Kurtmullaev R.Kh., Masalov
V.D. and Semenov V.N., 1971 JETP Lett. 13 139
- Andrew M.L., Daviation H., Fleischmann H.H., Kusse B.,
Kribel R.E. and Nation J.A., 1971 Phys. Rev.
Lett. 27 1428
- Bagratashoili V.N., Knyazev I.N., Kudryartsev Yu - A.
and Letikhov V.S., 1973 Optics Communications
9 135
- Berk H.L. and Pearlstein D., 1976 Phys. Fluids 19 1831
- Bernstein B. and Smith I., 1971 IEEE Trans. Nucl. Sci.
NS-18 294
- Bora D. and John P.I., 1981 IEEE Trans. Plasma Sci.
PS-9 80
- Breizman B.N. and Ryutov D.D., 1974 Nucl. Fusion
14 873
- Bruining H., Physics and Applications of Secondary
Electron Emission (Pergamon, London, 1954) P. 47

- Christofilos N.C., 1958 Proc. 2nd U.N. Int. Conf. on
the Peaceful Uses of Atomic Energy 32 279
- Chu K.R. and Rostoker N., 1973 Phys. Fluids 16 1472
- Chu K.R. and Rostoker N., 1974 Phys. Fluids 17 813
- Chu K.R., Kapetanakis C.A. and Clark R.W., 1975 Appl.
Phys. Lett. 27 185
- Coensgen F.H., Cummins W.F. and Sherman A.E. 1959 Phys.
Fluids 2 350
- Cox J.L. and Bennet W.H., 1970 Phys. Fluids 13 182
- Ekdahl C., Greenspan M., Kriebel R.E., Sethian J.
and Wharton C.B., 1974 Phy. Rev. Lett. 33 346
- Fainberg Ya. B., Shapiro V.D. and Shevchenko V.I., 1970
Sov. Phys. - JETP 30 528
- Ferch R.L. and Sudan R.N., 1975 Plasma Phys. 17 905
- Friedman M., 1970 a Phys. Rev. Lett. 24 1098
- Friedman M., 1970 b Phys. Rev. Lett. 25 567
- Friedman M. and Sprangle P., 1972 Plasma Phys. 14 207
- Gerber K.A., Spector D.N. and Sethian J.D., 1977
Rev. Sci. Instrum. 48 1408

Goldenbaum G.C., Dove W.F., Gerber K.A. and Logan B.G.,

1974 Phys. Rev. Lett. 32 830

Graybill S.E. and Uglum J.R., 1970 J. Appl. Phys. 41 230

Hammer D.A. and Rostoker N., 1970 Phys. Fluids 13 1831

Jain K.K., John P.I., Punithavelu A.M. and Rao P.P.,

1980 J. Phys. E 13 928

John P.I. and Jain K.K., 1981 Pramana 17 279

Kapetanakos C.A. and Hammer D.A., 1973 Appl. Phys.

Lett. 23 17

Kapetanakos C.A., Black W.M. and Chu K.R., 1973

Phys. Rev. Lett. 34 1156

Kapetanakos C.A., 1974 Appl. Phys. Lett. 24 112

Kapetanakos C.A., Black W.M. and Striffler C.D., 1975 App. Phys. Lett.

26 368

Korn P., Sandel F. and Wharton C.B., 1973 Phys. Rev.

Lett. 31 579

Lali K.S., Pujara H.D. and Saxena Y.C., 1979

PRL Technical Note No. TN-79-03

Lawson J.D., 1959 J. Nucl. Energy C 1 31

Lawson J.D., The Physics of Charged Particle Beams
(Clarendon Press, Oxford 1977) P. 118

Lee R.E. and Sudan R.N., 1971 Phys. Fluids 14 1213

Little R.G., Uglum J.R. and Lowell R.A., 1975 IEEE
Trans. Nucl. Sci. NS-22 2351

Lovelace R.V.E. and Sudan R.N., 1971 Phys. Rev. Lett.
27 1256

Miller P.A., 1975 Appl. Phys. Lett. 27 107

Molvig K. and Rostoker N., 1977 a Phys. Fluids
20 494

Molvig K. and Rostoker N., 1977 b Phys. Fluids
20 504

Nation J.A., 1970 Appl. Phys. Lett. 21 491

Nation J.A., 1979 Cornell University Report No. LPS-263

Nebenzahl I., 1973 Plasma Phys. 15 1149

Okamura R., Nakamura Y. and Kawashima N., 1977
Plasma Phys. 19 997

Oswald R.B., Eisen R.A. and Conrad E.E., 1966

IEEE Trans. Nucl. Sci. NS-13 229

Papadopoulos K., 1975 Phys. Fluids 18 1769

Rhee M.J. and Destler W.W., 1974 Phys. Fluids 17 1574

Roberson C.W., 1978 Nucl. Fusion 18 1693

Rudakov L.I. and Samarsky A.A., 1973 Proc. Vith
European Plasma Physics Conference,
Moscow P. 487

Sandel F.L., 1973 Cornell University Report No. LPS -131

Saxena Y.C., Lali K.S. and Jain K.K., 1979 PRL
Technical Note No. TN-79-02

Segall S.B. and Koopman D.W., 1973 Phys. Fluids 16 1149

Sethian J.D., Gerber K.A., Spector D.N. and Robson A.E.,
1978 Phys. Rev. Lett. 41 789

Schmidt G., 1962 Phys. Fluids 5 994

Striffler C.D. and Kapetanacos C.A., 1975 J. Appl.
Phys. 46 2509

Thode L.E. and Sudan R.N., 1975 Phys. Fluids 18 1552

Thode L.E., 1976 Phys. Fluids 19 305 and 831

Toepfer A.J. and Poukey J.W., 1973 Phys. Fluids
16 1546

Wharton C.B., 1977 Proc. 2nd Int. Conf. on High Power
Electron and Ion Beam P. 407

Wild J.P. and Swerd S.F., 1972 Ann. Rev. Astron.
Appar. 10 159

Yonas G., Poukey J.W., Prestwich K.R., Freeman J.R.,
Toepfer A.J. and Clauser M.J., 1974 Nucl.
Fusion 14 731.

QUACEND

1005 8AM